The Dissertation Committee for Alicia Jen Allen
certifies that this is the approved version of the following dissertation:

Analysis of Transmission System Events and Behavior using Customer-level Voltage Synchrophasor Data

Committee:

Surya Santoso, Supervisor

Mircea Driga

William M. Grady

Alexis Kwasinski

Jaime Ramos

Analysis of Transmission System Events and Behavior using Customer-level Voltage Synchrophasor Data

by

Alicia Jen Allen, B.S.E.E.; M.S.E.

DISSERTATION

Presented to the Faculty of the Graduate School of

The University of Texas at Austin

in Partial Fulfillment

of the Requirements

for the Degree of

DOCTOR OF PHILOSOPHY

THE UNIVERSITY OF TEXAS AT AUSTIN

May 2013

Dedicated to Mohit Singh.

Acknowledgments

I would like to express my thanks to Dr. Surya Santoso, my supervisor, for his excellent guidance during this project, his mentorship, his role in providing support for me throughout my career at the University of Texas, and for his faith in my capabilities as a researcher. I would also like to thank my committee member Dr. W. Mack Grady for setting up the Texas Synchrophasor Network to make possible the work presented here and to thank committee members Dr. Mircea Driga, Dr. Alexis Kwasinski, and Dr. Jamie Ramos for their valuable guidance and input.

I would also like to thank Joe Mooney for his help and encouragement during my internships at Schweitzer Engineering Laboratories and to thank Dr. Eduard Muljadi and Yih-Huei Wan at the National Renewable Energy Laboratory for their valuable guidance and input.

I am very grateful to my collaborators at the University of Texas, namely Sang-Wook Sohn, Moses Kai, and David Burnham, with whom I worked on parts of this project. I am also grateful to my lab colleagues for their help and support. I am especially grateful to Mohit Singh, who has been so patient with me and so helpful with my work.

I would also like to thank my dad, Loy Ray Allen, and sister, Ashley May Allen, for their encouragement and support.

I would like to acknowledge the contribution of Schweitzer Engineering Laboratories, Inc. for providing the equipment and technical support necessary for this work. This work is made possible by funding provided by the Center for the Commercialization of Electric Technologies, the Electric Power Research Institute and the National Renewable Energy Laboratory.

Analysis of Transmission System Events and Behavior using Customer-level Voltage Synchrophasor Data

Publication No. _____

Alicia Jen Allen, Ph.D.
The University of Texas at Austin, 2013

Supervisor: Surya Santoso

The research topics presented in this dissertation focus on validation of customer-level voltage synchrophasor data for transmission system analysis, detection and categorization of power system events as measured by phasor measurement units (PMUs), and identification of the influence of power system conditions (wind power, daily and seasonal load variation) on low-frequency oscillations. Synchrophasor data can provide information across entire power systems but obtaining the data, handling the large dataset and developing tools to extract useful information from it is a challenge. To overcome the challenge of obtaining data, an independent synchrophasor network was created by taking synchrophasor measurements at customer-level voltage. The first objective is to determine if synchrophasor data taken at customer-level voltage is an accurate representation of power system behavior. The validation process was started by installing a transmission level (69 kV) PMU. The customer-level voltage measurements were validated by comparison of long

term trends and low-frequency oscillations estimates. The techniques best suited for synchrophasor data analysis were identified after a detailed study and comparison. The same techniques were also applied to detect power system events resulting in the creation of novel categories for numerous events based on shared characteristics. The numerical characteristics for each category and the ranges of each numerical characteristic for each event category are identified. The final objective is to identify trends in power system behavior related to wind power and daily and seasonal variations by utilizing signal processing and statistical techniques.

Table of Contents

List of Tables

List of Figures

Chapter 1

Introduction

This chapter presents an outline of the research carried out to obtain and analyze high-quality power system data from phasor measurement units (PMUs). PMUs are a "Smart Grid" technology that provides an improvement in data synchronization and resolution over traditional supervisory control and data acquisition (SCADA) technologies. The data obtained from PMUs is called synchrophasor data and consists of GPS-synchronized time stamps, voltage and current magnitudes, phase angles and frequencies calculated from the phase angles. The research objectives presented here are the validation of customer-level voltage synchrophasor data for transmission system analysis, identification of the influence of power system conditions (wind power, daily and seasonal load variation) on low-frequency oscillations, and detection and categorization of power system events as measured by PMUs. The chapter begins by providing an overview of the importance and applications of synchrophasor data and describes the unique contributions a customer-level voltage synchrophasor network can provide. The research objectives are then enumerated and followed by a summary of the approaches taken to achieve these objectives. The resulting technical contributions to the area of wide area monitoring systems and synchrophasor data are discussed and a list of

publications is provided.

1.1 Background and Motivation

Monitoring power system stability has become increasingly important as power systems operate closer to their operating limits while incorporating ever increasing amounts of variable generation. Stability evaluation can be accomplished through monitoring of phase angle separations in the system and monitoring of electromechanical oscillations. Electromechanical oscillations are inherent to the power system, and the damping of these oscillations should be monitored in order to evaluate the stability of the power system. If monitoring systems were not in place to alert system operators, underdamped oscillations may cause transmission lines to temporarily exceed their stable transfer limits, which could potentially lead to system wide blackouts. The stability impacts on the grid of increased penetration of renewable sources are not completely known but better monitoring can assist in evaluating these impacts. Though power system simulations and models can provide some idea of the impacts of high penetration of renewable sources, synchrophasor data can provide a way to monitor the system and include details that are not present in power system models.

Synchronized voltage phasor measurements, or synchrophasor data, taken by phasor measurement units (PMUs) at substations and generating units allow for the wide area monitoring of the electric power system covering a large geographical area. This measurement technology is relatively new and

has so far been applied in a limited manner. It has the potential to greatly improve power system reliability [8] by providing a clear snapshot of the system state rather than the "blurry" image from the SCADA system. Synchrophasor measurements are taken at high speed (typically thirty times a second as compared to SCADA rates of once every four seconds) and time-stamped using a common time reference, typically derived from global positioning system (GPS) signals. The common time reference allows for the direct measure of the voltage phase angle at each PMU location. The voltage phase angle is used as an indicator of power system stress.

Though synchrophasor data provide insightful information, the placement of PMUs and use of synchrophasor data are generally dictated by utilities and the independent system operators (ISOs) that install them, and synchrophasor data are not always readily available for research. To overcome this obstacle, the University of Texas at Austin introduced the Texas Independent Synchrophasor Network to monitor power system events and analyze low-frequency electromechanical oscillations from the electric power grid through PMU measurements taken at customer-level voltage (120 V). The network consists of a central PMU station located on the University of Texas at Austin campus and remote PMU stations located throughout ERCOT. The central PMU station equipment includes a local PMU, phasor data concentrator (PDC) to collect and sort PMU data, and a PC to archive, display, and analyze the PMU data. The PMUs within the network are not installed at substations but measure single-phase, 120 V from a standard wall outlet. The

Texas Independent Synchrophasor Network has been producing voltage synchrophasor data from two to up to seven PMUs within ERCOT since it received its first remote measurements from the University of Texas McDonald Observatory in West Texas in January 2009 [9, 10]. Even though the PMUs in the network are taking measurements at customer-level voltage, only transmission system behavior is of interest for the research presented in this dissertation. The main purpose of synchrophasors is their ability to provide a wide-area view of the power system and hence gaining insight into transmission system behavior (such as phase angle separation and oscillations) is the main target of synchrophasor data analysis.

As stated, synchrophasor data can provide information across entire power systems but obtaining the data has been difficult and handling the large dataset and developing tools to extract useful information from the data is a challenge. There are also concerns that the customer-level voltage synchrophasor data contains distribution level information that will interfere with transmission system analysis. The research presented here tackles these problems of data acquisition, data analysis and data quality.

1.2 Objectives

The overall objective of the research presented in this dissertation is to demonstrate that customer-level voltage synchrophasor data can be used for power system analysis and consequently to use the synchrophasor data to extract useful information about power system behavior. Validation of

customer-level voltage synchrophasor data for transmission system analysis purposes will allow for the confident ease of expansion of synchrophasor networks and ease of dissemination of synchrophasor data for academic research. Customer-level voltage PMUs are much quicker and inexpensive to install because they do not require signing of non-disclosure agreements with utilities. Furthermore, since they are at a lower voltage they do not require expensive equipment to measure higher voltage quantities such as potential transformers (PTs). By extracting information on the behavior of the power system from synchrophasor data by applying signal processing and statistical methods, the impact power system events and changing penetration levels of renewable energy have on the grid is studied. The specific objectives are provided below.

Objective 1: *Determine if customer-level voltage synchrophasor data is an accurate representation of power system behavior.* Objective 1 involves demonstrating that customer-level voltage PMU data is an accurate representation of transmission level measurements and can be used to analyze transmission system behavior, e.g., power system events and low-frequency electromechanical oscillations.

Objective 2: *To develop automatic algorithms to detect and identify power system events in the synchrophasor data.* The purpose of Objective 2 is to create a novel algorithm to help extract useful information for power system analysis out of the large volume of synchrophasor data. The new algorithm will extract information about power system events such as

generator unit trips, transmission line trips, and other types of events as recorded by the synchrophasor network.

Objective 3: *Propose power system event categories for voltage synchrophasor data.* Objective 3 is an extension of Objective 2 and includes taking the detected events and creating categories based on common visual characteristics. Part of the objective is to also identify numerical characteristics for each category and to determine the ranges of characteristics for each event category.

Objective 4: *Identify trends in power system behavior related to wind power and daily and seasonal variations.* Objective 4 involves identifying trends in power system behavior in the synchrophasor data that is influenced by different levels of wind power penetration. Power system behavior information is extracted from the synchrophasor data using signal processing techniques. Wind power and generation data were taken from the ERCOT website to determine the approximate level of wind power penetration during the time period of synchrophasor data being examined.

1.3 Approach

1.3.1 Validation of customer-level voltage synchrophasor data for analysis of transmission system behavior

The Texas Independent Synchrophasor Network allows for easy access to real world power system measurements in the form of customer-level volt-

age synchrophasor data. However, because power system information in the form of a voltage signal is distributed from the transmission power system through a series of cables, equipment and parallel loads, the voltage measured by PMUs at the distribution level could potentially be polluted with noise and unwanted information. Even though the voltage signal is filtered to remove high frequency noise and harmonics before it is used for monitoring and analysis, phase shifts and other unwanted information may appear in the data [11].

The first step in this approach is to show that customer-level voltage synchrophasor data accurately captures power system response to known large disturbances. An example of a large disturbance type examined for this approach are generating unit trips as provided in the Electric Reliability Council of Texas' daily grid reports [12, 13]. The drop in frequency and the low-frequency oscillations induced by the disturbance as seen in the synchrophasor data are examined. Next, to show that even though the customer-level voltage synchrophasor data may contain additional distribution events it is still an accurate representation of transmission system voltages, customer-level voltage data is compared to voltage data taken from the nearest 69 kV bus. Bus voltages as calculated by ERCOT state estimators using SCADA and network data are compared to the customer-level voltage synchrophasor data. However, the timestamp and sampling rate of the ERCOT data significantly differs from the synchrophasor data. This next step taken to ensure that the customer-level voltage synchrophasor data are accurate is the installation of a PMU at a 69 kV bus located near the UT-Austin campus. The voltage synchrophasor data

from this PMU is compared to the customer-level voltage synchrophasor data. Signal processing methods are used to compare the information extracted from synchrophasor data taken at customer-level voltage to information extracted from synchrophasor data taken at 69 kV as well. The relative phase angle difference between the 69 kV and customer-level voltage PMUs at the UT-Austin campus is also examined. A simple simulation is built to verify behavior seen in the measured relative phase angle difference.

1.3.2 Automatically identify response of the power system to events as measured by the synchrophasor network

Synchrophasor networks generate large volumes of synchrophasor data making it difficult to discover meaningful information about power system behavior and events. In order to help discover useful information in the synchrophasor data, a novel algorithm is created which is applied to automatically detect power system events in the synchrophasor data. The algorithm detects events based on the abnormal response of the power system to events compared to normal operating conditions. When an event occurs, the normally occurring low-frequency electromechanical oscillations increase in amplitude. This observation is used by the algorithm to screen the synchrophasor data for events.

Three different signal processing techniques are utilized to help detect events. These techniques are fast Fourier transform method, Matrix-Pencil method, and the Yule-Walker Spectral method. A fourth method uses the

maximum difference in a window of data to help detect events. All four methods are applied to a moving window of data for an entire hour of synchrophasor data. For the signal processing methods, the peak values for each window are saved. For the maximum difference method, the calculated maximum difference is saved for each window. Statistical methods are applied to the saved peak values to determine if an event occurred for a particular window of data. If two or more methods detect a possible event, the window is marked as containing an event and the data is saved for further analysis. This method is applied to all frequency and relative phase angle difference signals available at the time of the analysis. The number of signals is dependent on the number of network PMUs in operation.

1.3.3 Propose power system event categories for synchrophasor data

The results from the screening algorithm described in Section 1.3.2 are used to propose power system event categories. For the first step in this approach, the event categories are created based on common visual characteristics seen in events detected by the screening algorithm. The event categories are based on the synchrophasor signal examined; either the relative phase angle difference signal or the frequency signal. The relative phase angle difference event categories include impulse, transient, and step change. The frequency event categories include impulse, transient, and drop or rise in frequency. Next, after many days of data are screened for events and those events that are found categorized, the numerical characteristics are extracted from each event. The

characteristics examined include the magnitude, the rate of change, the frequency content of the signal, the duration, and the step change amount. The typical ranges for characteristics for each category are provided and can easily be applied to the screening algorithm to automatically categorize events after they are detected.

1.3.4 Identify trends in power system behavior related to wind power and daily and seasonal variations by utilizing signal processing and statistical techniques

The impact of increasing penetration of wind power on power system behavior is not completely known. The grid operated by ERCOT provides a unique opportunity to study the impact of high levels of wind penetration. Wind power penetration levels of 26% of total power generation have been observed during a record wind power output of 8,521 megawatts in November of 2012. With the installation of PMUs across ERCOT, the impact of wind power on power system behavior can now be analyzed in new ways. Wind power and total generation data was captured from ERCOT's website. This information was collected over a period of 2 years and is compared to the synchrophasor data collected by the Texas Independent Synchrophasor Network over the same period of time. The relationship between the relative phase angle difference (between West Texas where many wind farms are located and Central Texas) and the wind power penetration are examined first. The low-frequency electromechanical oscillations present in the synchrophasor data are analyzed and the damping and frequency content are compared to different

wind power penetration levels.

All synchrophasor data are taken from the Texas Independent Synchrophasor Network and are used in all the listed research objectives. Additional data is provided by ERCOT as used in the approach for Objective 1 and Objective 4. Analysis of all data was done in MATLAB.

1.4 Original Research Contribution

This section summarizes key results and the original research contributions made while achieving the objectives for this work. A complete list of publications resulting from the research is also provided.

1.4.1 Major Contributions

Major contributions and the resulting publications are provided below:

- To achieve Objective 1, the customer-level voltage synchrophasor data is analyzed during large disturbances and during ambient or normal operating conditions. After applying the approach described in Subsection 1.3.1, it was found that the customer-level voltage synchrophasor data accurately represents power system behavior at the transmission voltage level. Large disturbances that were published by ERCOT on their website were seen clearly in the customer-level voltage synchrophasor data. Specifically, the frequency drop recorded by ERCOT matched the frequency drop in the synchrophasor data. Next, customer-level volt-

age synchrophasor relative phase angle data matched the relative phase angle data from SCADA and state estimator provided by ERCOT. The customer-level voltage synchrophasor data from UT-Austin also matches the transmission level voltage synchrophasor data at Harris Substation which connects the UT-Austin campus to the grid. The data from both PMUs were examined during ambient and transient conditions and found to match. When the relative phase angle difference between UT-Austin and Harris Substation is examined, the difference typically is negligible but it has been observed that the difference can jump to 2 to 3 degrees. These jumps are explained by changes in load current and a small model of the UT-Austin campus was created in PSSE software to illustrate the influence of load on the relative phase angle difference between UT-Austin and Harris Substation. Chapter 3 describes the methods used on the synchrophasor data to extract information on the low-frequency oscillations. Chapter 4 provides a description of the analysis and the results extracted from the analysis as well. The results from this analysis are published in [14] and will be published in the National Renewable Energy Laboratory (NREL) report [15]:

– Allen, A.J.; Sohn, S.W.; Grady, W.M.; Santoso, S.; "Validation of distribution level measurements for power system monitoring and low frequency oscillation analysis," Power Electronics and Machines in Wind Applications (PEMWA), 2012 IEEE , vol., no., pp.1-5, 16-18 July 2012

  - Allen, A.J.; Santoso, S.; Muljadi, E.; "Phasor Measurement Unit (PMU) for Wide Area Monitoring, Protection, and Control (WAMPAC) Applications," NREL Report, December 2012

- To achieve Objective 2, a novel algorithm to screen synchrophasor data to automatically identify power system events was created. The screening algorithm was based on the observation that the amplitude of the low-frequency oscillations typically present in the synchrophasor data are much larger during a power system event. The algorithm used signal processing techniques described in Chapter 3 and applied statistical analysis to identify power system events. The frequency and relative phase angle difference signals that were available at the time of the analysis were analyzed. A description of the screening algorithm and examples of the events detected are provided in Chapter 5. The results from this analysis are published in [16, 17]:

  - Allen, A.J.; Sohn, S.W.; Grady, W.M.; Santoso, S.; "Algorithm for Screening PMU Data for Power System Events," IEEE International Smart Grid Technologies, October 2012, Berlin, Germany
  - Sohn, S.W.; Allen, A.J.; Kulkarni, S.; Grady, W.M.; Santoso, S.; "Event detection method for the PMUs synchrophasor data," Power Electronics and Machines in Wind Applications (PEMWA), 2012 IEEE , vol., no., pp.1-7, 16-18 July 2012

- For Objective 4, it was initially observed that the relative phase angle difference between UT-Austin and McDonald Observatory (West Texas) was highly correlated to high wind power penetration levels within ERCOT. Early on in the analysis an approximate 2 Hz oscillation also appeared during high wind power penetration levels. However, as more synchrophasor data and wind power data was collected, the relationship between the 2 Hz oscillation and the wind power penetration levels changed. Many changes to the grid occurred between the initial observations made in 2008-2009 to observations made in 2010 and may be the cause of the changes in the relationship between oscillations and wind power levels. When more detailed wind power and generation data is available, a more detailed analysis on the relationship between wind power and low-frequency oscillations can be made. The initial observation on the relationship between the wind power penetration levels and synchrophasor data is published in [18].

  – Allen, A.J.; Santoso, S.; Grady, W.M.; "Voltage phase angle variation in relation to wind power," Power and Energy Society General Meeting, 2010 IEEE , vol., no., pp.1-7, 25-29 July 2010

  As wind power capacity increases and replaces conventional generation, changes in system inertia may occur. The changes in the 2 Hz oscillation may be caused by changes in inertia rather than the influence of wind power penetration levels. The impact changes in inertia have on

low-frequency oscillation is described in [19]. The extended abstract of the paper has been well received and the complete paper is invited for submission:

  - Allen, A.J.; Singh, M.; Muljadi,E.; Santoso, S.; "Measurement-Based Investigation of Inter- and Intra-Area Effects of Wind Power Plant Integration," IEEE TPWRS, submitted for review, April 2013

1.4.2 Supporting Contributions

The supporting contribution and resulting publications are given below:

- To achieve Objective 3, the categories created based on the events detected by the screening algorithm are identified based on common visual characteristics. The characteristics that are identified include magnitude, rate of change, frequency content of the signal, duration, and step change amount. Examples of the events and typical ranges of the event characteristics are provided in Chapter 6. The results from this analysis are published in [15]:

  - Allen, A.J.; Santoso, S.; Muljadi, E.; "Phasor Measurement Unit (PMU) for Wide Area Monitoring, Protection, and Control (WAMPAC) Applications," NREL Report, December 2012

1.4.3 Dissertation Outline

The organization of the chapters of this dissertation is as follows. Chapters 2 and 3 contain background information on the synchrophasor network and analysis methods used throughout this dissertation. Chapter 2 provides an introduction to synchrophasors and a description of the customer-level voltage Texas Independent Synchrophasor Network. The description of the network includes a description of the equipment and synchrophasor data format. A description of an algorithm created to help decide the best placement of PMUs for power system monitoring purposes is also provided. Chapter 3 describes the signal processing methods used to evaluate synchrophasor data and the performance of the selected methods is tested. Chapters 4 to 7 use the synchrophasor data as measured by the synchrophasor network. The customer-level voltage synchrophasor data is evaluated for its ability to accurately represent power system behavior in Chapter 4. Once the customer-level voltage PMU data is shown to be accurate representation of transmission level measurements, Chapter 5 introduces an algorithm that is used to automatically screen synchrophasor data for events that occur on the power system. Chapter 6 uses the results from the screening algorithm to create categories for the power system events. The common numerical characteristics from each category are extracted and used to automatically classify events. In Chapter 7, the influence of wind power penetration levels on the power system as seen in the synchrophasor data is analyzed. Finally, an overview and concluding remarks are given in Chapter 8.

Chapter 2

The Texas Independent Synchrophasor Network

Synchronized voltage phasor measurements, or synchrophasors, taken by phasor measurement units (PMUs) allow for the wide area monitoring of the electric power system covering a large geographical area. However, the placement of PMUs and use of synchrophasor data are generally controlled by utilities and the independent system operators (ISOs) that install them and synchrophasor data are not always readily available for research. To overcome this obstacle, the University of Texas at Austin introduced an independent synchrophasor network to monitor events and analyze low-frequency electromechanical oscillations from the electric power grid through PMU measurements taken at customer-level voltage (120 V).

This chapter provides a brief introduction on synchrophasors and their applications and introduces the Texas Independent Synchrophasor Network. Introductory information on synchrophasors and their applications is provided in Section 2.1. Section 2.2 analyzes possible locations for PMU placement within the Electric Reliability Council of Texas (ERCOT) for power system event monitoring purposes. The Texas Independent Synchrophasor Network

is introduced in Section 2.3 and includes the PMU locations and a description of the network equipment. Section 2.4 describes the Texas Independent Synchrophasor Network file format of archived synchrophasor data and the adjustments to the synchrophasor data required before analysis of the data can begin.

- **Publication**: Part of the work presented in this chapter has been published in [20]
  - S. Kulkarni, A. Allen, S. Santoso, and W. M. Grady. "Phasor measurement unit placement Algorithm" in *Power & Energy Society General Meeting, 2009 IEEE*, July 2009, pp. 1-6.

2.1 Synchrophasor and Phasor Measurement Unit Background

In Subsections 2.1.1 to 2.1.4, the definitions of phasor and synchrophasor are provided. A description of frequency estimation using voltage phase angle measurements is provided in Subsection 2.1.5. Subsection 2.1.6 provides an example of a synchrophasor network and Subsection 2.1.7 describes synchrophasor applications that can be used to improve power system wide area monitoring, control, and protection.

2.1.1 Phasor Definition

Phasors are mathematical representations of sinusoidal waveforms typically taken during steady-state conditions. An example of a steady-state sinusoidal waveform expressed as a function of time is provided in Eq. 2.1.

$$x\left(t\right) = X_m cos\left(\omega t + \phi\right) \tag{2.1}$$

where, X_m is the peak value of the waveform, ω is the frequency of the signal in radians per second, and ϕ is the phase angle in degrees. The *phasor representation* is a complex number consisting of the magnitude and phase angle and is independent of the system frequency. In order to express Eq. 2.1 as a phasor, Euler's identity is first employed resulting in Eq. 2.2.

$$x\left(t\right) = \Re[X_m e^{j(\omega t+\phi)}] \tag{2.2}$$

As mentioned, the phasor is independent of the system frequency so the term $e^{j\omega t}$ is suppressed and is rewritten in Eq. 2.3. The magnitude of the phasor, $V_M/\sqrt{2}$, is the root mean square (rms) value of the sinusoidal waveform.

$$x\left(t\right) \Leftrightarrow X = \frac{X_m}{\sqrt{2}} e^{j\phi} \tag{2.3}$$

Fig. 2.1 illustrates the phasor representation of the sinusoidal signal described in Eqs. 2.1 and 2.3. The phasor representation is of the waveform

at time $t = 0$. Information on how sampled waveforms and the digital Fourier transform (DFT) are employed to calculate the phasor representation is provided in [21].

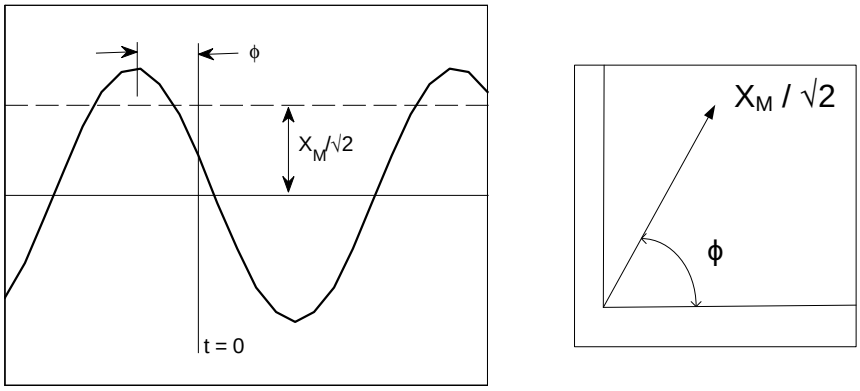

Figure 2.1: Representation of a phasor

2.1.2 Phasor representation for off-nominal frequency

The impact of off-nominal frequency (when the waveform frequency is above or below nominal) on phasor representation is illustrated here.

If a phasor representation is made for a waveform at nominal frequency for each kT_0 where $k = 0, 1, 2, \ldots, n$ and T_0 is the interval period for nominal frequency $T_0 = 1/f_0$, then a constant phasor results. In other words, the phase angle is constant for all kT_0. However, if the frequency of the waveform is off-nominal, the phase angle of the observed phasor will change at a rate of $2\pi(f - f_0)T$ where f is the off-nominal frequency. The change in phase

angle when the waveform is of off-nominal frequency is shown in Fig. 2.2. The dotted line shows the times where the phasor is calculated, kT_0, and the peaks of the off-nominal frequency waveform are indicated as well. If the waveform were nominal frequency, the phase angle ϕ_k would remain the same, and in this case $\phi_k = 0$ for all k. However, since the waveform frequency is off-nominal, the phase angle ϕ_k is increasing for each phasor representation.

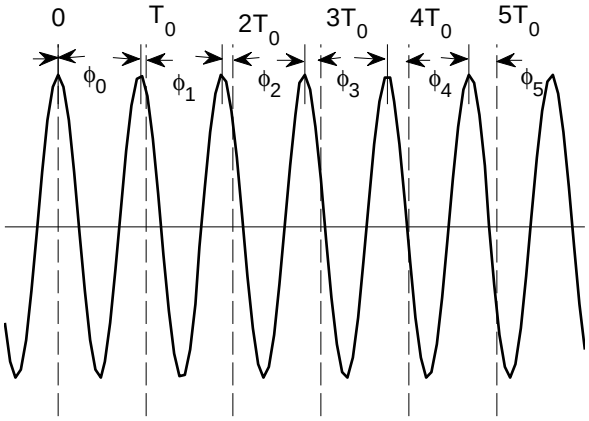

Figure 2.2: Phasor taken at kT_0 for off-nominal frequency alters the phase angle ϕ_k

2.1.3 Synchrophasor Definition

A common time reference allows for the synchronization of phasor measurements. This also allows for the direct measure of the phase angle quantity ϕ which now represents the phase angle relative to a reference cosine wave-

form at nominal frequency [22]. The signals are synchronized using a common timing source from a reliable source such as Global Positioning System (GPS) satellites. Synchrophasors are timestamped at the time of the measurement.

2.1.4 Positive Sequence Synchrophasor

Phasor representations for each phase can be calculated but for the evaluation of power system performance, positive sequence phasors are of more use than phasors from each individual phase [23]. Positive sequence phasors also reduce the amount of memory required to store synchrophasor data since only a single phasor is recorded rather than three phasors. The positive sequence phasor, V_1, is calculated using Eq. 2.4.

$$V_1 = \frac{1}{3}\left(V_a + \alpha V_b + \alpha^2 V_c\right) \tag{2.4}$$

Where, $\alpha = e^{j2\pi/3}$ and rotates the V_b and V_c phasors .

2.1.5 Frequency Estimation

As mentioned in Subsection 2.1.1, the phasor representation is a steady-state concept that is independent of the system frequency. However, in the actual power system, the frequency is constantly changing due to imbalances between the load and generation. Here frequency estimation is introduced and is derived directly from the synchrophasor phase angle measurements. More information on frequency and phasor estimation during off-nominal conditions is given in [21].

The frequency estimation based on balanced three-phase inputs is described here and is taken from [21]. First, if the nominal frequency is ω_0, the actual frequency deviation from nominal is $\Delta\omega$, and the rate of change of frequency is ω', the frequency $\omega(t)$ at time t is given by Eq. 2.5.

$$\omega(t) = (\omega_0 + \Delta\omega + t\omega') \tag{2.5}$$

Next, the relationship between phase angle and frequency as described in [21] is shown in Eq. 2.6.

$$\phi(t) = \phi_0 + t\Delta\omega + \frac{1}{2}t^2\omega' \tag{2.6}$$

Eq. 2.6 is next rewritten as a second degree polynomial in Eq. 2.7.

$$\theta(t) = a_0 + ta_1 + t^2a_2 \tag{2.7}$$

Where $\Delta\omega$ and ω' are written in terms of the a_1 and a_2 coefficients as shown in Eq. 2.8.

$$\Delta\omega = a_1, \omega' = 2a_2 \tag{2.8}$$

Using a window of N phase angle data points, the frequency is calculated using the matrix of equations in Eq. 2.9

$$\begin{pmatrix} \phi_0 \\ \phi_1 \\ \phi_2 \\ \cdots \\ \phi_{N-1} \end{pmatrix} = \begin{pmatrix} 1 & 0 & 0 \\ 1 & \Delta t & \Delta t^2 \\ 1 & 2\Delta t & 4\Delta t^2 \\ \vdots & \vdots & \vdots \\ 1 & (N-1)\Delta t & (N-1)^2\Delta t^2 \end{pmatrix} \times \begin{pmatrix} a_0 \\ a_1 \\ a_2 \end{pmatrix} \tag{2.9}$$

The calculated a coefficients are then used to find the frequencies using Eq. 2.8. The frequency in terms of Hz and the rate of change of frequency can also be calculated using Eq. 3.9.

$$\Delta f = a_1/(2\pi), f' = a_2/\pi \tag{2.10}$$

Since the estimated frequency is based on a measurement taken at a single bus, the frequency offers a more localized view of the response of the power system rather than demonstrating the behavior between two areas within a power system as apparent through the voltage phase angle difference between two different buses. The frequency estimate for unbalanced three-phase inputs and nonlinear frequency estimators are provided in [21].

2.1.6 Synchrophasor Network Architecture

To measure and collect synchrophasor data, a synchrophasor network that consists of PMUs placed throughout the grid and a system to collect data is required. An example of a synchrophasor network is given in Fig. 2.3 and is taken from [1]. In the network, data from PMUs are sent directly to a phasor data concentrator (PDC). A PDC is equipment that waits for and sorts data

from multiple PMUs in the synchrophasor network. In Fig. 2.3, the flow of data to and from PDCs in the network is indicated by the orange arrows. The data from PDCs can be sent to other PDCs in the network or sent directly to a variety of applications. The University of Texas independent synchrophasor network and its equipment are described in Subsection 2.3.

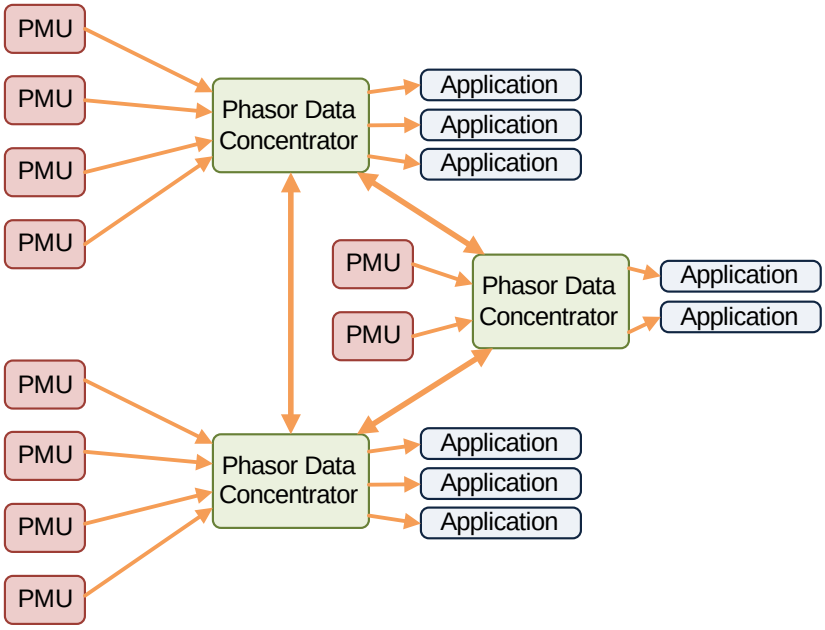

Figure 2.3: Synchrophasor network diagram example [1]

2.1.7 Synchrophasor Applications

Synchrophasor networks offer many benefits and can be used in applications such as a real-time system wide monitoring, control, and protection and rapid assessment of system conditions. Examples of potential synchrophasor applications are described here.

Synchrophasors for monitoring purposes have the capability of providing information to system operators in order to take corrective actions before voltage collapse occurs and to increase system performance. Oscillation monitoring systems have been designed to alert power system operators to poorly-damped oscillations in the power system [24]. A GPS-synchronized frequency monitoring network - the frequency monitoring network (FNET) - have allowed for wide-area real-time visualization and monitoring [25]. Other commercial software use synchrophasor data to help utilities monitor and visualize power system conditions [26].

Synchrophasors for improved power system protection and for use in power system control functions increasingly contribute to improved power system operation [27–31]. Currently, many system protection practices are based solely on locally measured voltage and current quantities and assumed static system conditions. By providing a near real-time system wide view of power system conditions, synchrophasors allow for protective actions that could potential prevent incorrect decisions that would lead to deterioration of power system conditions. In other words, synchrophasors allow for the use of adaptive protective devices capable of adjusting to changing power system conditions.

Synchronized phasor measurements can also be used to improve state estimation or drastically change the the way state estimation is done by introducing phasor-based state estimation [32]. At this time, power system measurements such as voltage and current magnitudes and real and reactive power flows are used in conjunction with network topology data to estimate

the power system state or elements of the state vector. The state vector is a collection of positive sequence bus voltage phasors and can take several minutes to estimate from the time the measurements are taken to the time the calculations are completed. The states are estimated based on the iterative solution found using weighted least square techniques. However, with synchronized phasor measurements, it is possible for the state vector to be directly measured and to view the dynamic behavior of the power system in near real-time. Synchronized current phasor measurements can also be used for redundancy purposes. The question of how many PMUs are required to make this possible is a problem of observability and is discussed in [33–35]. Research in [33] shows that a minimum of 1/5 to 1/4 of the buses should be equipped with PMUs to completely observe the network. Other research topics on implementing synchrophasor data into improving state estimation performance are discussed in [32, 36].

Synchrophasor data can also be used for other applications such as validation of power system models, transient instability prediction [37, 38], post-mortem analysis, and fault location systems [39].

2.2 PMU Placement Algorithm

One important issue that needs to be addressed is the strategic placement of PMUs on the power system for the purposes of power system event monitoring. The number of PMUs in the network is limited by the high cost of the equipment and the availability of communication facilities. The cost of

a synchrophasor network includes the costs of PMUs, PDCs, and communications to the PDC and to applications using the synchronized phasor data [1]. A variety of methods for determining "optimal" placement for PMUs in an interconnected grid have been devised where observability of the system is desired [35]. These methods base optimal placement of PMUs on the availability of communication facilities.

In order to increase the ability of a synchrophasor network to monitor power system events while reducing cost by limiting the number of PMUs in the network, an algorithm is created to identify buses that are the best candidates for PMU placement in an interconnected grid for monitoring purposes. The proposed algorithm does not consider the limitations of communications facilities, however, the algorithm satisfies the following requirements. Firstly, the PMU readings reflect changes occurring on the electric grid such as changes in system topology, loss of generation, or large increase in load. This will guarantee that important events do not go unnoticed and corrective action can be taken immediately. Secondly, by monitoring the selected buses, ideally the health of the system will be monitored as well. This requires that critical parts of the grid are visible. Thirdly, there should be little or no redundancy in the PMU readings unless intentionally providing additional data for increased reliability. The algorithm detailed in the Subsection 2.2.1 addresses the above requirements. In addition, mathematical indices are developed to quantify the three requirements. The algorithm is created with a large electrical grid in mind. If the bus selected for PMU placement is not an acceptable choice (lack

of communications, remote location, older control house equipment, costs at chosen location, etc.) the algorithm provides other possibilities for PMU placement that also satisfy the three requirements given above. If the electric grid is too small, the choices for PMU placement are limited and the bus selected by the algorithm might not be suitable.

The algorithm is described in Subsection 2.2.1. The algorithm is applied to a case study involving the application of the developed algorithm to the electric grid directed and operated by the Electric Reliability Council of Texas (ERCOT). The results from the case study are discussed in Subsection 2.2.2.

2.2.1 Proposed PMU Placement Algorithm

The approach taken to satisfy the requirements for PMU placement is described in 5 steps.

2.2.1.1 Step 1

The first requirement states that by monitoring the phase angles at PMU locations the slightest change in the electric grid should be detected. In other words, the algorithm should find the bus phase angles which are the most sensitive to electric grid events. The approach taken to satisfy this requirement is to calculate the difference between the phase angle during normal operating conditions and the phase angle during a change in the electric grid. Normal operating conditions of the electric grid are referred to as the base case. The phase angle difference is calculated for many different electric grid events. The

reference phase angles are compared to the calculated phase angles during a contingency case. A contingency case can be any change in the electric grid (i.e., changes in topology, removal of generation, or large increase in load). The greater the change in the bus phase angle, the greater the sensitivity of the bus to changes in the electric grid.

2.2.1.2 Step 2

The second requirement is to be able to monitor the health of the *entire* electric grid by observing the phase angles at the selected buses. The algorithm addresses this requirement in Steps 2 to 4. To make sure that the PMUs are distributed evenly throughout the grid, the buses are grouped into areas defined by bus ownership. The proposed algorithm then finds the most sensitive buses in each area by calculating the standard deviation of the phase angle differences in each area. The formula used to calculate standard deviation σ is given in Eq. 2.11.

$$\sigma = \sqrt{\frac{1}{N}\sum_{i=1}^{N}(x_i - \bar{x})^2} \tag{2.11}$$

Where, x_i is the phase angle difference of each bus in a particular area, $\bar{x}$ is the arithmetic mean of the phase angle differences of all the buses in the area, and N is the total number of buses in the area.

2.2.1.3 Step 3

In this step, only areas containing more than 30 buses are considered. For the areas with more than 30 buses, the buses with phase angle differences of more than 3 standard deviations are selected as PMU placement candidates. If the phase angle differences were normally distributed, only 5% of the phase angle differences would be above three standard deviations. However, the phase angle differences in an area or even the electric grid may not be normally distributed and the number of buses in any area having a phase angle difference above three standard deviations for a particular contingency case will vary greatly. This same process is repeated for each of the areas (with more than 30 buses).

Each bus is assigned a frequency of occurrence value. Once a bus is selected, its frequency of occurrence value is incremented by 1. Hence, the frequency of occurrence value of any particular bus indicates the number of times the phase angle difference of that bus was above 3 standard deviations. If 60 contingency cases are tested the frequency of occurrence can vary between 0 and 60. In this way, frequency of occurrence is used as the measure of sensitivity of the bus phase angle to changes in the electric grid.

2.2.1.4 Step 4

The process explained in Step 1 to Step 3 is repeated for all contingency cases applied. At the end of the process, the buses in each area are arranged according to their frequency of occurrence. The buses with the 20 maximum

frequency of occurrence values are selected for further analysis.

2.2.1.5 Step 5

The third requirement sates that the phase angle information measured at each bus should be unique and there should be little or no redundant measurements. In other words, it has to be made sure that the buses determined as sensitive do not perceive the exact same changes in the phase angles for all of the contingency cases applied. For example, if the phase angles of two buses in an area change by an identical amount for every contingency case, then placing PMUs at these two buses, even if they happen to be the most sensitive buses, is not a good option. Instead, a PMU should be placed at only one of the above buses. A mathematical measure of finding out if two buses are experiencing similar phase angle changes is to calculate the coefficient of linear correlation between all the phase angle differences of the buses in each area for all contingency cases applied. Coefficient of linear correlation is defined in Eq. 2.12.

$$\rho\left(X,Y\right)=\frac{\sum\left(x-\bar{x}\right)\left(y-\bar{y}\right)}{\sqrt{\sum\left(x-\bar{x}\right)^{2}\left(y-\bar{y}\right)^{2}}} \tag{2.12}$$

Where, x is the phase angle difference of bus X for a particular contingency case and $\bar{x}$ is the average value of phase angle differences for all contingency cases for bus X. Similarly, y is the phase angle difference of bus Y for the same contingency case and is the average value of phase angle dif-

ferences for all contingency cases for bus Y. A coefficient of linear correlation of magnitude 1 indicates that there is an exact linear relationship between X and Y, while a coefficient of linear correlation of 0 indicates that X and Y are linearly uncorrelated.

In step 5, the coefficient of linear correlation between all the selected buses in each area is calculated. The buses that have a coefficient of linear correlation close to a magnitude of 1 are experiencing similar changes in their phase angles during electric grid events. For each area, the selected buses showing a coefficient of linear correlation of more than a magnitude of 0.8 are put into a cluster. In other words, a cluster is defined as a group of selected buses with phase angle differences that are closely correlated to one another. An area can contain any number of clusters. A PMU can be placed on any bus in the cluster.

For convenience, the bus with the maximum frequency of occurrence value in a cluster was selected for PMU placement. If two or more buses in a cluster have the same frequency of occurrence then the bus for PMU placement is selected at random. In practice, the PMU can be located at any bus in the cluster. For areas with less than 30 buses, the PMU should be located at a bus that has the highest frequency of occurrence and there is no need to form clusters.

2.2.2 Case Study Results

The algorithm is applied to network data based on the electric grid managed and operated by the Electric Reliability Council of Texas (ERCOT). The grid connects 38,000 miles of transmission line and 550 generation units [40]. The total number of buses in the electric grid is divided into N areas based on bus ownership. The number of buses in each area varies greatly. An area can be a contiguous geographical region or may be made up of disjointed regions located in different parts of the electric grid. Only buses with a voltage level of 69 kV and above are considered in this case study. This voltage level is chosen because PMUs are generally located in the transmission system rather than in the distribution system.

The network element data of the electric grid was made available in the Siemens/PTI PSS/E software platform. Network element data for normal operating conditions or base case was provided by ERCOT. ERCOT also provided a list of X contingencies that were selected based on operating experience and therefore were the most likely events to occur on the electric grid. The contingency cases include the tripping or failure of one or more transmission lines. Each of the contingencies is simulated in PSS/E by taking the respective transmission line or lines out of service. The Full Newton Raphson method is then applied to obtain the phase angles at each bus for the new system topology. For consistency, the same bus is selected as the swing bus for all cases. MATLAB is used as the analysis tool for processing the phase angle information obtained from the power flow study.

After applying the algorithm to the ERCOT network data for the contingency cases provided, the approximate locations of the PMUs within ERCOT based on the clusters of buses in each area is given in Fig. 2.4. If PMUs are placed at these locations, common events that occur within ERCOT will heavily impact the voltage phase angles and be easily monitored by the synchrophasor network.

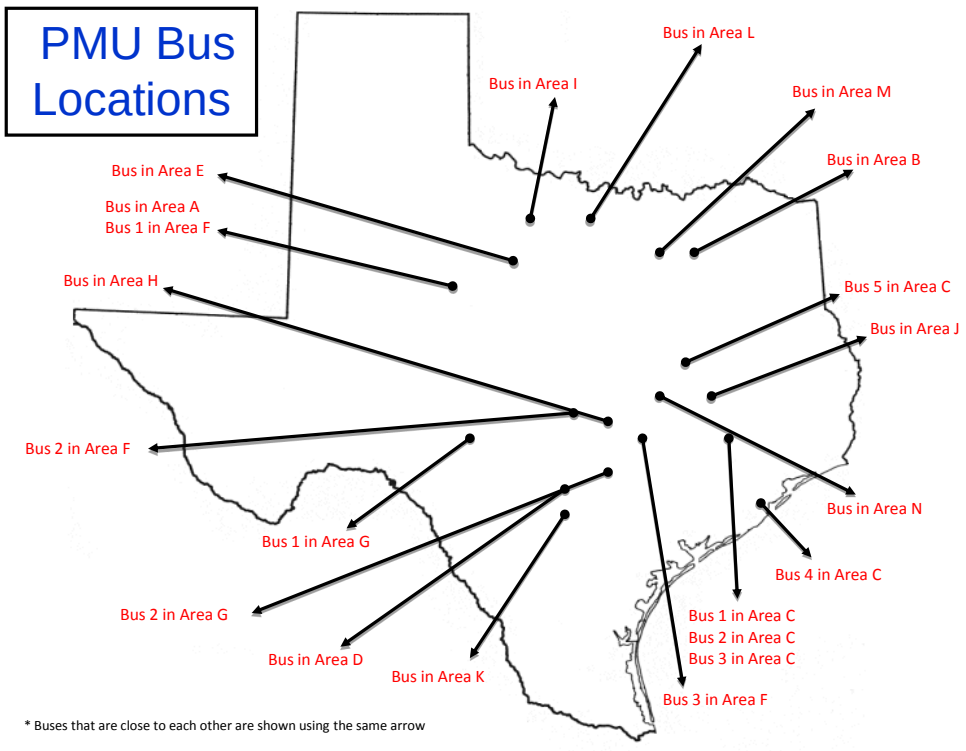

Figure 2.4: Location of buses for proposed PMU placement

In the next sections, a description of the University of Texas at Austin's Independent Synchrophasor Network and the pre-processing of the PMU data

before analysis can begin is given.

2.3 Independent Synchrophasor Network and PMU Data

At customer-level voltage, PMUs can now be placed virtually anywhere throughout the electric power system and measurements are freely available to use for power system analysis. A map of the locations of UT Austin independent synchrophasor network PMUs within Electric Reliability Council of Texas (ERCOT) is shown in Fig. 2.5. Each PMU station is placed within the different zones of ERCOT. The Waco PMU station is located within the North Zone, the UT-Pan American and UT-Austin PMU stations are located in the South Zone, the SEL-Houston PMU station is located within the Houston Zone, and the McDonald Observatory PMU is located in the West Zone. The McDonald Observatory PMU location was also selected because of its proximity to wind farms in West Texas as shown in Fig. 2.6. These locations closely align with the PMU locations in Section 2.2.

The equipment that makes up the Texas Independent Synchrophasor Network is described in the following Subsection.

2.3.1 Independent Synchrophasor Network Equipment and Software

A diagram of the equipment required for each remote PMU station within the independent synchrophasor network is shown in Fig. 2.7 in the box on the left and the equipment required for the central PMU station is shown

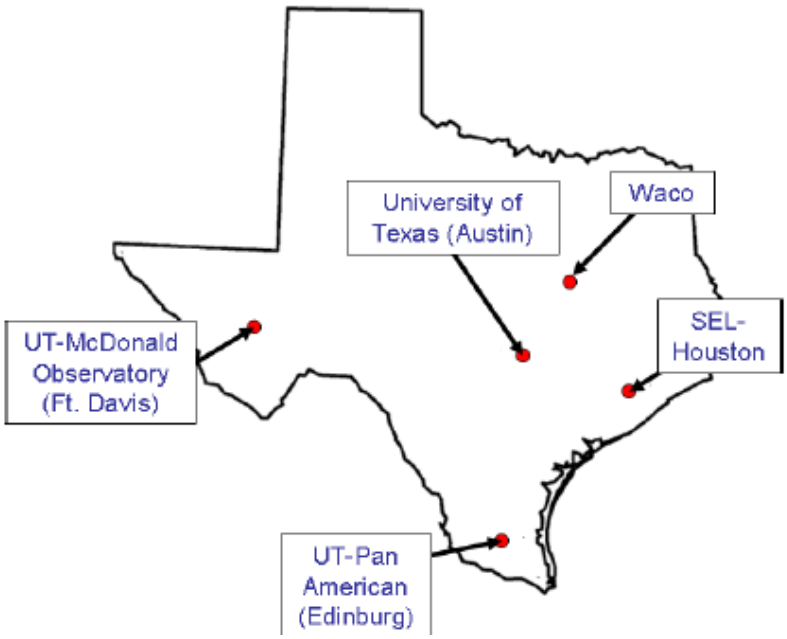

Figure 2.5: Map of Texas PMU stations within the University of Texas at Austin independent synchrophasor network

in Fig. 2.7 in the box on the right. As mentioned, there are four remote PMU locations: Waco, TX; McDonald; UT-PanAmerican; and Houston. The central PMU station is located at UT-Austin. All equipment was donated by Schweitzer Engineering Laboratories, Inc. [41].

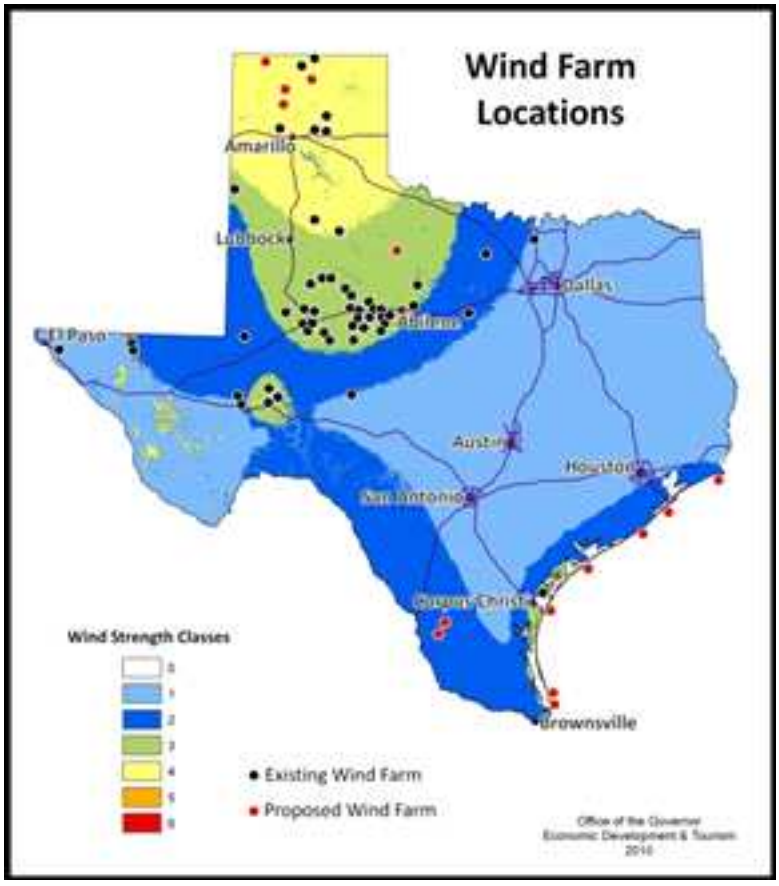

Figure 2.6: Map of wind farm locations within Texas [2]

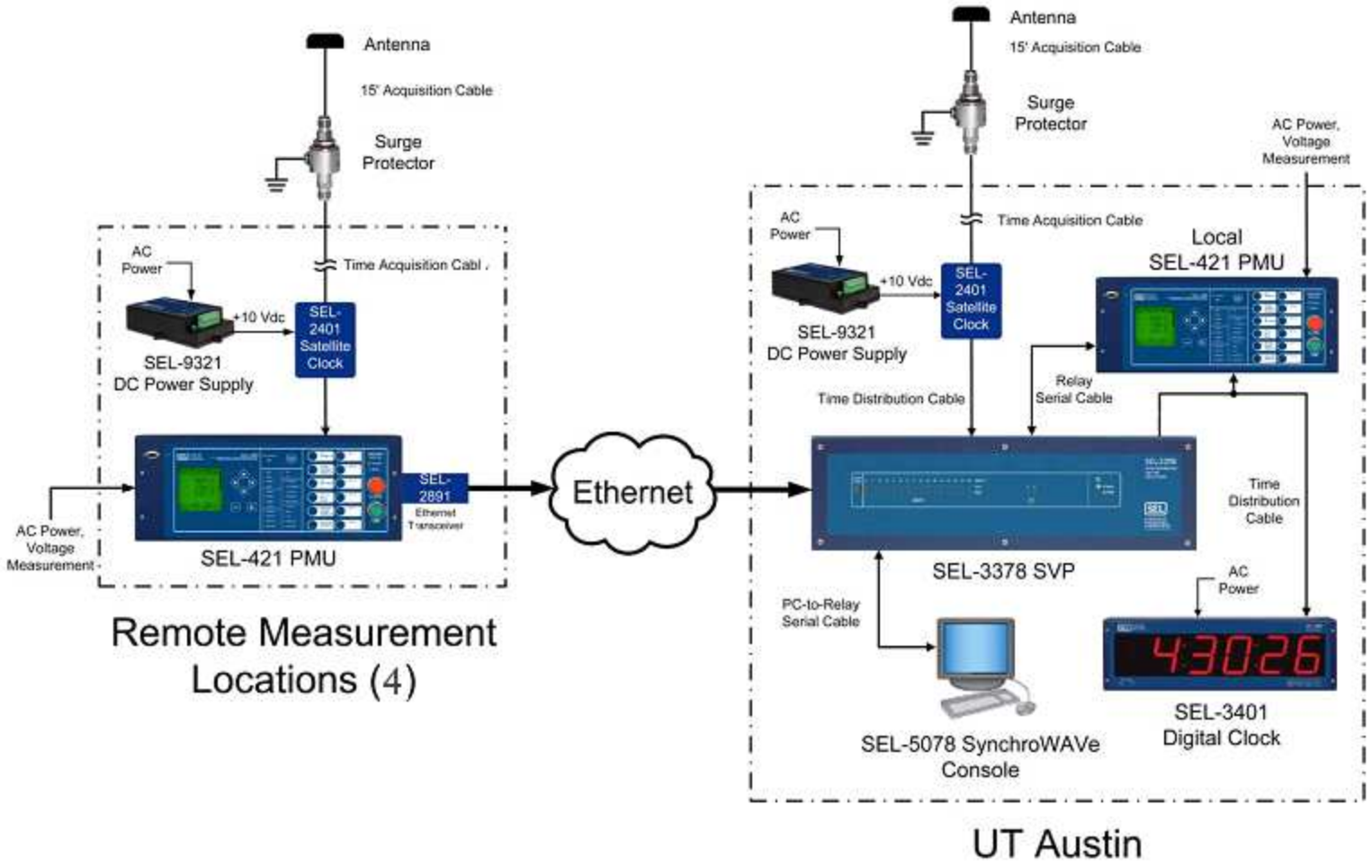

Figure 2.7: Equipment for each PMU station (right) and the phasor data concentrator and PC (left) within the Independent Synchrophasor Network

As shown in Fig. 2.7, each PMU station has an antenna to receive a GPS signal. Each PMU station GPS antenna is located outside with a clear view of the sky. This GPS signal is the common time reference required to make synchronous phasor measurements. A surge protector connects the antenna to the equipment located inside to provide protection from lightning strikes and to equalize the potential that can emerge between the central conductor and the shield of the coaxial cable [42]. The GPS signal is sent to the GPS receiver (SEL-2401) where it is converted to Coordinated Universal Time (UTC) and sent to each PMU to time-stamp the measured phasor quantity.

The SEL-2401 uses the GPS signal to create an unmodulated Inter-Range Instrumentation Group Time Code Format B (IRIG-B) output. The time code format for the SEL-2401 is HH:MM:SS:DDD. More information on PMU time input can be found at [22]. The SEL-2401 GPS receiver and clock has three indicator LEDs on the front panel: enable, satellite lock, and output. The enable LED indicates if all SEL-2401 self tests have passed. The satellite lock LED indicates when the SEL-2401 has tracked four or more GPS satellites and is currently tracking at least three GPS satellites. The satellites that have been tracked must be done so with a signal strength of at least 3.4 Antenna Measurement Unit (AMU) [42]. The satellite lock must maintain tracking of three satellites or more in order to remain locked. The output LED indicates if an accurate (within a $\pm$ nanosecond average) clock time is being sent.

The SEL-421 relays are used as PMUs in the synchrophasor network. The SEL-421 is a digital relay (providing distance and directional protection)

with PMU capabilities built in. More information on the SEL-421 can be found at these sources [43]. The time stamped phasor from each PMU station is sent either through public Internet at the remote PMU locations or serial cable at the central PMU location to the Phasor Data Concentrator (PDC). The SEL-2891 Ethernet transceiver is used to send PMU data through public Internet as shown in Fig. 2.7. The PDC waits for data from all PMU locations, collects, and time sorts the PMU data once it is received from up to 16 PMUs that support the IEEE Standard for Synchrophasors for Power Systems, IEEE C37.118-2005 [22]. The SEL-3378, the synchrophasor vector processor, is used as the PDC in the independent synchrophasor network. The SEL-3378 can use the collected and synchronized data in predefined and user-defined functions. Two of the predefined function blocks are the phase angle difference calculation and a modal analysis calculation. The SEL-3378 receives and outputs synchrophasor data according to IEEE standard C37.118-2005 [44]. The collected data is sent to a dedicated Desktop PC where software, SEL-5078, archives the data and displays the PMU data in real time [45].

The synchronized phasor measurements and calculated frequency are stored at a rate of 30 data points per second. Because the data has a 30 Hz sampling rate, only low frequency oscillations (below 15 Hz) can be analyzed. Events such as capacitor bank switching which induce oscillations of the order of a few hundreds of Hz to 1.5 kHz and are not visible in the PMU data. Even with a sampling rate of 30 Hz, the archived hourly reports are very large. For one PMU, an hourly report of the voltage phase angle data consists

of 108,000 data points. Since there are three signals for each PMU station (voltage phase angle, voltage magnitude, and frequency), each PMU station generates 324,000 data points each hour. These data points are stored hourly in a comma separated value (CSV) format. A network with 5 PMU stations generates hourly CSV reports that are 13.8 MB in size. The synchrophasor network is also in operation at all times.

An example of archived PMU data from the synchrophasor network is given in Table 2.1. The example is for a network with three PMUs. The GPS derived time stamp is located in the first column as well as the magnitude, phase angle, and frequency for each PMU. Dropped data points are expressed as a zero magnitude, zero phase angle phasor. The frequency for the dropped data point is also zero. In the Texas Independent Synchrophasor Network, dropped data points are typically caused by drops in public Internet.

t	MAG1 (V)	ANG1 (deg)	MAG2 (V)	ANG2 (deg)	MAG3 (V)	ANG3 (deg)	FREQ1 (Hz)	FREQ2 (Hz)	FREQ3 (Hz)
...	...	...	...	...	...	...	...	...	...
08:38.6	41.19	-22.83	79166.51	-45.65	73482	99.92	59.95	59.95	60.01
08:38.7	41.19	-23.46	79141.99	-46.27	0	0	59.95	59.95	0
08:38.7	41.19	-24.07	79138.84	-46.89	73484.74	100.14	59.95	59.95	60.01
08:38.7	41.19	-24.69	79162.91	-47.53	0	0	59.95	59.95	0
08:38.8	41.19	-25.33	79186.09	-48.16	73495.73	100.36	59.95	59.95	60.01
08:38.8	41.20	-25.96	79190.33	-48.79	73492.98	100.45	59.95	59.95	60.01
08:38.8	41.20	-26.56	79188.13	-49.41	0	0	59.95	59.95	0

Table 2.1: Example of archived PMU data

Since the first remote PMU was added in January 2009, the network has continuously been generating data. Because so much data is being generated, it is difficult to detect events of interest and analyze them for power system studies. Resources such as ERCOT Daily Grid Operations Reports [12] provide information on sudden loss of power above 450 MW caused by generating unit trips and information on line contingencies (total peak generating capacity in ERCOT is above 65 GW). In addition, it is generally straightforward to visually detect large sudden imbalances in generation and load by monitoring the frequency. However, information related to events like transmission line reclosing and trips and other equipment trips are not readily available. The research presented in Chapters 5 and 6 examines if these system events are visible in the PMU data and if it is possible to automatically detect events of interest.

2.4 PMU Data Format and Protocol

New PMU stations are installed and removed from the network for various reasons causing the format of the archived hourly PMU files to constantly change. The grouping of PMU quantities for each station changes as well, resulting in two types of data files. The two types of data files are shown in Table 2.2 and Table 2.3. The voltage magnitudes were arbitrarily selected. All measurements are taken at customer-level voltage of 120 V.

t	MAG1 (V)	ANG1 (deg)	FREQ1 (Hz)	MAG2 (V)	ANG2 (deg)	FREQ2 (Hz)
...	...	...	...	...	...	...
24:26.7	79924.90	120.18	59.98	40.80	-10.12	60.02
24:26.8	79930.60	119.89	59.98	40.81	-9.91	60.02
24:26.8	79933.17	119.60	59.98	40.82	-9.70	60.02

Table 2.2: Example of Type 1 PMU data in CSV format for two PMU stations with the magnitude, angle, and frequency for each station grouped together

t	MAG1 (V)	ANG1 (deg)	MAG2 (V)	ANG2 (deg)	MAG3 (V)	ANG3 (deg)	FREQ1 (Hz)	FREQ2 (Hz)	FREQ3 (Hz)
...	...	...	...	...	...	...	...	...	...
08:38.6	41.192	-22.827	79166.508	-45.7	73482	99.924	59.949	59.947	60.008
08:38.7	41.192	-23.457	79141.992	-46.3	0	0	59.948	59.947	0
08:38.7	41.187	-24.068	79138.844	-46.9	73484.742	100.14	59.948	59.948	60.009

Table 2.3: Example of Type 2 PMU data in CSV format for three PMU stations with the frequencies for each station listed in the last columns

Because of the two file types and the large variety in the number and location of stations in operation, it is cumbersome to read in PMU data and begin analysis of the data. Without an automated method, it is first necessary to open the PMU file and count the number of stations and the order of the stations in order to conduct accurate analysis. In addition, dropped data points show up in the voltage magnitude and frequency as zeros and need to be removed before analysis on the data can begin.

A protocol was created to analyze the PMU data files and indicate the type of file format, the number of PMU stations, and the quality of the PMU data. The file format type indicates if the PMU frequency for each station is grouped with the other PMU station data or if all PMU frequencies are grouped together as shown in Table 2.2 and Table 2.3 respectively. The number of PMU stations provides the number of PMU stations in operation at the time the data was archived. The quality of the PMU data is "true" if the PMU station contains zero or a limited number of dropped data points and "false" if the data contains many dropped data points or if the PMU station is not sending data to the PDC. An example of the Protocol output is given in Table 2.4. This information is used to determine how to label the data type and how to label the data by PMU location.

Type	Number of measurement point (NMP)	NMP 1					
		Mag		Ang		Freq	
		Col Index	Fault	Col Index	Fault	Col Index	Fault
2	6	1	true	2	true	13	true

Table 2.4: The Protocol function determines the PMU file type, the number of PMU stations, indicates the column locations for each PMU station magnitude, angle, and frequency, and indicates if the PMU data is 'faulty' or contains missing data

2.4.1 Relative Phase Angle Difference

In this research, the voltage phase angle difference between two PMU locations is used to detect events in the voltage phase angle. However, ideally when there are a large number of PMUs installed in the system, a common reference phase angle for all PMUs is desired. This reference phase angle can be determined by applying a center of gravity (COG) concept to PMU-derived local frequencies. A common phase angle reference can then be subsequently obtained from this COG frequency. Any PMUs located within the interconnected system can be referenced to this COG derived reference frequency or reference phase angle. There are many power system measurements available to estimate center of gravity as is well known in literature [3] and will not be discussed here.

Data from five PMUs are available at five separate locations with the distances between any two PMUs being very large. For example, the shortest geographical distance between two PMUs is approximately 105 miles apart. The closest two PMUs in the network is between Waco and The University of Texas (Austin). The longest distance between two PMUs is between McDonald (Ft. Davis) and UTPA (Edinburg). The geographical distance between these two PMUs is approximately 560 miles apart.

These PMUs are located among many generation buses and many of those buses are PV buses; maintaining the scheduled generation and the scheduled bus voltage (V = 0.95 p.u. to 1.05 p.u.). The McDonald PMU is located among wind power plants which are operated as a PQ bus (delivering power

at specified real and reactive power, many of wind plants are operated at unity power factor). For the case where two PMUs are installed at buses located at opposite ends of a transmission line, the voltage phase angle difference and power transfer between the two adjacent buses can be measured and computed. However, when there are many generators and loads connected to the network between these two PMUs, the measured data between the two PMUs at opposite ends of the power system network cannot be used to directly measure the voltage phase angle difference or the power transfer.

The voltage phase angle difference between any two PMUs available in this project cannot be used to estimate the power transfer, but, the PMUs are instead used to measure power system oscillations and other power system events. Two different PMU signals are used to screen for power system events, voltage phase angle and frequency. As previously stated, due to the limited number of PMUs installed in this area, the COG concept is not applied, but, instead, the difference in phase angle between two PMUs (*relative phase angle difference - RPAD*) is used as a sensing variable to detect power system events. Note that the frequency is computed at each PMU.

2.4.2 Unwrapping Voltage Phase Angles

Once the file format type is known, the columns of the PMU data are identified and the voltage phase angle data is modified before analysis can begin. Since the rotation of the voltage phasors is not constant and not always at nominal frequency (60 Hz), the voltage phase angles increase or decrease

depending on if the speed of rotation is greater or less than nominal. When the voltage phasor is rotating at greater than nominal speed it is rotating counterclockwise and crosses from 180° to −180° degrees, the voltage phase angle jumps as shown in Fig. 2.8. When the voltage phasor is rotating at less than nominal speed it is rotating clockwise and crosses from −180° to 180°, the voltage phase angle also jumps as shown in Fig. 2.8. Therefore, the change in frequency from less than 60 Hz to greater than 60 Hz can be seen in Fig. 2.8 when the angle goes from −180° to 180° jumps to 180° to −180° jumps.

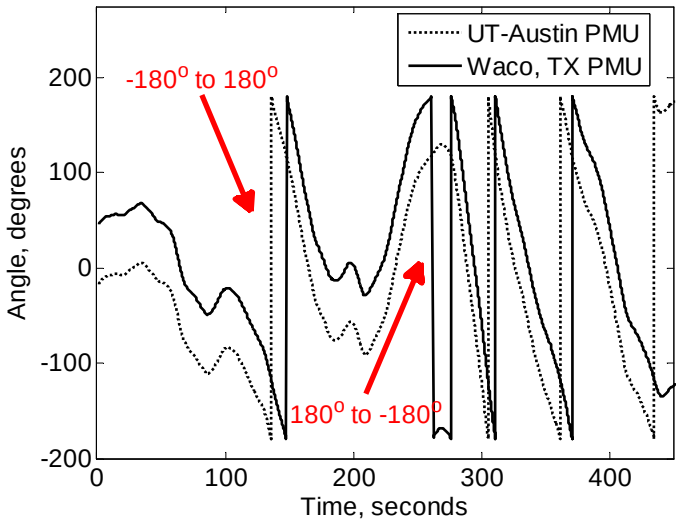

Figure 2.8: Raw voltage phase angle for two PMU stations

The voltage phase angle at each PMU station is unwrapped before the difference in the voltage angle between the two stations is taken (RPAD). The code for the function written in Matlab to unwrap each PMU station phase angle is given in Appendix B. The unwrapped voltage angle for each PMU

station is shown in Fig. 2.9. The frequency of the system changes from less than 60 Hz to greater than 60 Hz around 210 seconds in Fig. 2.9 when the direction of the phase angle changes from decreasing in value to increasing in value.

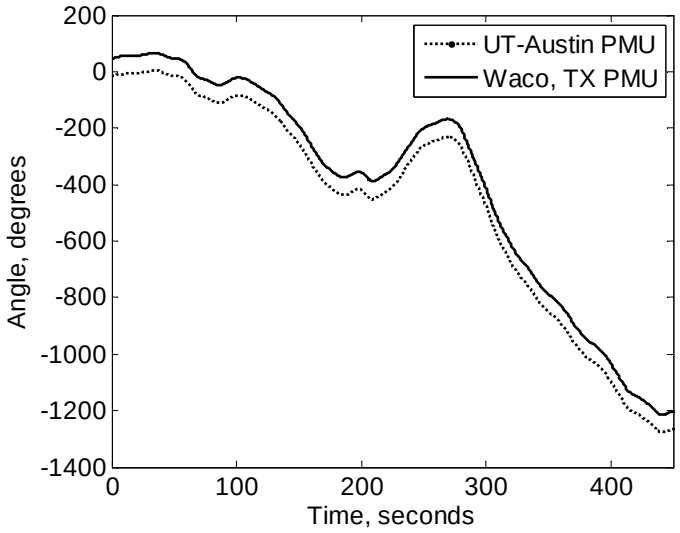

Figure 2.9: Unwrapped voltage phase angle for two PMU stations

The RPAD between the unwrapped voltage angles is shown in Fig. 2.10. It is easy to see the electromechanical oscillations present in the system in the unwrapped RPAD. All possible RPAD combinations are calculated for each PMU file.

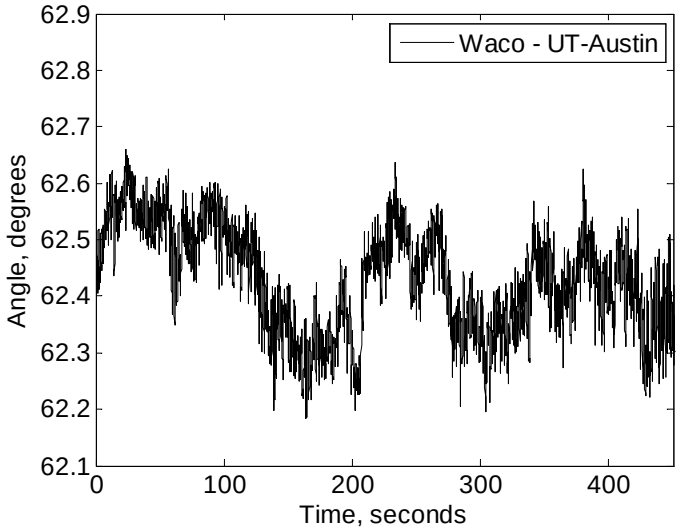

Figure 2.10: RPAD between the same two PMU stations corrected by individually unwrapping and taking the difference

2.5 Summary

In this chapter, the Texas Independent Synchrophasor Network was introduced. A brief introduction to synchrophasors and their applications was provided in Section 2.1. The use of synchrophasor phase angle to estimate frequency was given as well. An algorithm created to determine the best placement of PMUs in a network for power system event monitoring purposes was described in Section 2.2. The algorithm was applied to and used ERCOT network data. A description of equipment used in the Independent Synchrophasor Network was provided in Section 2.3. The PMU data format and necessary adjustments to the data before power system analysis can begin are provided in Section 2.4.

Chapter 3

Methods Used for Monitoring Power System Stability in Synchrophasor Data

It is important to monitor the stability of power systems as they are being pushed closer to their operating limits. Poorly damped oscillations could limit power transfer capabilities or worse lead to system instability and could result in system wide blackouts such as seen in the blackout on August 10, 1996 in the Western Interconnect [46]. Stability monitoring is the monitoring of electromechanical oscillations which are inherent to a system of interconnected synchronous machines. Electromechanical oscillations are excited by input to the system such as unit generating trips, clearing of faulted equipment, or random switching of power system components such as load switching. However, in power system stability monitoring, the input to the system cannot be measured and therefore, stability is monitored only through the measured system output. The measured system output of the power system in response to unknown input can be analyzed to monitor system stability using a variety of techniques.

This chapter provides background on power system dynamic behavior and how the measured power system responses are used to evaluate power

system stability. The concept behind estimation of power system stability by examining measured response is presented in Section 3.1. The different types of system responses that are studied are presented in Section 3.2. The different methods used to estimate the frequency, damping, amplitude, and phase components of the measured signal are presented in Section 3.3.

- **Publication**: The methods described and tested in this chapter are also applied in the research presented in the following publications [14, 16]
  - A. Allen, S. W. Sohn, W. M. Grady, S. Santoso. "Validation of distribution level measurements for power system monitoring and low frequency oscillation analysis" in *Power Electronics and Machines in Wind Applications (PEMWA), 2012 IEEE*, July 2012.
  - A. Allen, S. W. Sohn, W. M. Grady, S. Santoso. "Algorithm for Screening PMU Data for Power System Events" in *IEEE International Smart Grid Technologies (ISGT), 2012 IEEE*, October 2012.

3.1 Power System Stability

Power system stability is the ability of the power system to maintain operating equilibrium under normal operating conditions and to be able to restore the system to a state of equilibrium after a large disturbance occurs [3]. Traditionally, the ability of the power system to maintain stability has been defined as the ability of the system to maintain synchronous operation. However, there are many classes of power system stability as shown in Fig. 3.1. *Voltage*

stability is the ability of the power system to maintain acceptable levels of voltage at every bus in the power system. This type of stability is not examined in this dissertation. *Angle stability* is the ability of the synchronous machines in the system to remain in synchronism. This type of stability problem involves the study of the electromechanical oscillations inherent to the power system. The angle stability problem is broken down into two types: *small-signal stability* and *transient stability*. Both types are described in Subsections 3.1.1 and 3.1.2, respectively.

As shown in Fig. 3.1, small-signal stability can be a *mid-term stability* or *long-term stability* issue. The study period of mid-term stability can be up to several minutes and the study period of *long-term stability* can be up to several tens of minutes [3]. *Short-term stability* is also known as transient stability and has a study period of up to 10 seconds.

3.1.1 Small-Signal Stability

Small-signal stability is the ability of the power system to maintain synchronism during small disturbances in the power system. Small power system disturbances are the typically random, low-amplitude variations in power system load and generation. The small disturbances in the system can lead to two types of instability as shown in Fig. 3.1: non-oscillatory instability which is the steady increase in rotor angle or oscillatory instability which is the increase in amplitude of rotor oscillations [3]. The system response to small disturbances depends on many factors such as the strength of the

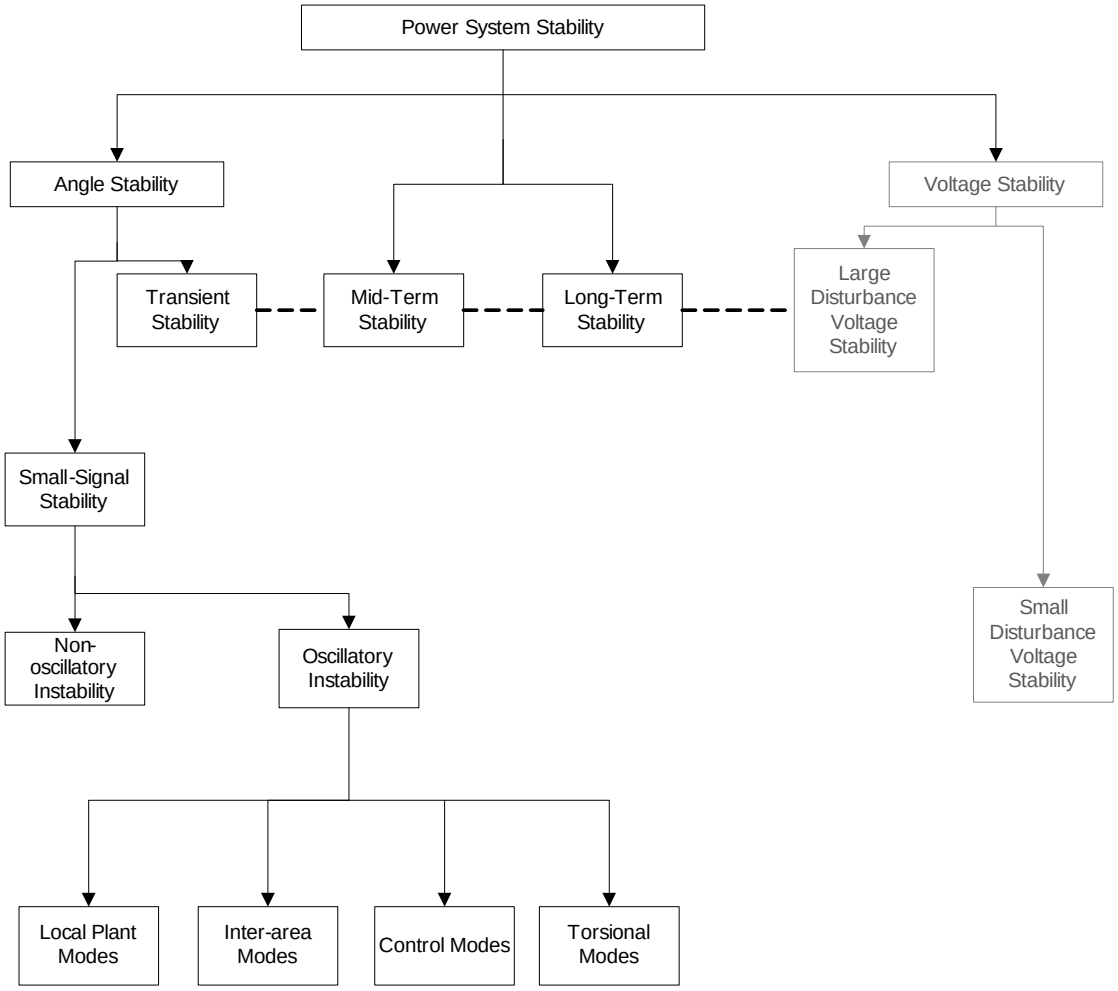

Figure 3.1: Classification of power system stability [3]

system, the system's initial operating point, and generator controls. Since small disturbances result in low-amplitude variations, it is assumed that the power system can be linearized around an operating point. This allows for the use of linear system concepts to describe power system small-signal stability. The low-amplitude variations of the power system are described by the set of

coupled first order linear differential equations shown in Eq. 3.1.

$$\dot{\mathbf{x}}(t) = A\mathbf{x}(t) + B_L\mathbf{q}(t) + B_E\mathbf{u}_E(t) \tag{3.1a}$$

$$\mathbf{y}(t) = C\mathbf{x}(t) + D_L\mathbf{q}(t) + D_E\mathbf{u}_E(t) + \mu(t) \tag{3.1b}$$

In Eq. 3.1, $\mathbf{x}$ is a vector that contains all system state variables such as generator rotor angles. Inputs to the system are represented by vectors $\mathbf{u}_E$ and $\mathbf{q}$. The vector $\mathbf{u}_E$ is an exogenous input to the system and represents known actions such as the application of probing signals. The use of a known probing signals can significantly increase the accuracy of mode estimation. A probing signal may be injected into the power system through a variety of actuator actions such as resistive brakes, generator excitation, or modulation of DC intertie signals [4]. The vector $\mathbf{q}$ is a random vector and represents small-amplitude perturbations to the system, i.e., the small-amplitude changes in load and generation that are always present. The elements of vector $\mathbf{q}$ have been shown to behave as independent stationary Gaussian white noise [4]. The vector $\mathbf{y}$ represents the measured output signals of the system and contains measurement noise μ. The matrix A is the state or plant matrix, B is the control matrix, C is the output matrix, D is the feedforward matrix, and t is time.

The representation of a dynamic system model as a set of coupled first-order differential equations in Eq. 3.1 is also known as the state space representation and allows for the application of *modal analysis*. Modal analysis is

the study of the electromechanical modes of the system. A mode's properties are the frequency, damping, and shape. The mode's frequency and damping indicate the system's stress which typically increases as load increases or generating capacity decreases. The mode shape is used to provide critical information for making operational control decisions [4]. *Therefore, small-signal stability is monitored by monitoring the modal frequency and damping of the system.* The output vector of the system $\mathbf{y}$ is used to estimate the modal properties. The signal-processing methods used to analyze the modes present in $\mathbf{y}$ is described in Section 3.3.

Electromechanical modes can be broken down into four groups as shown in the oscillatory instability small-signal stability subcategory in Fig. 3.1. Only local (or intra-area) and inter-area modes are studied in this dissertation. Local modes occur when one machine oscillates against a group of machines. Since the inertia of this type of oscillations is higher and is associated with lower impedance connections, the frequencies of local modes are higher, in the 1 - 2 Hz range. Inter-area modes occur when one group of machines are oscillating against another group of machines and this type of mode's frequencies are in the 0.2 - 1.0 Hz range. Typically, power system stability issues associated with modes arise from the inter-area category of modes [4].

3.1.2 Transient Stability

Transient stability is the ability of the power system to maintain synchronism during a large disturbance. The power system response during a

transient disturbance involves large swings in generator rotor angles. Stability of the power system depends on both initial operating conditions and the severity of the disturbance. It often occurs that after a large disturbance the steady-state operating conditions differ from conditions prior to the event. For transient stability studies, the period of interest is usually from 3 to 10 seconds following the disturbance.

3.2 Transient and Ambient Power System Response

As described in Section 3.1, angle stability is broken down into two types: small-signal stability and transient stability. Small-signal stability deals with system stability in response to small disturbances and transient stability deals with system stability in response to large disturbances. These concepts are expanded upon in this section as shown in the block diagram in Fig. 3.2 from [4, 5]. Fig. 3.2 shows a structure describing the source of the electromechanical oscillations resulting from the power system response to small and large disturbances. The power system is represented by the linear multiple-input and multiple-output (MIMO) system G and network topology changes are represented by the gain matrices K and K'. The gain matrix K represents known changes and the matrix K' represents unknown changes in topology. The vectors $\mathbf{q}$ and $\mathbf{u}_E$ represent the inputs to the system as described in Subsection 3.1.1. The measured output $\mathbf{y}$ and measurement noise μ are also the same. The output $y_i(t)$ is the i^{th} element of $\mathbf{y}$ colored by measurement noise $\mu_i(t)$.

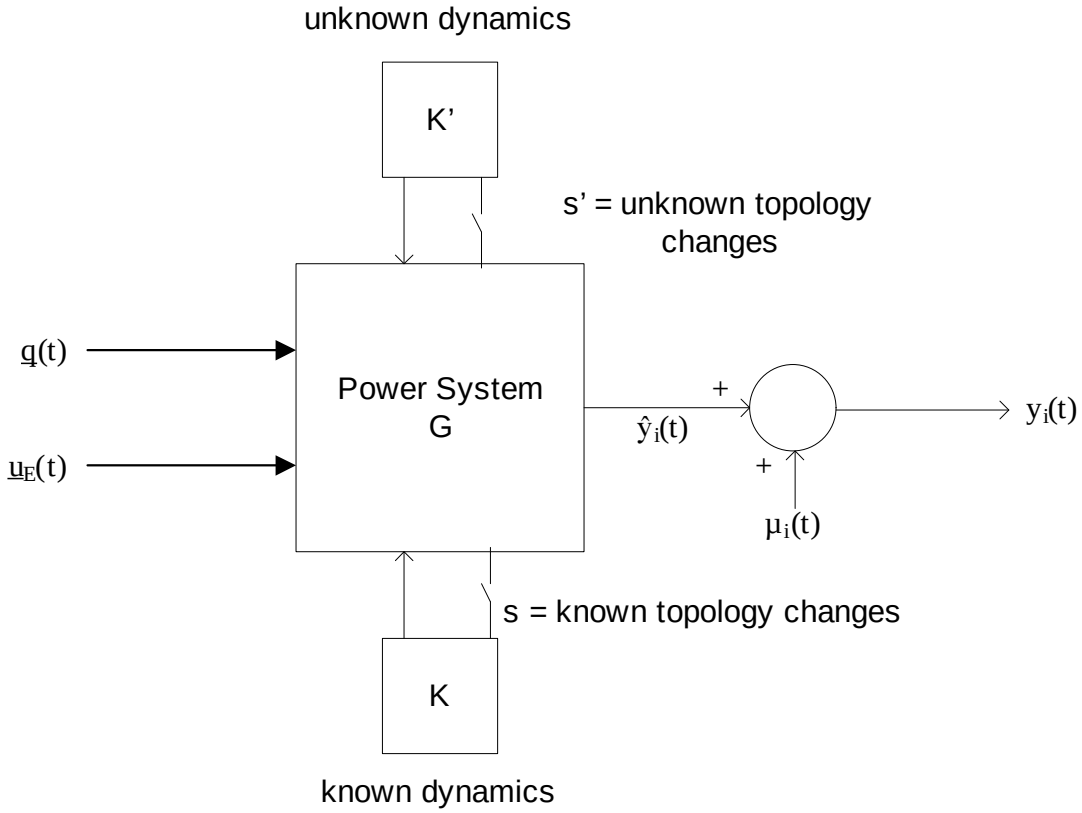

Figure 3.2: A diagram showing the sources of power system dynamic information [4, 5]

Based on the representation of the dynamics of the power system shown in Fig. 3.2, the response of the system can be classified into two types: ambient and transient. For the ambient response, the power system is excited by random, low-amplitude variations represented by $\mathbf{q}$ and u_E. The transient response is typically larger in amplitude and caused by sudden switching represented by **s** or **s'** or by a sudden step impulse represented by $\mathbf{u}_E$. The resulting time-domain response $\hat{y}_i(t)$ is colored by the dynamics of G.

An example of measured ambient and transient power system responses is shown in Fig. 3.3. Prior to the disturbance which occurs at 29 seconds, the ambient response of the system is measured. After the start of the disturbance, the transient response of the system is seen. After the ringdown of the transient response at 37 seconds, the system returns to conditions where the system is excited by low-amplitude variations and the ambient response is measured.

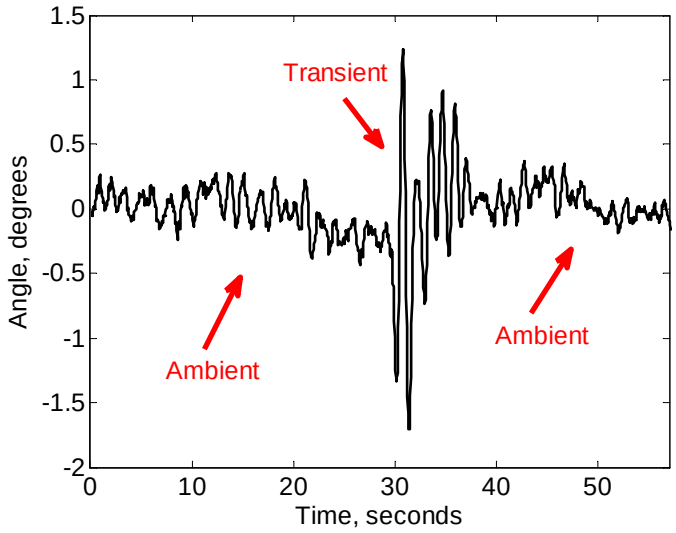

Figure 3.3: The measured ambient and transient power system responses

Signal processing methods are applied to measured system outputs during ambient and transient responses to estimate power system electromechanical modes. The types of signal processing methods used to analyze these two responses are ringdown analysis and mode-meter analysis. These methods are described in Section 3.3.

3.3 Mode Estimates

This section describes the methods used in this dissertation to analyze power system behavior, specifically power system modal behavior. First, a description of each method will be provided. Next, the accuracy of the method is tested. Finally, the parameters for each mthod are examined to determine how they influence the results. Mode estimation methods for power system application avaliabel in literature are categorized in Fig. 3.4 [6] based on the concepts described in Sections 3.1 and 3.2. The acronyms for each method in Fig. 3.4 are extended in Appendix A. In Fig. 3.4, the methods are first categorized by type of measured power system response: ambient response or transient response. Ambient response methods are broken down into two further categories: probing and non-probing. The probing category involves interjection of a known probing signal into the power system using different actuator methods such as dynamic resistve brakes, generator excitiation, or modulation of the control signal of DC intertie signals [47–49]. The methods are further categorized based on the calculation method used.

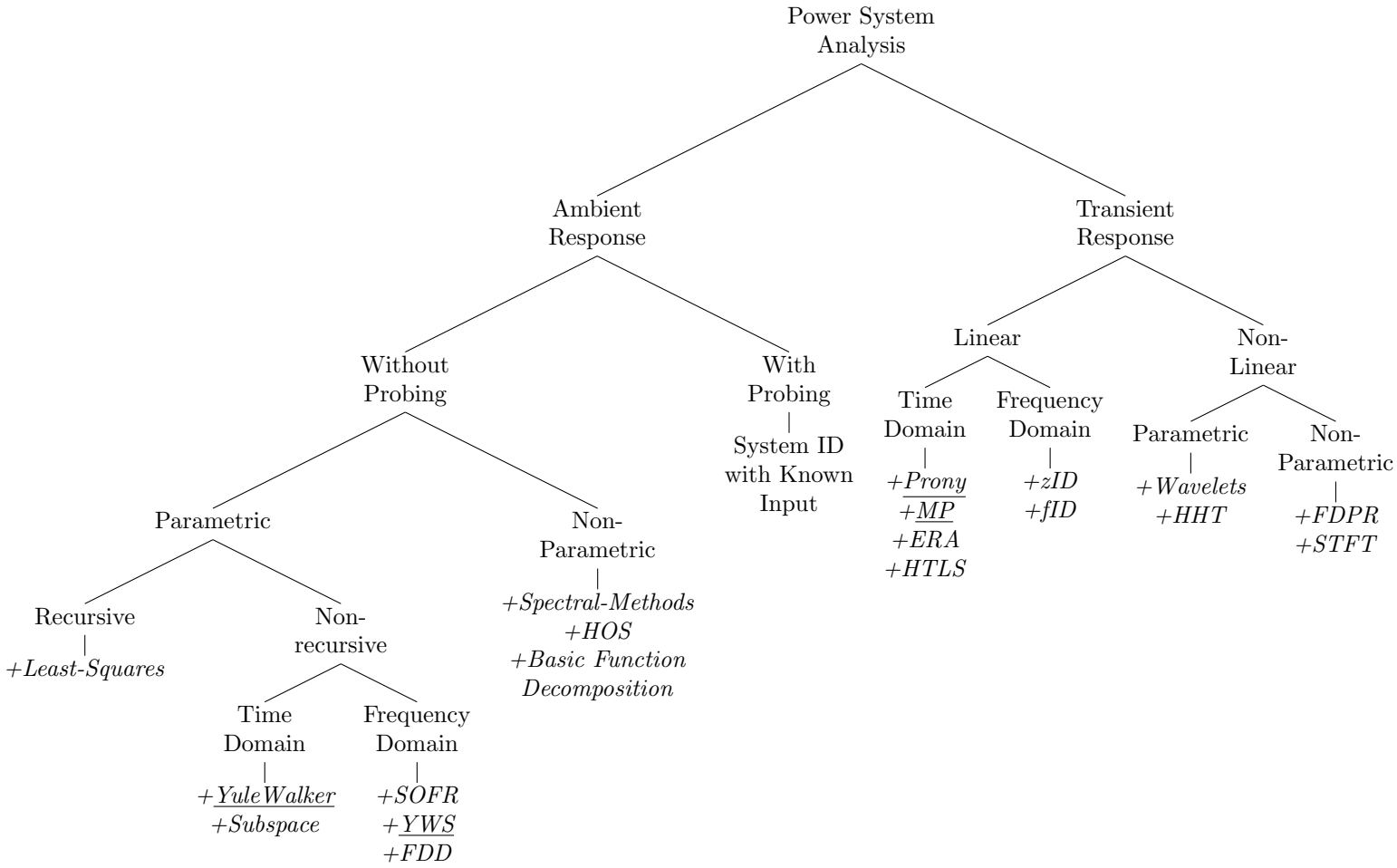

Figure 3.4: Classification of methods used to monitor power system stability based on type of measured power system response [6]. Underlined methods are used in the research presented in this dissertation and are described in Section 3.3

The underlined methods (Yulewalker YWS, Prony, Matrix-Pencil) are used in this dissertation and are described in this section. The Prony and Matrix-Pencil methods are linear, time-domain approaches and are described in Subsections 3.3.1 and 3.3.2, respectively. The non-recursive parametric methods described in this section are methods that estimate the autregressive (AR) coefficients from a measured signal. These methods provide parametric and spectral results and are described in Subsection 3.3.3. Some non-parametric methods are used for ambient analysis as well, such as the fast Fourier transform (FFT) and Welch, and are described briefly in Subsection 3.3.4.

3.3.1 Prony Method

The Prony method is used to fit a signal to a parametric linear model and is described in this subsection. The accuracy of the Prony method for estimating signal components is examined as well.

3.3.1.1 Prony Method Theorem

The Prony method has been used extensively in power systems analysis to monitor power system response to large disturbances or during normal operating conditions [50–55]. The Prony method fits a linear combination of damped sinusoids to an evenly sampled signal as shown in Eq. 3.2.

$$y(t) = \sum_{i=1}^{n} A_i e^{\sigma_i t} sin(2\pi f_i t + \phi_i) \tag{3.2}$$

The evenly sampled signal in Eq. 3.2 is $y(t)$. Each damped sinusoid consists of four components: magnitude A_i, frequency f_i, damping factor σ_i, and phase ϕ_i. Each damped sinusoid is considered one of n modes of the signal.

Applying Euler's theorem and letting $t = kT$, Eq. 3.2 is rewritten as Eq. 3.3. In the equation, T is the sampling period of the signal.

$$y[k] = \sum_{i=1}^{n} R_i z_i^k \tag{3.3}$$

The poles of the system, z_i, are shown in Eq. 3.4 and the complex pole weights, R_i, are shown in Eq. 3.5.

$$z_i = \exp^{(\sigma_i \pm j\omega_i \Delta)t} \tag{3.4}$$

$$R_i = \frac{A_i}{2} e^{(j\phi_i)} \tag{3.5}$$

The Prony method estimates z_i and R_i using the following three steps. The first step is to use the signal, $y[k]$, of length N to create a linear prediction model (LPM) of order n as shown in Eq. 3.6.

$$y[k] = a_1 y[k-1] + a_2 y[k-2] + \ldots + a_n y[k-n] \tag{3.6}$$

In order to estimate the coefficients, a, of Eq. 3.6, the values of $y[k]$ are calculated for $n \leq k \leq N-1$ as shown in matrix form in Eq. 3.7.

$$\begin{pmatrix} y[n] \\ y[n+1] \\ y[n+2] \\ \vdots \\ y[N-1] \end{pmatrix} = \begin{pmatrix} y[n-1] & y[n-2] & \cdots & y[0] \\ y[n] & y[n-1] & \cdots & y[1] \\ y[n+1] & y[n] & \cdots & y[2] \\ \vdots & \vdots & \ddots & \vdots \\ y[N-2] & y[N-3] & \cdots & y[N-n-1] \end{pmatrix} \times \begin{pmatrix} a_1 \\ a_2 \\ a_3 \\ \vdots \\ a_n \end{pmatrix} \quad (3.7)$$

Eq. 3.7 can also be written in the abbreviated form shown in in Eq. 3.8.

$$d = Da \quad (3.8)$$

The a coefficients in Eq. 3.8 can be solved for using Eq. 3.9. The a coefficients are known as the linear prediction coefficients.

$$a = D \backslash d \quad (3.9)$$

In the second step, the roots of the characteristic polynomial equation, z_i, associated with the linear prediction coefficients are solved for. The characteristic polynomial equation is shown in Eq. 3.10.

$$z^n - a_1 z^{n-1} - \ldots - a_{n-1} z - a_n = (z - \hat{z_1})(z - \hat{z_2}) \ldots (z - \hat{z_n}) \quad (3.10)$$

The final step is to solve for the original set of linear equations shown in Eq. 3.3 to calculate the complex pole weights R_i. The roots of the characteristic polynomial, $\hat{z}_i$ are used to find the complex pole weights R_i as shown in the matrix formula in Eq. 3.11.

$$\begin{pmatrix} y[0] \\ y[1] \\ y[2] \\ \vdots \\ y[N-1] \end{pmatrix} = \begin{pmatrix} 1 & 1 & \cdots & 1 \\ \hat{z_1^1} & \hat{z_2^1} & \cdots & \hat{z_n^1} \\ \hat{z_1^2} & \hat{z_2^2} & \cdots & \hat{z_n^2} \\ \vdots & \vdots & \ddots & \vdots \\ \hat{z_1^{n-1}} & \hat{z_2^{n-1}} & \cdots & \hat{z_n^{n-1}} \end{pmatrix} \times \begin{pmatrix} R_1 \\ R_2 \\ R_3 \\ \vdots \\ R_n \end{pmatrix} \tag{3.11}$$

Eq. 3.11 can be rewritten as shown in Eq. 3.12.

$$Y = UR \tag{3.12}$$

The complex weights, R_i, are calculated using Eq. 3.13.

$$R = U \backslash Y \tag{3.13}$$

The estimates for the poles, $\hat{z}_i$, and the complex pole weights, R_i, are used to calculate the frequency, damping, amplitude, and phase using Eqs. 3.4 and 3.5. The reconstructed signal using the estimated frequencys, damping, amplitude, and phase angle is calculated using Eq. 3.3.

3.3.1.2 Prony method Estimates for a Test Signal

The accuracy of the frequency and damping estimates made using the Prony method is tested by applying the Prony method to a noisy signal containing known frequency and damping components. The test signal is given in Eq. 3.14.

$$y_{noise} = \sum_{i=1}^{n} A_i e^{\sigma_i t} sin\left(2\pi f_i t + \phi_i\right) + A_n n\left(t\right) \tag{3.14}$$

For the test signal, y_{noise}, the number of damped sinusoids, n, is set to 3. The damping, σ_i, and frequency, f_i, for each of the damped sinusoids is given in Table 3.1. The amplitude for all the damped sinusoids, A_i, are set to 1 and the phase shift for all sinusoids, ϕ_i, is set to 0. The signal $n(t)$ is the Gaussian noise added to the signal. The amplitude of the noise, A_n, for the test case is set to 0.4.

Table 3.1: Frequency and damping components for the test signal

Damped Sinusoid No. i	Frequency (Hz)	Damping Factor	Damping Ratio (%)
1	0.6	-0.1	2.65
2	1.4	-0.05	0.57
3	0.9	-0.2	3.53

The signal, y_{noise}, is sampled at 30 Hz and the length of the signal is set to 10 seconds. A plot of the noisy signal and the estimated signal using the Prony method is shown in Fig. 3.5. The order of the system is set to 170, $n = 170$.

From Fig. 3.5, the estimate appears to be very accurate. The quality of the Prony method's ability to fit the original noisy signal is quantified by calculating the signal-to-noise ratio (SNR). A higher value of SNR (greater than 80 dB, for example [56]) indicates a good fit between the Prony estimated signal and the original noisy signal. The SNR is calculated using Eq. 3.15.

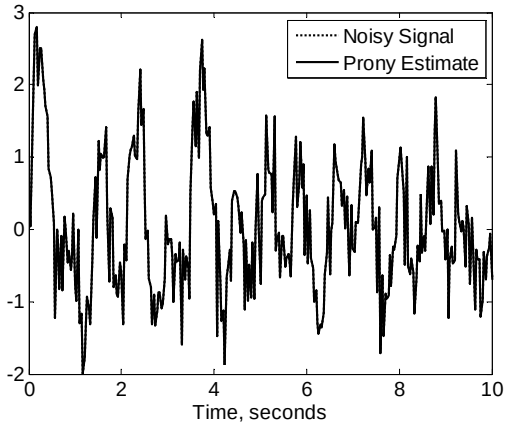

Figure 3.5: Reconstructed signal using Prony method parameter estimates compared to the original noisy signal

$$SNR = 10log_{10}\left(\frac{\sum_{k=0}^{N} y[k]^2}{\sum_{k=0}^{N}\left(y[k]-\hat{y}[k]\right)^2}\right) \tag{3.15}$$

In Eq. 3.15, $y[k]$ is the original signal, $\hat{y[k]}$ is the Prony estimated signal, and N is the number of samples in the signal. For the example test signal and Prony estimate shown in Fig. 3.5, the SNR is 253 dB, indicating that the Prony method estimate is a very good fit to the original signal. The selected order of the system influences the SNR between the original signal and the Prony method estimated signal. To show the influence the system order has on the accuracy of the Prony estimate, the Prony method with changing system order is used to estimate the components of the original signal. The SNR is calculated for each selected system order. The results are shown in Fig. 3.6. The plot shows the SNR along the y-axis and the system order along

the x-axis.

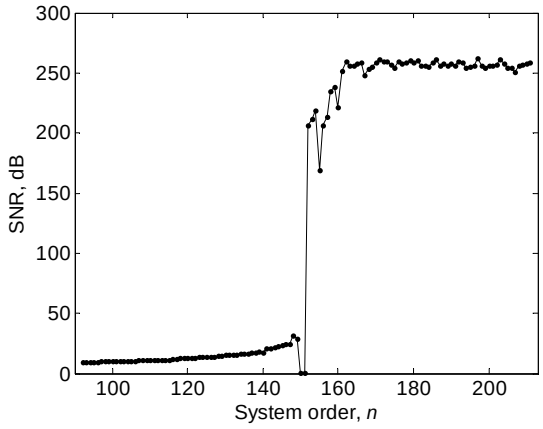

Figure 3.6: The SNR between the Prony estimate and the test signal as a function of the Prony system order, n

In Fig. 3.6, the higher the system order, the more accurate the Prony estimate. However, the high system order results in components estimates that "overfit" the original signal [57],[50]. This results in trivial components that are not representative of the actual components in the system. An example is provided in Figs. 3.7 and 3.8 to illustrate how a high order selected for the Prony method overfits the original signal. From the signal shown in Fig. 3.5, the estimated frequencies and their corresponding estimated amplitude are plotted in Fig. 3.7. The estimated frequency is along the y-axis and the estimated amplitude is along the x-axis. The estimated damping factors and their corresponding estimated amplitude are plotted in Fig. 3.8. The estimated damping factor is along the y-axis and the estimated amplitude is along the x-axis.

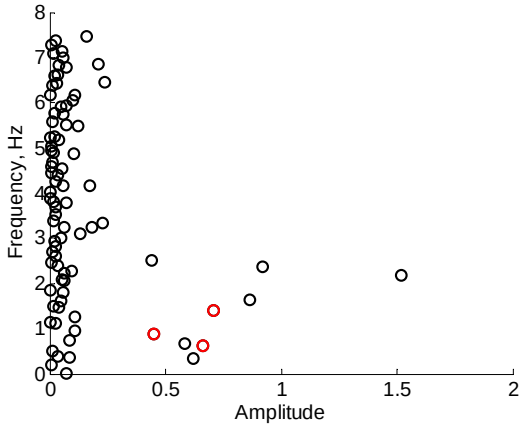

Figure 3.7: Prony method frequency estimates "overfit" the test signal with the estimates closest to the actual frequencies of the test signal highlighted in red

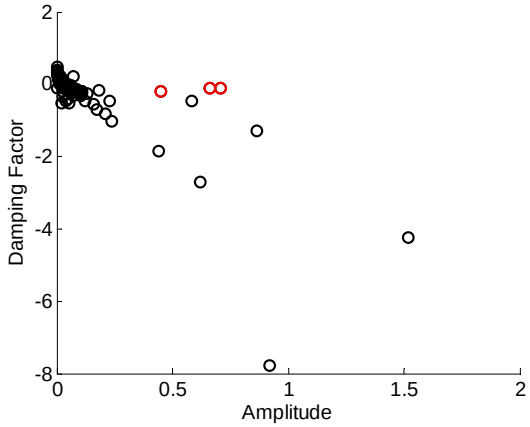

Figure 3.8: Prony method damping factor estimates "overfit" the test signal with the estimates closest to the actual damping factors of the test signal highlighted in red

Figs. 3.7 and 3.8 show that a large number of the frequency and damping factor estimates have a very small amplitude and are located close to the

y-axis. The Prony method is still able to accurately detect the actual frequency and damping factor components as highlighted in red. If the Prony method is to be used, a filter should be applied to remove low amplitude estimates or to remove noise from the original signal [56]. However, from the case presented here, it would be difficult to determine which frequency estimates were "true" and which are trivial since there are some frequency estimates located near the true frequencies of the signal. The Prony method is applied to a signal where the noise of the signal is reduced (A_n is set to 0.05). The order of the system is also reduced so that $n = 50$. The estimated frequencies and their corresponding estimated amplitude are shown in Fig. 3.9 and the estimated damping factors and their corresponding estimated amplitude are shown in Fig. 3.10. For the less noisy signal, the frequency and damping factor estimates that correctly represent the frequencies in the signal have a much larger amplitude and are easy to detect. Therefore, for the analyses in this dissertation that involve noisy signals, the Prony method will not be used. The Prony method can be used for large transient events where there is a small number of modes with large amplitude in the measured signal.

Subsection 3.3.2 describes the Matrix-Pencil method, another parametric linear method used for power system analysis that utilizes singular value decomposition to the LPM to remove the trivial components.

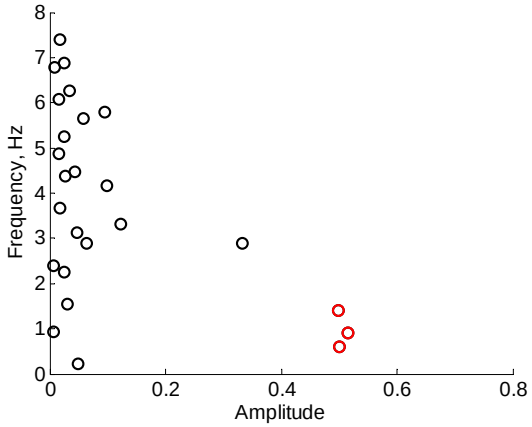

Figure 3.9: Prony method frequency estimates for a test signal with less noise; the estimates closest to the actual frequencies of the test signal are highlighted in red

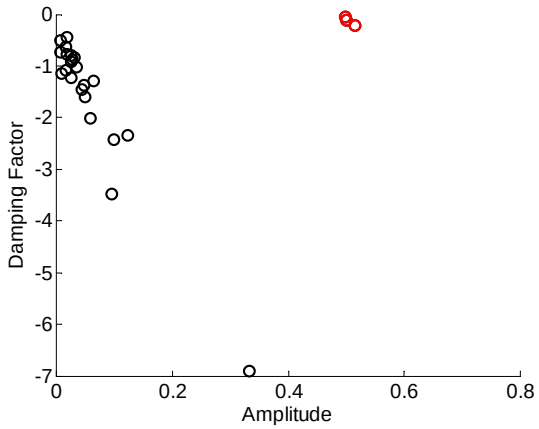

Figure 3.10: Prony method damping factor estimates for a test signal with less noise; the estimates closest to the actual damping factors of the test signal are highlighted in red

3.3.2 Matrix-Pencil Method

The Matrix-Pencil method is used to fit a signal to a parametric linear model and is described in this section. The Matrix-Pencil method is less

sensitive to noise compared to the Prony method. The accuracy of the Matrix-Pencil method for estimating signal components is examined as well.

3.3.2.1 Matrix-Pencil Theorem

The Matrix-Pencil method [24] fits a sum of damped sinusoids to an evenly sampled signal, similar to the Prony method described in Subsection 3.3.1. The goal is to estimate the complex weights R_i and poles z_i from the noisy signal. The mathematical representation of the sum of damped sinusoids estimates fitted to an evenly sampled signal, $y[k]$, is given in Eq. 3.16.

$$y[k] = \sum_{i=1}^{n} R_i z_i^k \tag{3.16}$$

Again, the signal, $y[k]$, in Eq. 3.16 is equal to the sum of the product of the complex weights R_i and the poles z_i. The parameter n is the number of sinusoids or modes to be estimated. The damping and frequency estimates for the signal are extracted from each z_i as shown in Eq. 3.17. The amplitude and phase estimates for the signal are extracted from each R_i as shown in Eq. 3.18.

$$z_i = \exp^{(\sigma_i \pm j\omega_i \Delta)t} \tag{3.17}$$

$$R_i = \frac{A_i}{2} e^{(j\phi_i)} \tag{3.18}$$

This method also utilizes singular value decomposition (SVD) to effectively remove noise from the signal before the estimates are made. Because

a Matrix-Pencil function is not available in Matlab, a user-defined function was created to calculate the parameters using the Matrix-Pencil method and is described briefly by the following equations.

For a noisy signal, a matrix Y is created from the data points of the signal as shown in Eq. 3.19.

$$Y = \begin{pmatrix} y[0] & y[1] & \cdots & y[L] \\ y[1] & y[2] & \cdots & y[L+1] \\ \vdots & \vdots & \ddots & \vdots \\ y[N-L-1] & y[N-L] & \cdots & y[N-1] \end{pmatrix} \tag{3.19}$$

The parameter L is referred to as the pencil parameter and N is the total number of data points in $y[k]$. For effective removal of noise, the pencil parameter is chosen so that $N/3 < L < N/2$. This range was selected because the variance in the estimates of the z_i's is at a minimum [58]. The SVD of the matrix Y is shown in Eq. 3.20.

$$Y = U\Sigma V^H \tag{3.20}$$

The matrices U and V are unitary matrices and the operator H is the conjugate transpose. The singular values of Y are located along the diagonal of matrix Σ in descending order. At this point, the parameter n is selected and the noise from the signal is effectively removed. This is done by selecting a threshold value based on the ratio of the singular values along the diagonal of Σ to the maximum singular value, σ_1. A threshold value is selected so

that only the n singular values above the threshold are considered. This is illustrated in Eq. 3.21.

$$\frac{\sigma_c}{\sigma_1} > threshold \tag{3.21}$$

The selection of the threshold can be selected based on the known accuracy of the significant digits of the signal. So if the signal is accurate up to 3 significant digits, then singular values that fall below the ratio shown in Eq. 3.21 are considered noise [58]. Another method is to select a threshold that is 10% of the largest singular value, σ_1 [24]. Once the parameter n has been selected, it is used to create the following matrices shown in Eqs. 3.22 to 3.24.

$$V' = \begin{pmatrix} v_1 & v_2 & \cdots & v_n \end{pmatrix} \tag{3.22}$$

$$Y_1 = U\Sigma'[V_1']^H \tag{3.23}$$

$$Y_2 = U\Sigma'[V_2']^H \tag{3.24}$$

The v's are the first n column vectors of V from Eq. 3.20, matrix Σ' is the first n columns of Σ, V_1' is the matrix V with the final column removed, and V_2' is the matrix V with the final row removed. Using the Matrix-Pencil

as defined in [24], the matrices from Eqs. 3.22 to 3.24 can be used to create the following new Matrix-Pencil definition for noisy data as shown in Eq. 3.25.

$$Y_1^+ Y_2^+ = V_2'^H [V_1'^H]^+ \tag{3.25}$$

In Eq. 3.25, the $^+$ operator is the pseudo-inverse of the matrix. The z_i's are found by computing the eigenvalues for $V_2'^H [V_1'^H]^+$. Once the parameter n and z_i's are known, they are used to solve for the R_i's from Eq. 3.16. The R_i calculation is rewritten in Eq. 3.26.

$$\begin{pmatrix} y(0) \\ y[1] \\ \vdots \\ y[N-1] \end{pmatrix} = \begin{pmatrix} 1 & 1 & \cdots & 1 \\ z_1 & z_2 & \cdots & z_n \\ \vdots & \vdots & \ddots & \vdots \\ z_1^N - 1 & z_2^N - 1 & \cdots & z_n^N - 1 \end{pmatrix} \times \begin{pmatrix} R_1 \\ R_2 \\ \vdots \\ R_n \end{pmatrix} \tag{3.26}$$

The estimates for the damping factor and frequency are extracted from the z_i's as shown in Eq. 3.17 and the amplitude and phase is extracted from the R_i's as shown in Eq. 3.18.

3.3.2.2 Matrix-Pencil Estimates for a Test Signal

The accuracy of the frequency and damping estimates made using the Matrix-Pencil is tested by applying the Matrix-Pencil to a noisy signal containing known frequency and damping components. The test signal is given in Eq. 3.27 and is the same as shown in Subsection 3.3.1. The amplitude for all the damped sinusoids, A_i, are set to 1 and the phase shift for all, ϕ_i, is set to 0.

Gaussian noise, $n(t)$, is added to the signal. The amplitude of the noise, A_n, for the test case is set to 0.4. The frequencies and the corresponding damping factors are 0.6 Hz with -0.1 damping, 1.4 Hz with -0.05 damping, and 0.9 Hz with -0.2 damping.

$$y_{noise} = \sum_{i=1}^{n} A_i e^{\sigma_i t} sin\left(2\pi f_i t + \phi_i\right) + A_n n\left(t\right) \tag{3.27}$$

The signal, y_{noise}, is sampled at 30 Hz and the length of the signal is set to 10 seconds.

An example of the reconstructed signal from estimates made using the Matrix-Pencil method is compared to the original noisy signal in Fig. 3.11. As can be seen from Fig. 3.11, the SVD of the Matrix-Pencil is able to remove the noise from the signal and estimate the components of the "true" signal.

Because of the random nature of the signal, Monte Carlo simulations are employed to fully evaluate the estimated frequency and damping. The mean and standard deviation of frequency and damping factor estimates resulting from 100 runs are provided in Table 3.2. The average estimated frequency and damping components are very close to the actual frequency and damping components. The standard deviation for each component is also very small, especially for the frequency components, indicating the variation in the estimates are very low. However, the standard deviation is greater for the damping factor estimates, indicating that variation for estimates for the damping factor is greater and care should be taken when using the Matrix-Pencil to analyze

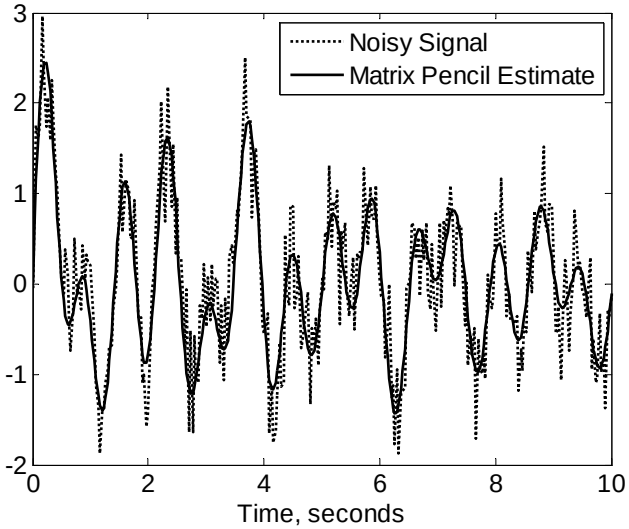

Figure 3.11: Noisy test signal

the damping factor.

Table 3.2: The test signal frequency and damping factor estimates using the Matrix-Pencil method

	Damped Sinusoid No.	Frequency (Hz)	Damping	Damping Ratio (%)
Mean	1	0.5970	-0.0882	2.3521
	2	1.4010	-0.0470	0.5335
	3	0.8990	-0.1978	3.4969
Standard Deviation	1	0.0043	0.5852	0.0219
	2	0.0026	0.1987	0.0175
	3	0.0061	0.6502	0.0370

The error between the mean value of the estimates and the actual components is calculated using the formula in Eq. 3.28 where x_{ref} is the actual

frequency or damping factor components and x_{est} is the estimated frequency or damping factor component.

$$error = \frac{(x_{est} - x_{ref})}{x_{ref}} \times 100 \tag{3.28}$$

The errors between the estimated frequency and damping components are given in Table 3.3. From Table. 3.3, the error in the frequency estimates is very low - the largest error is 0.5%. The errors in the estimates for the damping components are higher. The higher error rate should be taken into consideration when using Matrix-Pencil to estimate the damping factor components.

Table 3.3: Error in the estimated frequency and damping factor components

Damped Sinusoid No. i	Frequency (Hz)	Damping (%)	Damping Ratio (%)
1	0.50%	11.76%	11.30%
2	0.07%	6.07%	6.14%
3	0.11%	1.10%	1.06%

Factors such as the pencil parameter, L, the tolerance threshold selected for the ratio of σ's as shown in Eq. 3.21, and the data window size impact the estimated frequency and damping factor components. The estimates for the damping and frequency components for changing pencil parameter L are shown here. For each changing value of the pencil parameter L, the damping factor estimates are shown in Fig. 3.12 and the frequency estimates are shown in

Fig. 3.13. The dotted line indicates the actual damping factor and frequency components. From Figs. 3.12 and 3.13, it is obvious that the parameter L has a large impact on the damping estimates but not as large of an impact on the frequency estimates. If the parameter L is set to slightly less than half the length of the signal (in this case $L = 148$), the estimates for both the frequency and the damping are more accurate. This follows the rule mentioned in Subsection 3.3.3.1 where the variance of the estimates for z_i is reduced when the pencil parameter L is between $N/3$ and $N/2$. However, this rule was set for signals with a SNR of 20 to 25 dB. In this case, the SNR for the signal is much lower (the signal contains more noise) which might impact the selection of L for accurate estimates made by the Matrix-Pencil method.

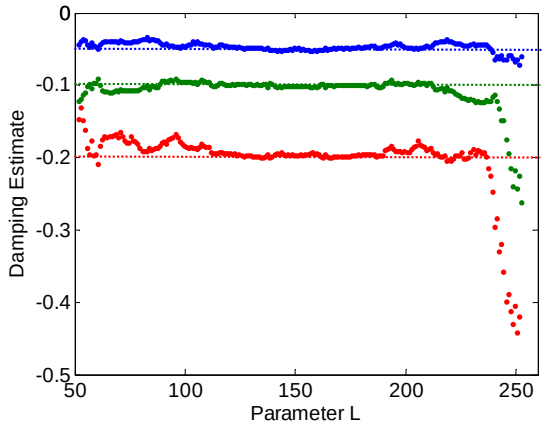

Figure 3.12: Impact of pencil parameter L on the Matrix-Pencil damping factor estimates, for changing L the damping factor estimates are indicated by a dot and the actual damping factors are shown by the dotted lines

Next, the impact of the selected threshold on the parameter n is exam-

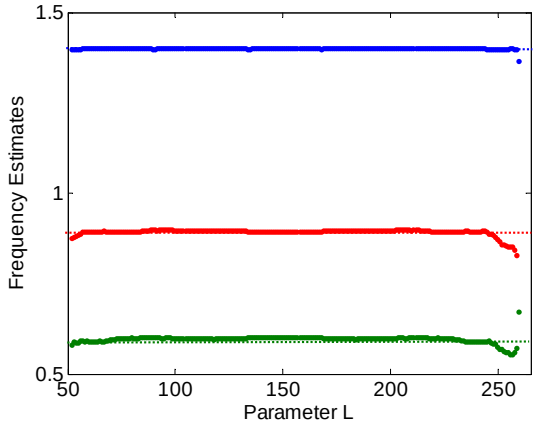

Figure 3.13: Impact of pencil parameter L on the Matrix-Pencil frequency estimates, for changing L the frequency estimates are indicated by a dot and the actual frequencies are shown by the dotted lines

ined. In Fig. 3.14 below, the ratio between each σ_c from the diagonal matrix Σ and the maximum value, σ_1, is plotted. The number of singular values σ_c, or order of the system n, used to estimate the frequency and damping components depends on the selected threshold. If the threshold is too low, too many σ_c values are used and erroneous estimates are made. If the threshold is too high, not enough σ_c values are used and not enough estimates are made. The impact the selected threshold has on the parameter n is shown in Fig. 3.15 where the value of n is a function of the selected threshold. From Fig. 3.15, the correct number of estimates (three estimates for the 0.6 Hz, 0.9 Hz, and 1.4 Hz components) are made when the threshold is set between 0.1 and 0.55. A threshold of 0.25 is used when the Matrix-Pencil is applied to a signal to estimate the damping factor and frequency components.

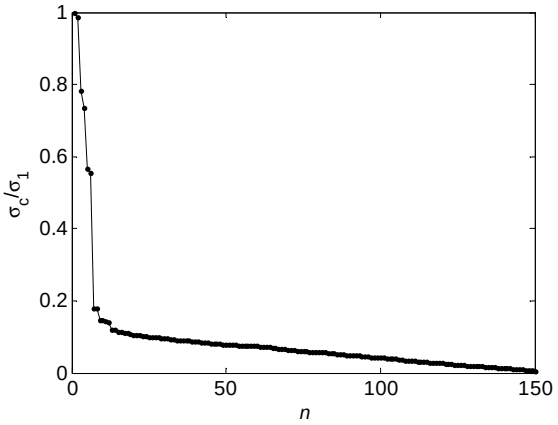

Figure 3.14: The ratio between sigma values for the SVD diagonal matrix Σ and the maximum sigma value

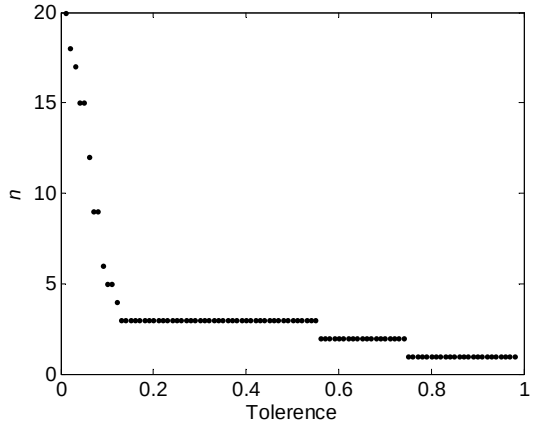

Figure 3.15: Impact of the selected threshold on the parameter n

Next, the impact window size has on the frequency and damping estimates is examined. The window lengths that are examined are 5 seconds, 10 seconds, 15 seconds, 20 seconds, and 25 seconds in length. For each window length, one hundred cases are run and the estimates from each case are saved.

The mean and standard deviation of estimates from the 100 cases for each window length are shown for the 0.9 Hz frequency component and for the -0.2 damping in Figs. 3.16 and 3.17, respectively. In Figs. 3.16 and 3.17, the mean value is shown by the gray circle and the actual value is shown by the blue circle. For the 5 second window, both the frequency and damping estimates have a higher variance compared to the other window lengths. However, a window length greater than 10 seconds does not seem to reduce variance. Also, the window length does not seem to improve the accuracy of the mean value when compared to the actual value. From the cases examined here, a window length of 10 seconds is sufficient for Matrix-Pencil application. The same is observed for both the 0.6 Hz and 1.4 Hz modes.

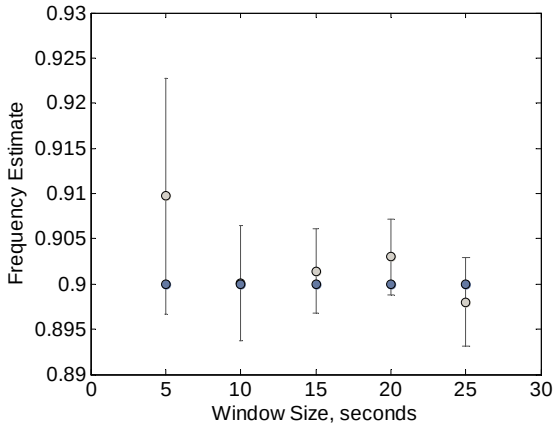

Figure 3.16: Impact of window size on the mean and standard deviation of Matrix-Pencil estimated frequency components

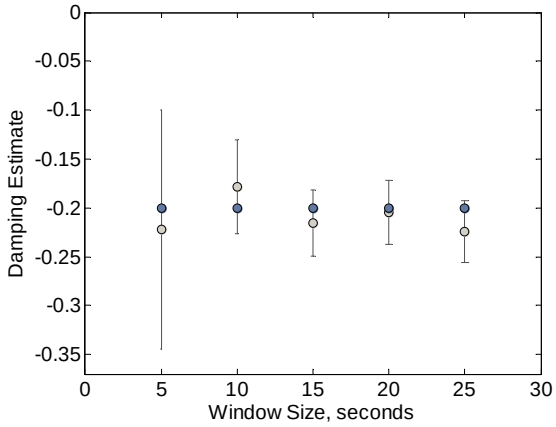

Figure 3.17: Impact of window size on the mean and standard deviation of Matrix-Pencil estimated damping components

3.3.3 Autoregressive Model Estimates

Estimates for frequency and damping components using parametric, non-recursive, time-domain methods are described here. Only methods that estimate the autoregressive (AR) coefficients are examined. The accuracy of these methods for analyzing signal components is examined as well.

3.3.3.1 Autoregressive model Background

A variety of functions are provided in Matlab to estimate the autoregressive coefficients from an input signal, y. The signal, y, is assumed to be the measured output of an AR system that is driven by white noise [59]. The order, n, for the AR model needs to be specified as well. One method used to fit an n^{th} order AR model is the Yule-Walker method [60]. The application of the parametric Yule-Walker method is described in [4, 61]. The `aryule` function in

Matlab returns the AR all pole model using the Yule-Walker algorithm. The estimated AR coefficients are used to calculate the frequency and damping as shown in the previous sections. A variet of methods to estimate parameters of AR models are available in the Matlab System Identification Toolbox.

The `pyulear` function returns the power spectral density (PSD) estimate for the measured system response and is described in detail in [62]. The PSD provides an estimate of the strength of the frequency as a function of frequency. The frequency content is easy to detect by examining the peaks in the PSD. The steeper the sides of the peaks in the PSD, the lighter the damping of the oscillations [4]. The application of the power spectral density Yule-Walker method is described in [4, 61, 63].

3.3.3.2 Estimates for a Test Signal

The accuracy of the frequency and damping estimates is tested by applying the Matlab functions to estimate the AR coefficients for a noisy signal containing known frequency and damping components. The test signal is again provided in Eq. 3.29. The amplitude for all the damped sinusoids, A_i, are set to 1 and the phase shift for all, ϕ_i, is set to 0. The signal $n(t)$ is the noise added to the signal and is random white Gaussian noise. The amplitude of the noise, A_n, for the test case is set to 0.4. The frequencies and the corresponding damping are 0.6 Hz with -0.1 damping, 1.4 Hz with -0.05 damping, and 0.9 Hz with -0.2 damping.

$$y_{noise} = \sum_{i=1}^{n} A_i e^{\sigma_i t} sin\left(2\pi f_i t + \phi_i\right) + A_n n\left(t\right) \tag{3.29}$$

The order of the system, i.e. the number of AR coefficients, is set to $n = 92$. Because of the random nature of the signal, Monte Carlo simulations are employed to fully evaluate the estimated frequency and damping factor components. The mean and standard deviation of frequency and damping factor estimates resulting from 100 runs are provided in Table 3.4.

Table 3.4: True frequency and damping components for the test signal

	Damped Sinusoid No.	Frequency (Hz)	Damping Factor	Damping Ratio (%)
Mean	1	0.6001	-0.1074	2.8463
	2	1.3993	0.8348	0.6147
	3	0.9008	-0.2137	3.7734
Standard Deviation	1	0.0042	0.0291	0.7710
	2	0.0040	0.0247	0.2809
	3	0.0071	0.0526	0.9330

From Table 3.4, it is obvious that the estimates for both the estimated frequency and damping components are very accurate. The standard deviation is low for estimated frequency components but the standard deviation is slightly higher for the estimated damping components. Overall, the performance is good for a very noisy signal, where the SNR is low.

Next, the estimates (+) along with the actual (indicated as red o's) frequency and damping components are plotted in Fig. 3.18. From Fig. 3.18,

the estimates are close to the actual frequency and damping components. The higher variance in the damping estimates can be seen in Fig. 3.18.

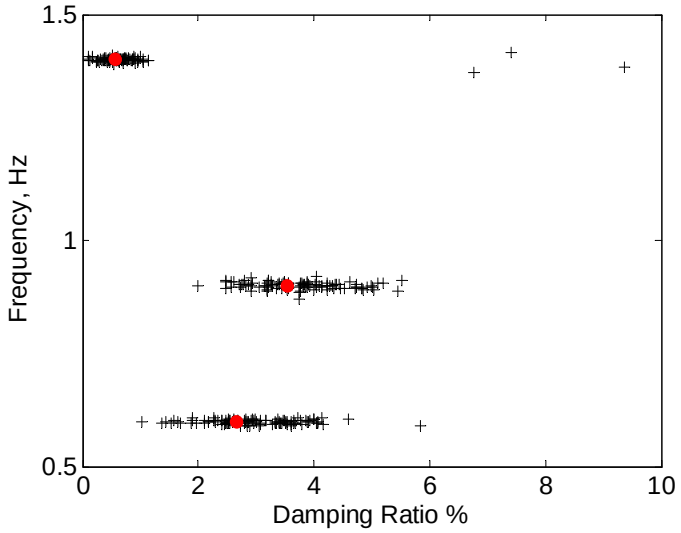

Figure 3.18: The estimated frequency and damping components (indicated as black +'s) for 100 runs and the actual frequency and damping components (indicated as red o's)

The PSD for the test signal is also estimated using the Yule-Walker method. Because of the random nature of the signal, Monte Carlo simulations are employed to fully evaluate the estimated PSD. The estimated PSD for each run and the mean PSD for all the runs is shown in Fig. 3.19. The peaks of the mean PSD in Fig. 3.19 are at 0.59 Hz, 0.90 Hz, and 1.4 Hz. The narrow peaks indicate the oscillations for each of the frequencies is lightly damped.

The damping in the test signal is changed to illustrate how the steepness of the peaks change for highly damped oscillations in the estimated PSD. The

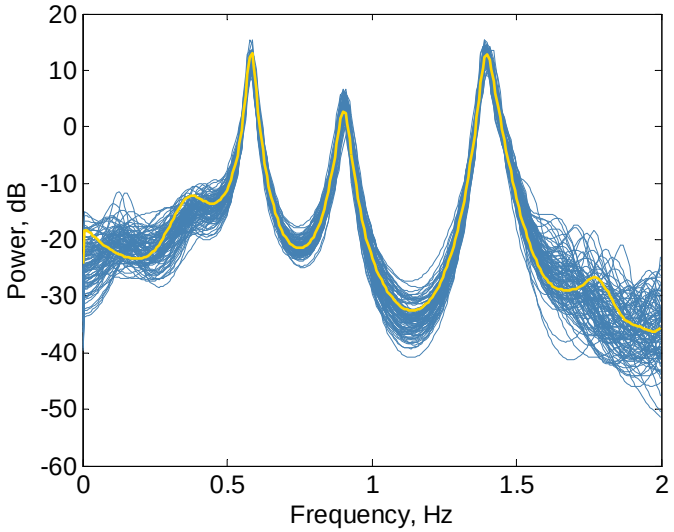

Figure 3.19: The Yule-Walker PSD estimated for each of 100 runs (blue) and the mean PSD for all the runs (yellow)

damping of the 0.6 Hz oscillation is increased significantly, from -0.1 to -0.6. The estimated PSD for the highly damped 0.6 Hz oscillation is compared to the lightly damped 0.6 Hz oscillation as shown in Fig. 3.20. The rate of change for the downward slope for the highly damped 0.6 Hz oscillation is -97.3 dB/Hz and for the lightly damped 0.6 Hz oscillation is -187.9 dB/Hz. From this analysis, it is apparent that the damping of the oscillation impacts the steepness of the peaks. The strength of the highly damped 0.6 Hz oscillation shown in Fig. 3.20 is also reduced compared to the lightly damped oscillation. This information can be used when analyzing the PSD as applied to PMU data to examine damping of oscillations as well as frequency content.

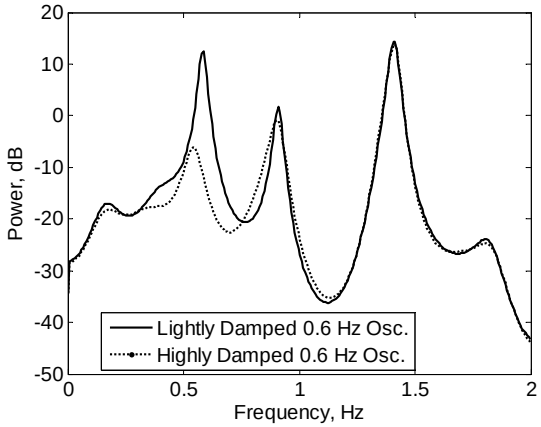

Figure 3.20: The sigma values for the SVD diagonal matrix Σ

3.3.4 Other Methods in Literature

In this dissertation, the Fast Fourier transform (FFT) and Welch periodogram methods are also used to analyze the frequency content of signals. Since these methods are well documented, this section provides an analysis of their performance for the test signal used in Subsections 3.3.1 and 3.3.2.

Because of the random nature of the signal, Monte Carlo simulations are employed to fully evaluate the estimated spectrum from both the FFT and Welch methods. The estimated FFT spectrum for each run and the mean spectrum for all the runs is shown in Fig. 3.21. The peaks of the mean Fourier transform in Fig. 3.21 are at 0.59 Hz, 0.88 Hz, and 1.40 Hz, an accurate representation of the frequency content of the test signal.

The estimated Welch PSD for each run and the mean spectrum for all the runs is shown in Fig. 3.22. The peaks of the mean PSD in Fig. 3.22 are

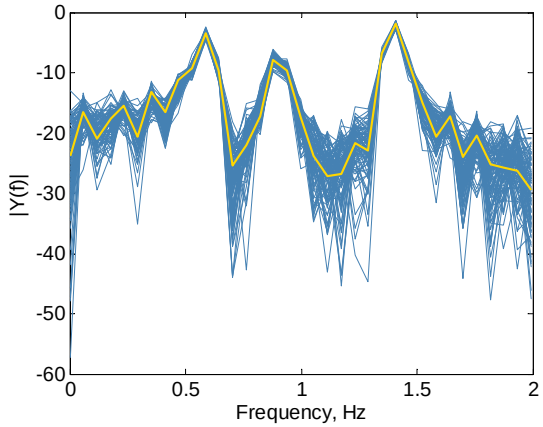

Figure 3.21: The Fourier transform estimated for each of 100 runs (blue) and the mean Fourier transform for all the runs (yellow)

at 0.59 Hz, 0.88 Hz, and 1.40 Hz, an accurate representation of the frequency content of the test signal.

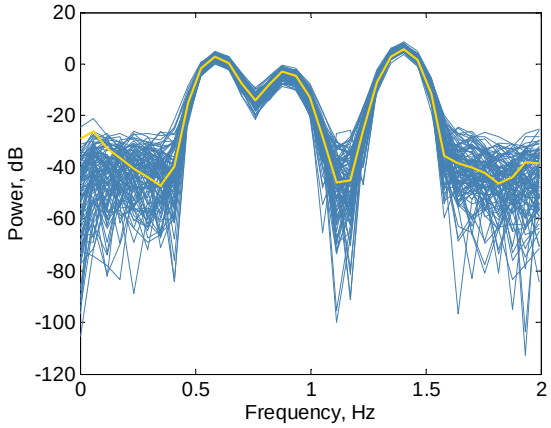

Figure 3.22: The Welch PSD estimated for each of 100 runs (blue) and the mean PSD for all the runs (yellow)

3.4 Summary

Methods used to monitor and analyze power system stability were introduced in this chapter. Two parametric, time-domain methods were described: the Prony method and the Matrix-Pencil method. The theorems for both methods was provided and the quality of their ability to estimate the signal components were quantified by applying the methods to a test signal. A parametric, linear, non-regressive method, to estimate AR coefficients, was also tested by applying the AR estimation methods to a test signal and calculating the power spectral density (PSD) of the test signal. The PSD was calculated using the Yule-Walker spectral method and the Welch method. The fast Fourier transform was also used to measure its ability to find the strength of the frequency content in the test signal. These methods are used throughout the following chapters to analyze actual power system measurements taken from phasor measurement units.

Chapter 4

Examination of the Value of Synchronized Voltage Measurements Taken at Customer-Level Voltage for Detection and Analysis of Transmission System Events

4.1 Introduction

The research objective presented in this chapter is to determine if customer-level voltage synchrophasor data is an accurate representation of power system behavior. Research into this objective involves demonstrating that customer-level voltage PMU data is an accurate representation of transmission level measurements and can be used to analyze transmission system behavior, e.g., power system events and low-frequency electromechanical oscillations.

4.1.1 Objective

As previously discussed in Chapter 2, synchronized voltage measurements taken by Phasor Measurement Units (PMUs) allow for the wide area monitoring of the electric power system covering a large geographical area. However, the placement of PMUs and use of PMU data are controlled by utilities and the Independent System Operators (ISOs) that install them. Data

are not always readily available for research from these entities. To overcome this obstacle, the University of Texas at Austin introduced an Independent Synchrophasor Network (now hosted at Baylor University) in order to monitor events and analyze low-frequency oscillations from the electric power grid through PMU measurements taken at the customer level voltage of 120 V. At this voltage level, PMUs can be placed virtually anywhere throughout the electric power system and measurements are freely available to use for power system analysis. The intent of the research presented in this chapter was to prove that:

- 120V PMU data contains information about large transmission level disturbances,
- 120V PMU data and state estimator data collected by the utility or system operator contain information about transmission system behavior that is similar,
- 120V PMU data and transmission level PMU data contain information about transmission system behavior that is similar, and
- 120V PMU data can provide information about the transmission system even during ambient (non-event) conditions.

4.1.2 Challenges

Since information in the form of a voltage signal is distributed from the transmission power system to the customer through a series of cables, equip-

ment and parallel loads, the voltage measured by PMUs at the customer-level voltages could potentially be polluted with noise and unwanted information. Even though the voltage signal is filtered to remove high frequency noise and harmonics before it is used for monitoring and analysis, phase shifts and other unwanted information may appear in the data [11]. Concerns about synchrophasor data taken from customer-level PMUs include:

- Voltage phase angle shifts that are introduced because of transformers with delta-wye connections, phase-shifting transformers, and voltage phase angle shifts caused by load current flowing through distribution voltage level transformers.
- The effect of distribution system events on cusstomer-level voltage synchrophasor data. Distribution system events include faulted lines and equipment within the distribution system, line trip and reclosing to clear faulted equipment, capacitor bank switching, and other events as described in [64].
- Unknown/unidentifiable distribution system influences.

The delta-wye connected transformer and phase-shifting transformer created phase angle shifts can range from -40° to $+40^\circ$ [65] and are not unique to PMU measurements taken at distribution voltage levels. Delta-wye connected transformers and phase-shifting transformers are present on the transmission system and need to be taken into account for transmission level

synchrophasor data as well. When system network data is known, delta-wye and phase-shifting transformer-induced phase shifts can be corrected in the synchrophasor data. The voltage phase angle shifts caused by load current are much smaller. Within the UT Independent Synchrophasor Network the voltage phase angle shift is approximately 3° (analyzed further in Section 4.5). The magnitude of the phase shift between the transmission system and customer level voltage depends on the number and size of the transformers and the load current (higher currents are seen at peak load). The impact of distribution level events on the PMU voltage phase angle is minimal and the effect on frequency may not be visible. However, the voltage magnitude will be heavily influenced by events that occur on the distribution system depending on the nearness of the event to the PMU location. For faults located on the distribution side, the voltage magnitude can drop to 0.9 p.u. [64]. Apart from known events and transformer configurations, other influences of the distribution system on PMU measurements could be present but their effects unknown (for example, effects of arc loads).

4.1.3 Strategy

The intent is to establish that 120V PMU data, particularly voltage phase angle data and frequency data, can be used to make conclusions about events occurring in the transmission system. In order to achieve this objective, synchrophasor data from multiple geographically distant PMUs are used. The transmission system is a strong and stiff system compared to the distribution

network, and as a result an event in the transmission system such as a line trip involves much more power re-routing than a comparable event at the distribution level. Such events are typically visible across the entire interconnection and can be detected in multiple PMUs if not all PMUs within an interconnected system. Using the observations that a) only the voltage magnitude is heavily influenced by distribution level events and that b) distribution level events only impact a single PMU, an event detected in the voltage phase angle or frequency can be further evaluated by examining if the event is visible in other PMUs and examining the drop in voltage magnitude.

The research presented in this chapter attempts to demonstrate that 120V PMU measurements contain accurate information about the behavior of the power system at the transmission level. Such behavior includes the power system response to large disturbances and trends in low frequency inter- and intra-area oscillations. The analysis comprised the following steps:

- Monitoring and analysis of the response of the transmission level electric power system to large disturbances as measured by 120V PMUs in order to confirm that transmission level phenomena is indeed visible at the 120V level,
- Comparison customer level voltage phase angle data to transmission level (69 kV) state estimator calculated voltage phase angle data,
- Comparison of the response of the power system to large disturbances as measured by customer level voltage PMUs to the response of the power

system as measured by transmission level PMUs, and

- Comparison of power system ambient response as observed by 120V PMUs and transmission level PMUs (comparison of modal frequency and damping estimates derived from 120V PMU measurements to estimates derived from transmission level PMU measurements.)

Section 4.2 examines if known transmission system events are visible in customer voltage level PMU data. This step is a prerequisite to proving the utility of the 120V data; since if the transmission system events were invisible (drowned out by distribution system noise, for example, or if the events failed to propagate to the distribution level) then analysis on the 120V data would be futile. The research described here proves that transmission system events are indeed visible in the 120V data. To demonstrate that customer level PMUs are able to accurately capture transmission system events, a comparison of 120V synchrophasor data time stamp and frequency drop to the event data from ERCOT Daily Grid Operations Reports [12] is made. Known transmission system events are listed in the ERCOT Daily Grid Operations Reports and these reports also include the system load at the time of the event, the cause, the start time, and if relevant, the drop in frequency caused by an event. First, the drop in frequency is examined to verify that the 120V PMU frequency drop during the event matches the frequency drop as recorded by ERCOT. In addition, the PMU measurements contain information on the electromechanical oscillations of the power system. A ringdown analysis is applied to the PMU

frequency signal during the event to estimate the modal damping and frequency of the electromechanical oscillations. The modal frequency estimates are compared to oscillations that are typical for the ERCOT power system during loading conditions at the time of the event as reported in [66]. The PMU voltage magnitude is also examined to find the impact, if any, that large transmission system disturbances have on customer-level voltage magnitude.

Section 4.3 describes comparison of ERCOT-supplied state estimator calculated voltage phase angle difference data to 120V PMU measured voltage phase angle difference data. This is the first comparison to indicate that 120V PMU measurements are accurate representations of the transmission system behavior during steady state conditions. The statistical information for both data sets (customer voltage level PMU and State Estimator voltage phase angles) are compared for a time span of 3 months. The results of the comparison show strong agreement between the two datasets.

In Section 4.4, the measurements of a PMU installed at 69 kV bus is compared to the UT-Austin customer level voltage synchrophasor. The 69 kV synchrophasor data are taken at Harris Substation which connects the UT-Austin campus to ERCOT. The 120V and 69kV measurements are compared during times of power system response to large events. The results of the comparison once again show strong agreement between the two datasets.

In Section 4.5, the electromechanical oscillations estimates based on PMU data measured at both customer voltage level and the transmission level are examined. The damping and frequency of these low frequency oscillations

are estimated using a block processing AR method as described in Chapter 3. The nearness of these estimates indicate that no new oscillations are introduced at the customer voltage PMU by the distribution system. However, it is observed that a small voltage phase angle difference between the 69 kV and 120 V PMU measurements exists during ambient conditions. A simple simulation is created to examine why small differences between the two measurements arise.

4.1.4 Publications

- **Publication**: Part of the work presented in this chapter has been published in [14]
  - Allen, A.J.; Sang-Wook Sohn; Grady, W.M.; Santoso, S.; , "Validation of distribution level measurements for power system monitoring and low frequency oscillation analysis," Power Electronics and Machines in Wind Applications (PEMWA), 2012 IEEE , vol., no., pp.1-5, 16-18 July 2012

4.2 120V PMU measurement analysis during a large events

In this section, it is shown that customer-level voltage synchrophasor data accurately capture the transmission system response to large events. A power system response to a large event can be observed as a sudden, large increase or drop in frequency, a temporary depression or rise in voltage magni-

tude, as damped (if the system is stable) oscillations, or as a sudden jump in the voltage phase angle. In this section, only large events caused by generating unit trips are examined. For this first validation step is accomplished by comparing data on disturbances detected in customer-level voltage synchrophasor data to event response information provided in ERCOT Daily Grip Operations Reports. The reports list the date and time of the event, the amount of power in mega-watts (MW) lost, the frequency decline, and the system load at the time of the disturbance. The reported frequency declines are based on transmission level measurements and are therefore accurate representations of power system responses to large disturbances.

The accuracy of customer-level voltage synchrophasor data are further examined by estimating the damping and frequency of the disturbance induced electromechanical oscillations as captured in the synchrophasor data. The Matrix-Pencil and Prony methods are used to estimate the damping and frequency and are described in detail in Chapter 3. These estimates are compared to the damping and frequency of oscillations typically seen in ERCOT during similar loading conditions as reported in [66]. The frequencies of the electromechanical oscillations are heavily influenced by transmission line congestion and power transfers and lightly damped oscillations are observed to be at a higher frequency ranging from 0.67 - 0.87 Hz [66]. The observations made in [66] are based on off-line small signal stability analysis studies.

Finally, the measured voltage magnitude is analyzed to determine if transmission level disturbances strongly influence customer-level voltage syn-

chrophasor data. The examples examined show that the voltage magnitude at customer-level voltage is too noisy at some PMU locations to use for reliable transmission system analysis.

4.2.1 Customer-level voltage PMU frequency during a large disturbance

In this section, it is shown that customer-level voltage PMU frequency accurately capture the transmission system response to large events, specifically generating unit trip events.

In Section 4.2.1.1, the shape of the frequency response caused by a generating unit trip event is analyzed. Two examples from ERCOT [7] are provided showing how the shape of the frequency response to an event is influenced by the system load. Next, the two frequency responses during the same events as captured by the customer-level voltage PMUs are compared to the ERCOT examples to illustrate the accuracy of the customer-level voltage measurements. Finally in Section 4.2.1.2, two separate disturbances are examined and compared to information provided in the ERCOT Daily Grid Operations Reports [12]. The ERCOT reports provide :

- the date and time of the disturbance,
- the total loss of generation in mega-watts,
- the frequency decline in hertz, and
- the ERCOT load at the time of the disturbance.

The accuracy of the customer-level voltage PMU is tested by comparing the time and frequency decline in the ERCOT reports to the customer-level voltage PMU data. Finally, the disturbance induced oscillations are analyzed by estimating their modal damping and frequency. The estimates are compared to typical damping and frequency seen within ERCOT based on small-signal stability analyses [66]. The Matrix-Pencil method is used to estimate the modal damping and frequency and a Yule-Walker spectral analysis is used to examine the frequency content of the PMU signals.

4.2.1.1 Customer-level voltage PMU frequency response

During a generating unit trip, the balance between the power consumed and power generated becomes unbalanced and results in a drop in the system frequency. The magnitude and rate of the frequency drop is dependent on the quantity of megawatts lost and inertia of the power system at the time of the event. The shape of the frequency drops and recoveries typically seen within ERCOT is reported in [7, 67]. Fig. 4.1 illustrates typical frequency drop and recovery and shows how the system inertia, or conventional generation online, influences the rate and magnitude of the frequency decline. The frequency response shown in Fig. 4.1 was taken from ERCOT [7]. For the two frequency responses, the mega-watts lost are approximately the same (837 MW for the dotted line and 890 MW for the solid line). However, the inertia of the system is different for the two responses. For the dotted line, the disturbance occurred in March 2010 with a system load of 23,655 MW and with 27,499 MW of

conventional generation online. For the solid line, the disturbance occurred in July 2009 and the system load was 49,209 MW with 55,609 MW of conventional generation online. For the disturbance that occurred in March 2010 and with lower inertia (dotted line), the rate of frequency decline was higher (0.066 Hz/s) and the frequency dropped to a much lower value (59.75 Hz). For the disturbance that occurred during July 2009 and with higher inertia (solid line), the rate of frequency decline was less (0.027 Hz/s) and the frequency dropped to a higher value (59.80 Hz).

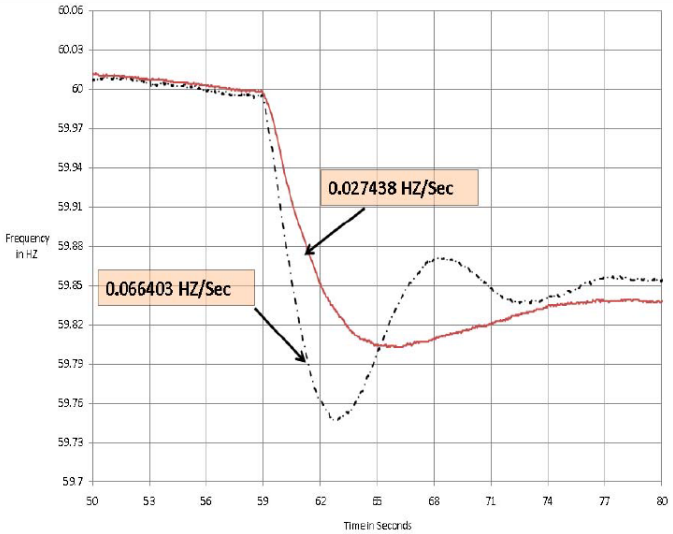

Figure 4.1: Frequency responses taken by ERCOT for two different load scenarios, lower inertia (dotted line) and higher inertia (solid line) [7]

The same events were recorded by the customer-level voltage PMUs and the same shape of the frequency response shown in the ERCOT data is seen in the PMU data. The frequency responses taken by the UT-Austin customer-level voltage PMU at the time of the events are shown in Fig. 4.1. The shape

and values of the frequency response taken by the PMUs are nearly identical to the frequency response taken by ERCOT. For the disturbance during lower inertia (dotted line), the rate of frequency decline was higher (0.0589 Hz/s) and the frequency dropped to a much lower value (59.75 Hz). For the disturbance that occurred during the summer and with higher inertia (solid line), the rate of frequency decline was less (0.0291 Hz/s) and the frequency dropped to a higher value (59.80 Hz). The rate of frequency decline was found by calculating the slope using the time and frequency values at the start of the event and the nadir (lowest point in the frequency). This first step shows how powerful and accurate synchrophasor data are, even when measurements are taken at a low voltage, i.e.m the frequency response of generating unit trips that occur on the transmission system are clearly visible at 120 V.

4.2.1.2 Customer-level voltage PMU frequency response examples

Next, two examples of the frequency signal during generating unit trip events taken from customer-level voltage PMUs are examined. The frequency response from the PMU network are shown in Figs. 4.3 and 4.6. The measured frequency drop and time of the event is compared to the frequency drop and time taken from the ERCOT Grip Operations Reports [12, 13] for these events. The first example shown in Fig. 4.3a are the frequencies from PMU stations located at UT-Austin, McDonald Observatory, and UT-Pan America. For this event, the ERCOT Grid Operations Report states the system response was caused by a unit trip of 783 MW. ERCOT load at the time of the event

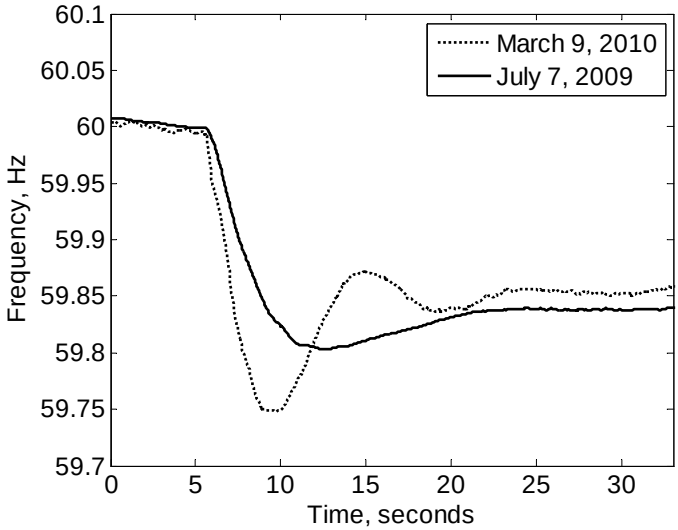

Figure 4.2: Frequency responses taken by the UT-Austin customer-level voltage PMU for two different load scenarios,lower inertia (dotted line) and higher inertia (solid line)

was 33,590 MW. The event starting time and recovery operations executed by ERCOT to maintain system stability began at 4:10 CST and recovery operations ended at 4:27 CST. The system frequency dropped to 59.80 Hz during the event. The customer-level voltage PMUs frequency signals show the frequency drops between 59.797 Hz and 59.799 Hz, equal to the frequency drop provided by the Operations Report. The time of the event, 10:09 UTC, is near that given in the ERCOT Operations Report. The slight difference in time may come from the different timing sources used to timestamp the two datasets.

In addition to the frequency drop, the high precision PMU data also

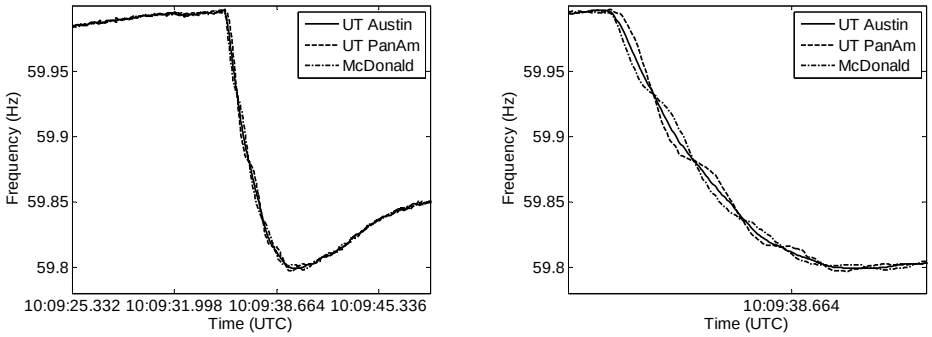

(a) Frequency of a generating unit trip event

(b) A zoomed view of the frequency response

Figure 4.3: Frequency of a unit trip event of 783 MW on July 26, 2010

provides additional information. Electromechanical oscillations are visible in the McDonald and UT-PanAM frequencies as shown in detail in Fig. 4.3b. The oscillations are nearly 180° out of phase indicating that two portions of the grid oscillate against one another. The modal damping and frequency for the McDonald, UT-PanAm, and UT-Austin PMU frequency signals are estimated using the Matrix Pencil method. The resulting modes with the two highest amplitudes are given in Table 4.1.

From Table 4.1, the UT-PanAm modal frequencies estimates are 0.59 Hz and 0.21 Hz. The damping for the estimated 0.21 Hz mode is negative, indicating a growing oscillation. However, the window of data containing the oscillation is small and the oscillation is damped out when the window of data is expanded. The 0.59 Hz mode is well damped with a damping ratio of 13.75%. The McDonald modal frequencies estimates are 0.23 Hz and 0.71 Hz. The same approximate 0.2 Hz mode is visible at McDonald and UT-PanAm.

Table 4.1: Matrix Pencil estimated modal damping and frequencies for July 26, 2010 event (frequency signal)

Location	*Amplitude*	*Damping (%)*	*Frequency (Hz)*
UT-PanAm	13.0	13.75	**0.59**
	6.8	-11.46	**0.21**
McDonald	10.03	1.68	**0.23**
	5.31	7.03	**0.71**
UT-Austin	15.9	-14.34	**0.12**

The 0.2 Hz mode is better damped at McDonald, but only very lightly damped with a damping ratio of 1.68%. The second McDonald modal frequency is 0.71 Hz. Electromechanical oscillations are not as strongly visible in the UT-Austin PMU frequency signal. The only modal frequency and damping detected by the Matrix-Pencil method at UT-Austin was 0.12 Hz and -14.34%, respectively.

The Yule-Walker power spectral density is applied to the UT-PanAm, McDonald, and UT-Austin frequency signals to measure the strength of the frequency content of each signal. The PSD for the PMU frequency signals are shown in Figs. 4.4 and 4.5. The UT-PanAm PSD shows the two modal frequencies around 0.2 Hz but the two modes are close to one another. It's possible that the Matrix-Pencil method was unable to detect the two separate modes. The same two modes near 0.2 Hz is also visible in the McDonald PSD. The UT-PanAm PSD shows a 0.56 Hz mode and the McDonald PSD shows a 0.76 Hz mode. These are approximately the same frequencies as estimated by the Matrix-Pencil method.

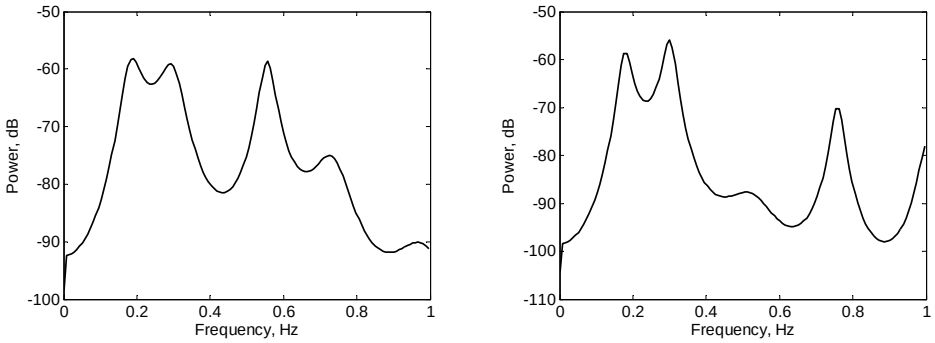

(a) UT-PanAm (b) McDonald

Figure 4.4: Power Spectral Density of July 26, 2010 PMU frequency signals

The PSD for the UT-Austin frequency signal in Fig. 4.5 reveals an additional mode at 0.54 Hz that was not detected by the Matrix-Pencil method. It's not clear why this frequency was not detected but it shows the importance of using multiple methods to estimate modes in PMU signals.

The second frequency response event in Fig. 4.6 shows the drop in frequency caused by a generating unit trip event that occurred on January 9, 2010 . Only two of the PMU stations in the independent synchrophasor network, McDonald and UT-Austin, were operational at the time. From [12], a unit trip of 1231 MW occurred at 10:28 CST, causing the system frequency to drop to 59.77 Hz. The ERCOT load at the time of the event was 47,871 MW. The customer-level voltage PMU frequencies at the time of the event are in Fig. 4.6a. The information from the PMUs indicate that the event occurs at the same time (16:28 UTC) and the frequency drops to 59.763 Hz at the McDonald station and 59.765 Hz at the UT-Austin station, similar to the frequency drop provided by ERCOT.

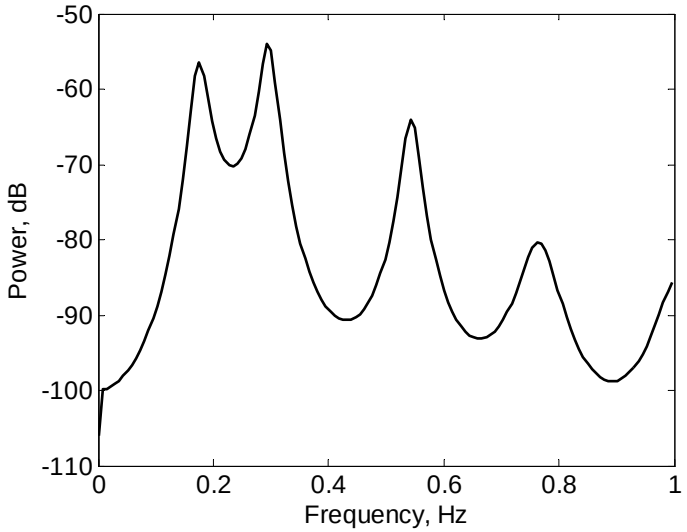

Figure 4.5: Power Spectral Density of UT-Austin PMU frequency signal during the July 26, 2010 generating unit trip event

The Matrix-Pencil estimated modal damping and frequency for the event are provided in Table 4.2. Only the modes with the two highest amplitudes are saved. The UT-Austin PMU frequency signal contains a 0.46 Hz mode and an underdamped 0.18 Hz mode. The McDonald PMU frequency signal contains the same approximate 0.20 Hz mode and a different 0.58 Hz mode.

Yule-Walker power spectral densities for the UT-Austin and McDonald PMU frequency signal is shown in Fig. 4.7. The two modes visible in the UT-Austin PSD shown in Fig. 4.7a are 0.5 Hz and 0.2 Hz modes, similar to the modes detected in Table 4.2. The two modes visible in the McDonald PSD shown in Fig. 4.7b are 0.62 Hz and 0.2 Hz modes, similar to the modes

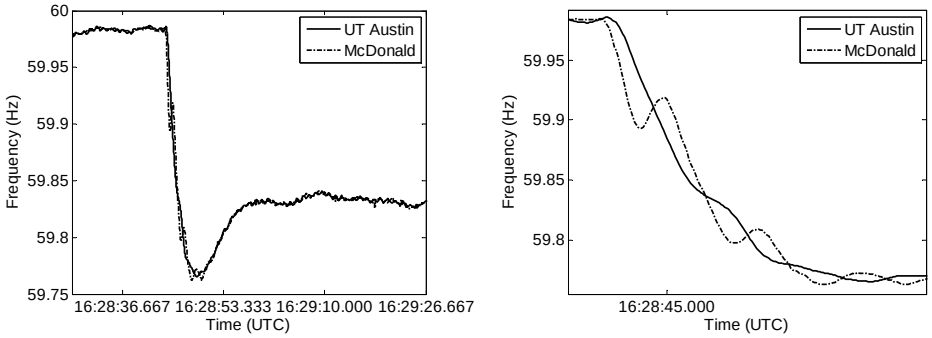

(a) Frequency of a generating unit trip event

(b) A zoomed view of the frequency response

Figure 4.6: Frequency of a unit trip event of 1231 MW on January 9, 2010

Table 4.2: Matrix Pencil estimated modal damping and frequencies for January 9, 2010 event (frequency signal)

Location	*Amplitude*	*Damping (%)*	*Frequency (Hz)*
UT-Austin	16.0	20.37	**0.46**
	8.3	-14.50	**0.18**
McDonald	15.6	7.10	**0.58**
	10.2	-2.93	**0.20**

detected in Table 4.2.

Section 4.2.2 examines the impact the same events have on the voltage magnitude as measured by customer-level voltage PMUs. The section will evaluate if the measured voltage magnitude for distribution level PMUs can be used for transmission system analysis.

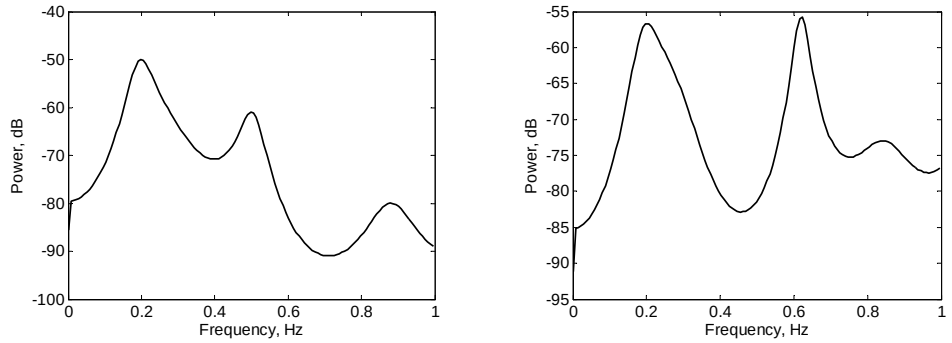

(a) UT-Austin (b) McDonald

Figure 4.7: Power Spectral Density of January 9, 2010 PMU frequency signals

4.2.2 Voltage Magnitude during Transient Response

In this section, the response of the power system to generating unit trips described in Section 4.2.1 are examined through the measured PMU voltage magnitude. Before analysis begins, it is assumed that even at the distribution level, an event that occurs at the transmission level can be observed in the voltage magnitude. The impact these events have on the voltage magnitude measured by customer-level voltage are evaluated to determine if this quantity can be used for transmission system analysis or if the impact of the distribution system interferes with transmission system analysis. It is expected that during a generating unit trip event the voltage magnitude is temporarily depressed with a duration of a few cycles. In the examples examined, the per unitized voltage magnitude is analyzed. To calculate the per unit voltage for each PMU station, the base value is defined as the averaged voltage magnitude one minute prior to the event start time. The measured voltage data are then divided by the base voltage.

The voltage magnitudes of the two generating unit trip events described in Section 4.2.1 are shown in Figs. 4.8 and 4.10. The voltage magnitude taken during the July 26, 2010 event in Fig. 4.8 was measured at UT-Austin, McDonald Observatory, and UT-PanAmerican. At the start of the event, the voltage magnitudes at UT-Austin and UT-PanAm begin to drop as shown in Fig. 4.8. However, the voltage drop at all of the locations does not fall below 0.995 p.u. and the voltage magnitude at McDonald does not seem to be affected by the generating unit trip event. The start of the event is marked with a red arrow in Fig. 4.8. Other isolated events are seen at McDonald and UT-PanAm, but these events are not system wide and are only seen at a single PMU location. The cause of the drop in voltage magnitude is unknown since the customer-level voltage magnitude can be influenced by events occurring on the distribution system as well as by events on the transmission system. The depression in the voltage magnitude is also influenced by the location of the event occurrence in relation to the PMU station and by the type of event that occurred.

An hour of per unitized voltage magnitude data for McDonald is given in Fig. 4.9. The amount of variation in the voltage magnitude indicates that the customer-level PMU measured voltage magnitude is too heavily influenced by the distribution system for accurate transmission system behavior analysis.

The voltage magnitude during the generating trip event that occurred on January 9, 2010 is shown in Fig. 4.10. The PMU stations located at McDonald and UT-Austin were operational during the event. It is apparent from

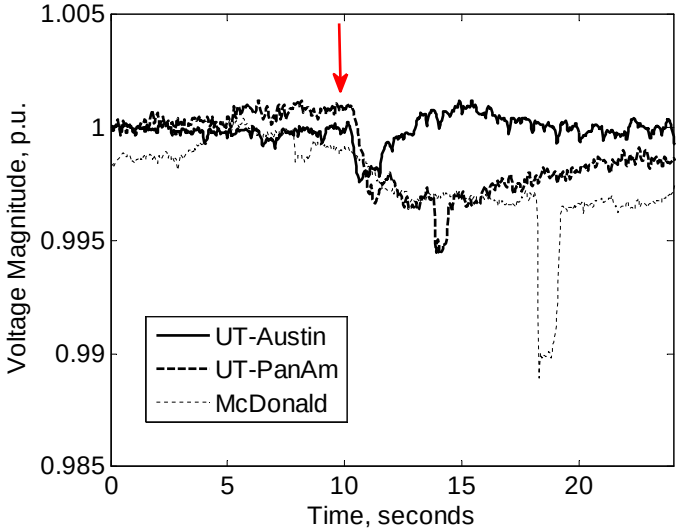

Figure 4.8: Voltage Magnitudes during a generating unit trip event causing a sudden loss of 783 MW on July 26, 2010

Fig. 4.10 that the depression in the voltage magnitude during the event (the event time is marked by the red arrow) in Fig. 4.10 is very small and detectable only in the UT-Austin measurement where the per unitized voltage magnitude drops to less than 0.1% of unity. The per unitized voltage magnitude at McDonald is noisy and contains events of unknown origin making it difficult or impossible to detect the start of the generating unit trip event.

Even though it was observed that the voltage magnitude is influenced by transmission system events, Figs. 4.8 to 4.10 show the strong influence of the distribution system on the voltage magnitude measurements. Therefore, it is unrealistic to analyze the power system transient response based solely on the voltage magnitude measured at the distribution level. However, if the voltage

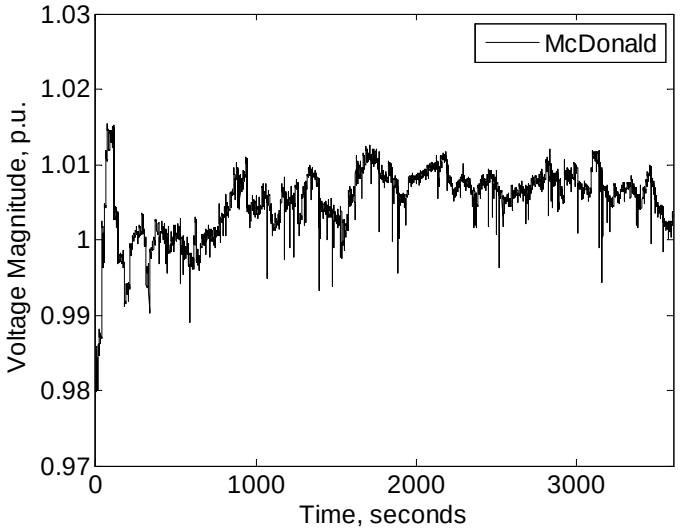

Figure 4.9: Voltage Magnitudes during a generating unit trip event causing a sudden loss of 783 MW on July 26, 2010

magnitude is used in conjunction with other voltage phasor quantities, the voltage magnitude may be helpful in identifying different types of transmission system events such as a fault, a line trip, or islanding event as described in [68].

4.2.3 Voltage Phase Angle during Transient Response

This section examines the impact generating unit trip events have on the voltage phase angle as measured by customer-level voltage PMUs. The section will evaluate if the measured voltage phase angle from customer-level voltage PMUs are accurate enough to be used for transmission system analysis.

The response of the power system to a generating unit trip is seen as a damped (if system conditions are stable) low-frequency oscillation in the

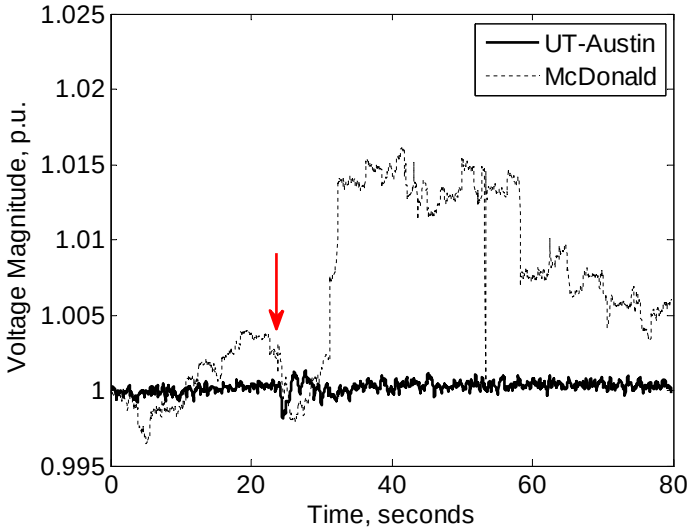

Figure 4.10: Voltage magnitude during a generating unit trip event causing a sudden loss of 1231 MW on January 9, 2010

PMU measured voltage phase angle. The estimated modal damping of the low-frequency oscillation is an indication of how well the system is able to absorb a disturbance without loss of stability. For example, if a large disturbance results in oscillations that are underdamped, this could be used as indication that the system might not be able to handle another large disturbance. There is an increased risk that if another disturbance occurred it might result in system wide blackouts as shown in the well documented blackout that occurred in the Western interconnect in August 1996 [69].

The voltage phase angle difference between two distribution level PMU stations during two generating unit trip events described in Section 4.2.1 are analyzed here. The first event, on July 26, 2010, recorded data from PMU

stations located at McDonald Observatory, UT-Austin, and UT-Pan American. The voltage phase angle difference between McDonald and UT-Austin in Fig. 4.11a shows a 1.81 ° change during the initial swing, the difference between UT-Austin and UT-Pan American in Fig. 4.11b shows a 2.36 ° change during the initial swing, and the difference between UT-Pan American and McDonald in Fig. 4.12 shows a change of 4.30 ° during the initial swing. The initial swings between UT-Pan American (located in south Texas) and McDonald Observatory (located in west Texas) are relatively large which is in agreement with the analysis on the PMU frequency signal at these locations during the same event as analyzed in Section 4.2.1. The UT-Pan American and McDonald PMU frequency signals in Fig. 4.3a shows an oscillation of larger amplitude between these two locations compared to the PMU frequency at UT-Austin.

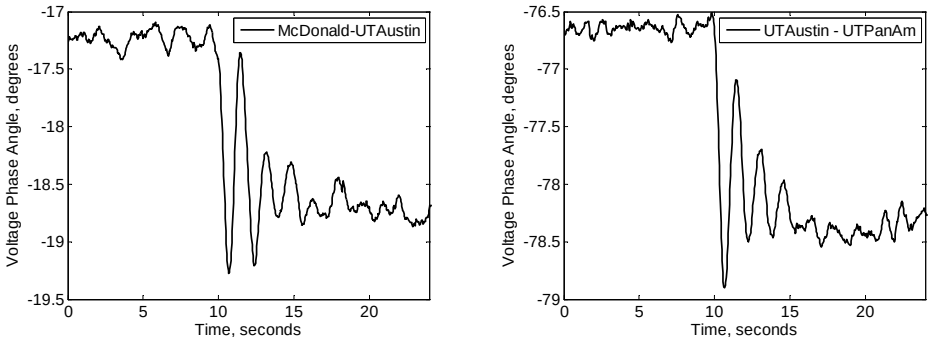

(a) McDonald and UT-Austin (b) UTAustin and UT-PanAm

Figure 4.11: Voltage Phase Angle Differences during a unit trip event of 783 MW on July 26, 2010

The modal damping and frequencies estimated by the Matrix-Pencil method are given in Table 4.3. The dominant modal frequency in all PMU

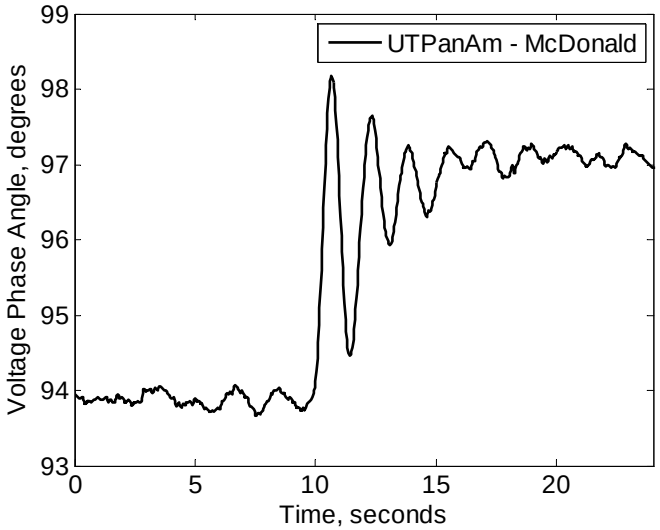

Figure 4.12: Voltage Phase Angle Difference between UT-Pan American and McDonald during a unit trip event of 783 MW on July 26, 2010

voltage phase angle differences analyzed is an approximate 0.6 Hz mode. A second 0.3 Hz mode was detected in the PMU voltage phase angle difference between McDonald and UT-Austin and between UT-Austin and UT-Pan American.

The Yule-Walker calculated power spectral density for the events are shown in Figs. 4.13 and 4.14 below. The frequencies in the PSD match the frequencies in Table 4.3. The 0.63 Hz mode in Fig. 4.14 is much stronger than the same 0.6 Hz mode in Fig. 4.13. It is possible that the 0.3 Hz mode that is visible in the PSD in Fig. 4.14 was not detected by the Matrix-Pencil method.

During the second event, the PMU stations at McDonald Observatory and UT-Austin were operational. The voltage phase angle during the event

Table 4.3: Matrix Pencil estimated modal damping and frequencies for July 26, 2010 event (voltage phase angle signal)

Phase Angle Diff (deg)	*Amplitude (deg)*	*Damping (%)*	*Frequency (Hz)*
McD-UT	0.70	9.78	0.61
	0.22	17.95	0.30
UT-UTPA	1.41	10.36	0.63
	0.33	21.04	0.31
UTPA-McD	0.67	9.79	0.64

Table 4.4: Prony estimated modal damping and frequencies for January 9, 2010 event (voltage phase angle signal)

Phase Angle Diff (deg)	*Amplitude (deg)*	*Damping (%)*	*Frequency (Hz)*
McD-UT	2.99	11.40	0.55
	0.62	46.35	0.13

in Fig. 4.15 shows a 10.3° initial swing. The large change in voltage phase angle, caused by a generating unit trip with 1231 MW loss, is clearly visible at customer-level voltage and demonstrates the ability of cusomter-level voltage PMUs to represent events that occur at the transmission power system.

The modal damping and frequencies estimated using Matrix-Pencil are given in Table 4.4. The modal frequencies are slightly different from the modal frequencies estimated from the PMU calculated frequency in Table 4.2.

Yule-Walker power spectral density shows 0.56 Hz and 0.23 Hz modes in Fig. 4.16. The estimate for the 0.23 Hz mode in the PSD differs from the

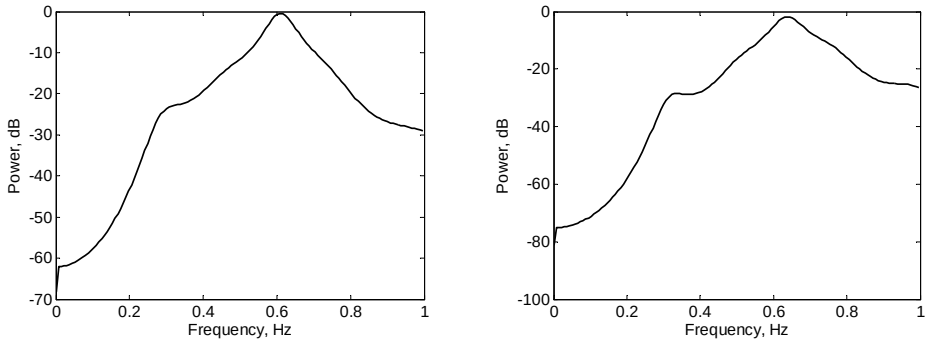

(a) McDonald and UTAustin (b) UTAustin and UT-PanAm

Figure 4.13: Yule Walker PSD for voltage phase angle differences during July 26, 2010 generating unit trip events

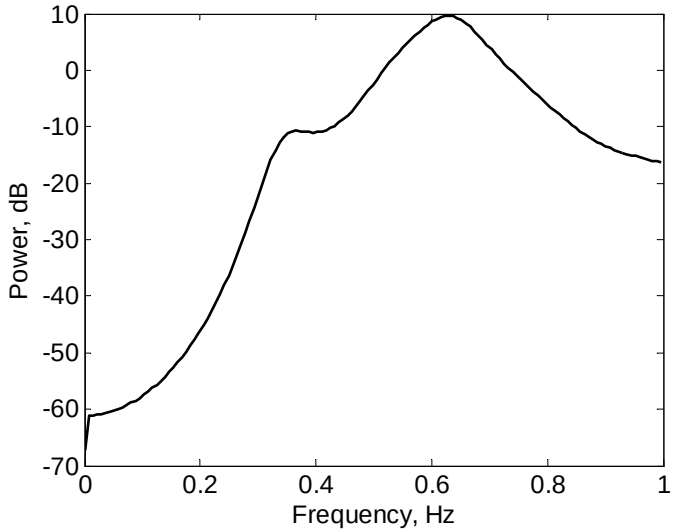

Figure 4.14: Yule Walker PSD for voltage phase angle difference between UT-PanAm and McDonald during July 26, 2010 generating unit trip event

Matrix-Pencil estimated 0.13 Hz mode. The 0.13 Hz mode is highly damped with a damping ratio of 46.35%, therefore, the frequency of the oscillation is

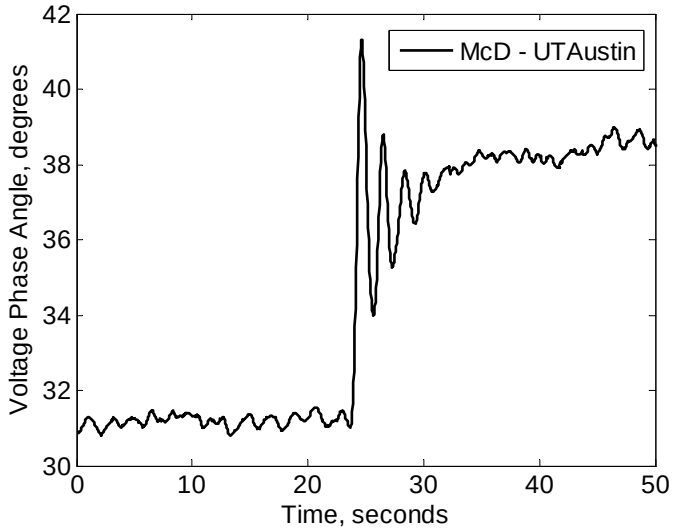

Figure 4.15: Voltage Phase Angle difference between McDonald and UT-Austin during a unit trip event of 1231 MW on January 9, 2010

more difficult to estimate.

4.2.4 Conclusion

From these initial measurements it is apparent that with customer-level voltage PMU measurements it is possible to clearly detect and analyze the transient response of events that occurred on the power system, specifically generating unit trip events. The transients response is most obviously visible in the voltage phase angle and the frequency measured at each PMU station. In Section 4.3, the customer-level voltage PMU measurements are further validated by comparing the PMU data to the state estimated voltage phase angle at buses located near UT-Austin and McDonald Observatory

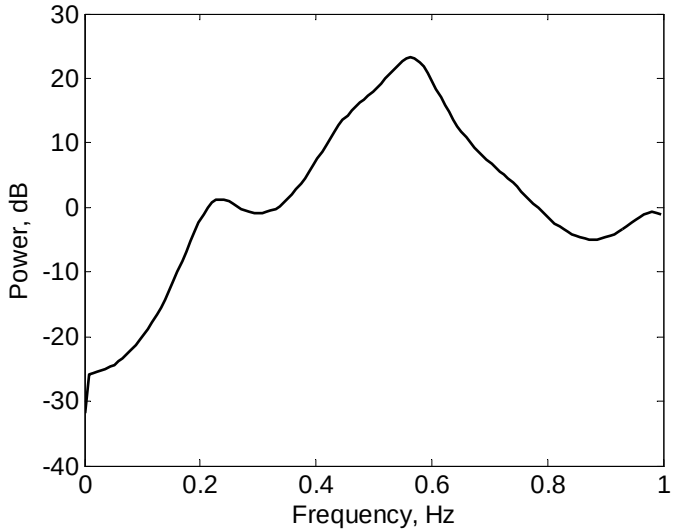

Figure 4.16: Yule Walker PSD for voltage phase angle difference between UT-PanAm and McDonald during January 9, 2010 generating unit trip event

PMU stations. In Sections 4.5 and 4.4, an additional PMU is installed at the transmission voltage level of 69 kV and is located at the transmission bus nearest the UT-Austin PMU station. Large power system events and steady state measurements are compared for measurements taken at customer-level voltage and at 69 kV in order to validate the customer-level voltage measurements for transmission system analysis.

4.3 State Estimator Voltage Phase Angle and Customer-Level Voltage Synchrophasor Data Comparison

In this section, the accuracy of customer-level voltage phase angle measurements as representation of the transmission level phase angle is analyzed

by comparing the customer-level voltage synchrophasor data to 69 kV voltage phase angle data as calculated by the system operator state estimator (SE). Only the state estimates calculated for buses located near a customer-level voltage PMU station are examined. For example, Harris Substation is the transmission level bus located nearest to the University of Texas at Austin PMU station. Therefore, the Harris Substation state estimated voltage phase angle is used to determine the accuracy of the UT-Austin PMU measured voltage phase angle. The other voltage phase angle examined is the customer-level voltage phase angle measured at McDonald. The 69 kV state estimated voltage phase angle taken from the McDonald 69 kV bus is also used for the validation of the customer-level voltage PMU measurements.

Since system operators use results from the State Estimator (SE) for applications such as contingency analysis and optimal power flow and are increasingly used in emerging energy markets [70] it can safely be assumed that the estimated voltage phase angle is an accurate representation of the true voltage phase angle at the transmission bus. If customer-level voltage synchrophasor data are comparable to the SE data then it can be stated that customer-level voltage PMU data are an accurate representation of transmission bus voltage phase angles. A brief background on state estimation is provided in Subsection 4.3.1. In Subsection 4.3.2 the voltage phase angle measured at customer-level voltage and the phase angle calculated by the system operator state estimator are compared. The SE voltage phase angle data was provided by ERCOT.

4.3.1 State Estimator Background

The operating conditions of a power system are known through analog and status measurements of the power system, however, some of the states of the power system cannot be measured. State estimation is the method of estimating the unknown states of the power system by using snapshots of real-time measurements and static network data [70]. Estimation of the unknown states is an optimization problem where estimates are made by minimizing error between the true states of the system and the measured states with equality and inequality constraints [71]. Weighted Least Squares (WLS) state estimation attempts to reduce error further by utilizing a weighted matrix which emphasize more accurate measurements. The WLS optimization problem with a nonlinear objective function and constraints is given in (4.1) and (4.2).

$$minimize\ f = \sum_{i=1}^{m} \frac{1}{\sigma_i^2}[z_i - h_i(x)]^2 \tag{4.1}$$

$$subject\ to\ g_i(x) = 0;\ i = 1,\ n_g \tag{4.2a}$$

$$c_i(x) \leq 0;\ i = 1,\ n_c \tag{4.2b}$$

Where $f(\cdot)$ is the objective function, m is the number of measurements, z is the vector of measurements, x is the vector of unknown states to be estimated, $h(\cdot)$ is the function relating x to z, σ_i is the variance of the i^{th} measurement, and $g_i(\cdot)$ and $c_i(\cdot)$ are the constraint functions representing power flow quantities.

State estimates are a quasi-static representation of the power system operating conditions [70]. Part of the reason the SE provides only a quasi-static representation is that SCADA measurements used by the state estimator are not synchronized. Measurements taken at each SCADA system scan can differ by a few seconds. In addition, the interval at which state estimates can be made is limited by large computations and therefore it is only practical for state estimators to run every few minutes. In the estimated voltage phase angles provided by ERCOT, the state estimator provides estimates approximately every 5 minutes. In addition to a lower resolution, the timestamp for each state estimate is not provided by GPS and introduces another time skew when comparing to GPS synchronized PMU measurements.

4.3.2 SE and PMU Voltage Phase Angle Comparison

In this section a visual comparison between estimated voltage phase angle and the customer-level voltage PMU measured voltage phase angle is used to analyze the accuracy of distribution level PMU measurements as representations of the transmission level voltage phase angle. The voltage phase angle difference between the distribution PMU station at UT-Austin and McDonald Observatory are compared to the state estimator voltage phase angle calculated at the nearest 69 kV buses. As has been mentioned before, the PMU data has a sampling frequency of 30 Hz and the SE voltage phase angle estimates are made approximately every 5 minutes. The PMU data is downsampled to match the 5 minute sampling rate of the SE voltage phase angle

in order to easily compare the two data sets. Three weeks of estimated and measured data taken in April 2009 is plotted in Fig. 4.17. The two data sets closely match during this time period. Steep changes in the the voltage phase angle closely match as can be seen between the 6^{th} and 7^{th} day.

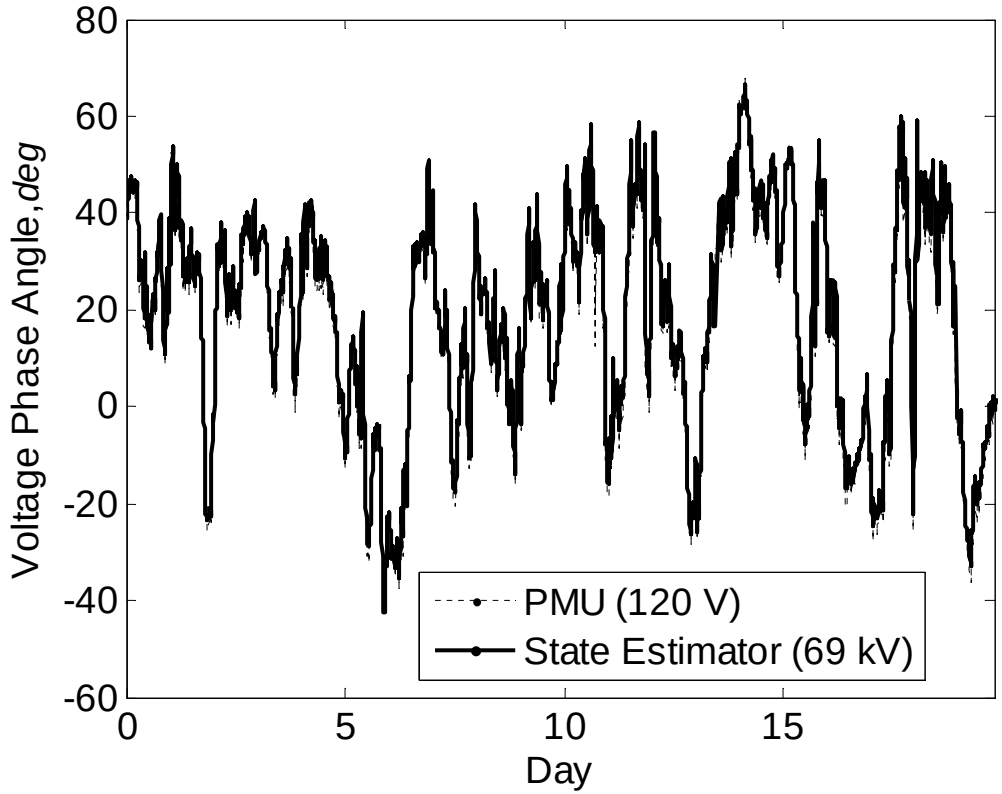

Figure 4.17: Comparison of the voltage phase angle between UT-Austin and McDonald Observatory as measured at the distribution level (dotted line) and as calculated at the transmission level using the state estimator (solid line)

A detailed view of the customer-level voltage measured phase angle (at its original 30 Hz sampling rate) and the state estimated voltage phase angle is given in Fig. 4.18. While the detailed view shows the nearness of the two different datasets, it also emphasizes that the PMU data provides more detail and therefore more information that can be utilized to monitor the health of the power system.

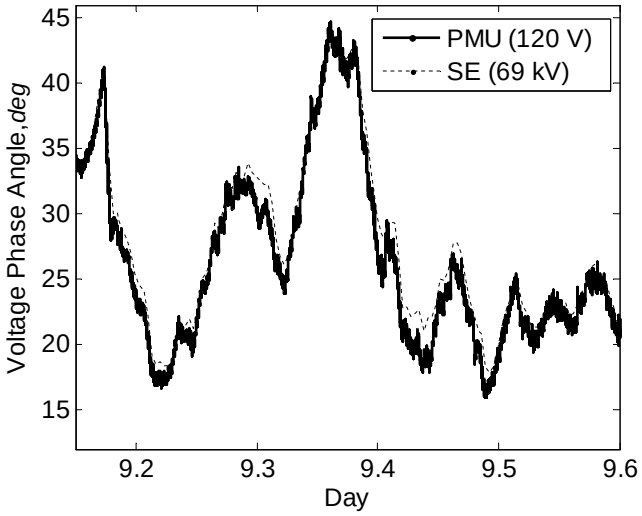

Figure 4.18: Detailed comparison of the voltage phase angle as measured at customer-level voltage (solid line) and as calculated at the transmission level using the state estimator (dotted line)

The comparison of the customer-level voltage PMU measured voltage phase angle to SE calculated transmission level voltage phase angle demonstrate the accuracy of the PMU measurements as representative of the voltage phase angle at the transmission level. However, the state estimated voltage phase angle is not a direct measure and therefore a more thorough approach is

used by comparing customer-level voltage synchrophasor data to synchrophasor data taken at the transmission level (69 kV) as provided in Sections 4.4 and 4.5.

4.4 Comparison of 69 kV PMU measurements to 120 V PMU measurements Transient Response

In Summer 2010, an additional PMU was installed at Harris Substation near the University of Texas at Austin at the 69 kV (transmission voltage) level. A satellite view of the University of Texas campus with the locations of the 120 V and 69 kV PMUs marked is shown in Fig. 4.19. The Harris Substation connects the University of Texas campus to the grid and, therefore, Harris Substation is the transmission level voltage bus closest to the customer-level voltage UT-Austin PMU station. Voltage phasor and frequency data from the 69 kV PMU are referred to as transmission level synchrophasor data or Harris Substation synchrophasor data.

After installation of the transmission level PMU, it was observed that events measured at both the distribution level and the transmission level are comparable. Two examples of PMU frequency signals from customer-level voltage and transmission level voltage during a generating unit trip are presented in this section. The PMU frequency signals are compared to show that customer-level voltage PMU data are accurate representations of transmission system frequency during a large event. The first example is of PMU measurements taken during a generating unit trip event occurred on July 10, 2010 at

Figure 4.19: Satellite view of the University of Texas campus with the UT-Austin (120 V) and Harris Substation (69 kV) locations indicated

9:10:46 UTC. During the July 10, 2010 event, a drop in the frequency measured at the UT-Austin customer-level voltage PMU station and the transmission level PMU is shown in Fig. 4.20a. The event causes the frequency to drop to 59.84 Hz at a rate of 2.51 mHz/s. As shown previously, the frequency is calculated from the voltage phase angle measurements. A detailed view of the frequencies in Fig. 4.20b measured at UT-Austin (120 V) and Harris Substation (69 kV) shows how closely the two PMU frequency signals match. The PMU frequency signal from UT-PanAm is plotted as well in order to show how a frequency signal can vary across the interconnected grid.

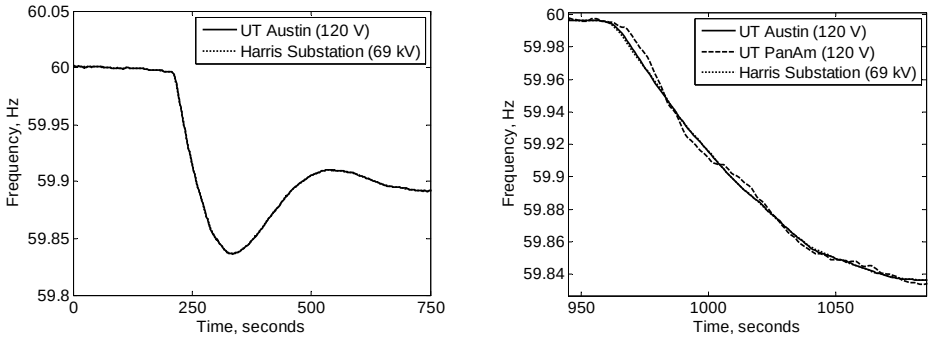

(a) Frequency response during July 10, 2010 generating unit trip event

(b) Detailed view of frequencies during July 10, 2010 event

Figure 4.20: Frequencies during July 10, 2010 generating unit trip event taken by distribution level (120 V) PMUs and transmission level (69 kV) PMU

The second example shows the frequency response as seen by UT-Austin customer-level voltage and Harris Substation 69 kV PMUs during a generating unit trip event on November 29, 2011. The sudden loss of 1,365 MW caused the frequency to drop to 59.69 Hz. The customer-level voltage and 69 kV PMU frequencies during the event are shown in Figs. 4.21a and 4.21b. The detailed view shows how the frequency signal at customer-level voltage is an accurate representation of the transmission level frequency. The PMU frequency from McDonald is plotted as well to show how how the frequency can differ during the same event at a different location within the interconnected grid.

The power spectral density is calculated for each event. The results are shown for both the customer-level voltage PMU and the transmission level voltage PMU. The PSDs for the July 10, 2010 event is shown in Fig. 4.22a.

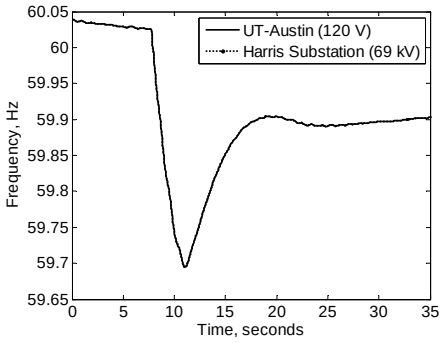

(a) Frequency response during November 29, 2011 generating unit trip event

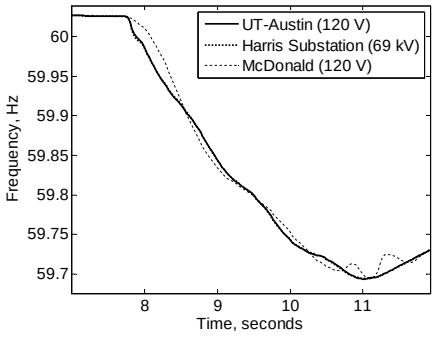

(b) Detailed view of frequencies during November 29, 2011 generating unit trip event

Figure 4.21: Frequencies during November 29, 2011 generating unit trip event taken by distribution level (120 V) PMUs and transmission level (69 kV) PMU

The PSDs for the November 29, 2011 event is shown in Fig. 4.22b. Both results show that the spectral content and strength is very similar for both customer-level and transmission level voltage PMU data.

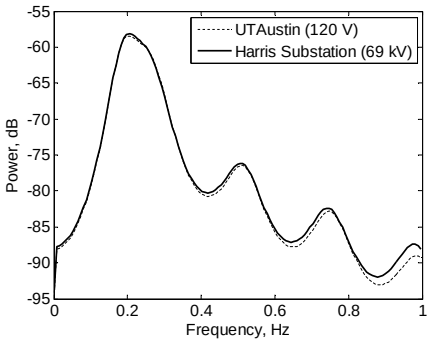

(a) July 10, 2010 Event

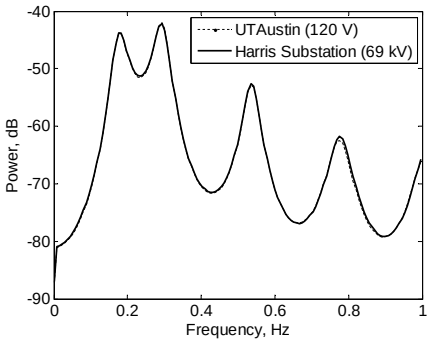

(b) November 29, 2011 Event

Figure 4.22: Comparison of the power spectral density of the frequency signal for customer-level voltage PMU at UT-Austin and transmission level voltage PMU at Harris Substation

In Section 4.5, the customer-level voltage PMU data will be compared to the 69 kV PMU data during steady state (ambient) conditions.

4.5 Comparison of 69 kV Synchrophasor Data to 120 V Synchrophasor Data during Ambient Conditions

In this section, customer-level voltage PMU measurements are compared to 69 kV PMU measurements during steady state or ambient conditions in order to further validate that customer-level voltage PMUs produce accurate data that can be used for transmission system analysis.

4.5.1 Analysis of PMU Measurements

To further illustrate the accuracy of the UT-Austin 120-V measurement as representative of nearby transmission voltage level measurements, the voltage phase angle difference between the UT-Austin and Harris Substation PMUs is examined during ambient conditions. A typical example of the voltage phase angle difference is shown in Fig. 4.23 over a period of 5 hours. In Fig. 4.23, the difference never exceeds 0.7° during the time period indicating the similarity of the distribution measured voltage phase angle to the transmission measured voltage phase angle. As expected, the difference is not constant nor is it exactly zero. The load current flowing through reactive elements causes a slight shift in the voltage phase angle difference and random load switching causes the fluctuations seen in the data.

Occasionally the voltage phase angle difference jumps 2° or 3° as shown

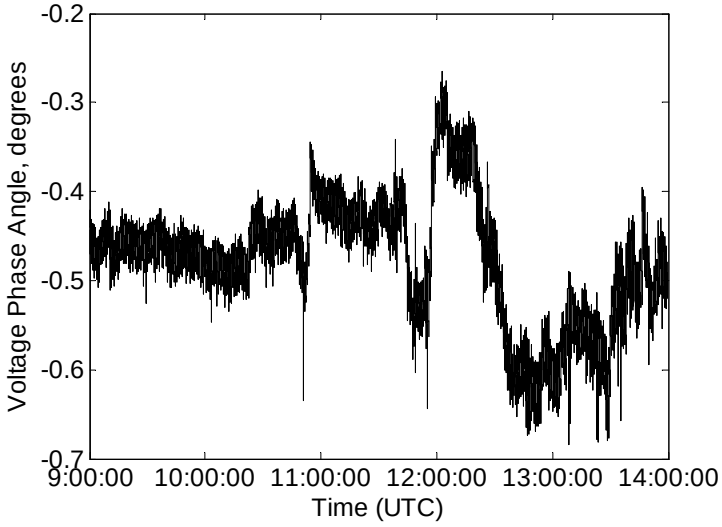

Figure 4.23: Voltage phase angle difference between UT-Austin and Harris Substation during ambient conditions

in Fig. 4.24. The phase angle difference is from Harris Substation to UT-Austin, a negative phase angle indicates power flowing from UT Austin toward Harris Substation. In Section 4.5.2, a simulation created in Siemens/PTI PSS/E software platform is used to analyze jumps in the voltage phase angle difference and how the phase angle difference is influenced by the power flow from the UT-Austin campus towards Harris Substation.

Next, to verify that customer-level voltage measurements provide an accurate representation of transmission system low frequency inter- and intra-area oscillations, the modal estimates made based on UT-Austin PMU measurements (120 V) are compared to modal estimates based on Harris Substation PMU measurements (69 kV). The detrended PMU frequency from each of

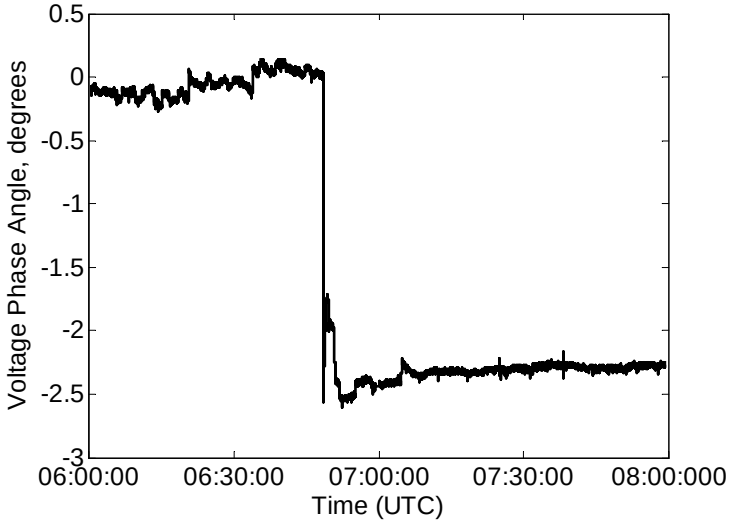

Figure 4.24: Example of a typical jump in the voltage phase angle between the UT-Austin (120 V) and Harris Substation (69 kV)

the two locations is used to estimate the modal frequency and damping. The detrend function is applied to the PMU frequency signal to remove the mean value. An autoregressive (AR) block-processing method as described in [72] is used to estimate the modal frequency and damping. A modified Yule-Walker method is used to estimate the poles, a_1,...,a_N, of the system. The method is applied to a moving window of 10 minutes of ambient data where the estimated system order, N, is set to 64. The AR modified Yule-Walker method is described in Chapter 3.

In Figs. 4.25a and 4.25b, two hours of ambient data are used to estimate the modal damping and frequency. The ambient data is taken from January 8, 2012. In Fig. 4.25a, the data is taken from 00:00 to 02:00 UTC. Modal

damping and frequency estimates are made for both customer-level voltage PMU frequency and transmission level voltage PMU frequency. The modal damping is along the x-axis and the frequency along the y-axis. In Fig. 4.25b, the data is taken from 10:00 to 12:00 UTC.

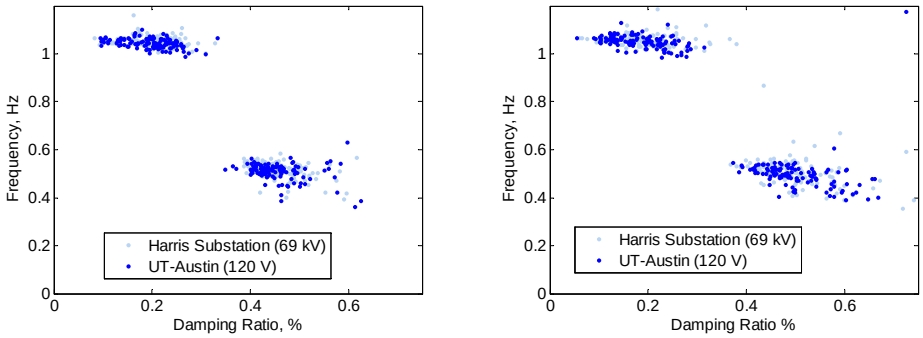

(a) January 8, 2012 00:00 to 02:00 UTC

(b) January 8, 2012 10:00 to 12:00 UTC

Figure 4.25: Two examples of frequency versus damping ratio estimate comparisons for January 8, 2012 ambient PMU data

For the PMU stations' location (central Texas) and at the time of the measurements, the dominant modal frequencies are approximately 0.5 Hz and 1.0 Hz and are present in both the customer-level voltage and transmission voltage level measurements. The 0.5 Hz mode falls under the defined inter-area mode range and the 1.0 Hz mode falls under the defined intra-area mode range [4]. It is evident from the modal estimates that customer-level voltage PMU measurements provide a good representation of the ambient response of the power system.

For the modal results from each two hour window of ambient PMU

data, a class identification algorithm is applied to group the estimates into meaningful subgroups. The class identification algorithm is described in [73]. An example of how the algorithm is used to detect a subgroup of modal estimates is given in Fig. 4.26. Each subgroup of estimates in Fig. 4.26 is assigned a unique color. For example, the subgroup of estimates identified as the 1.0 Hz mode are blue and the subgroups of estimates identified as the 0.5 Hz mode are pink. The mode estimates that do not belong to either of these subgroups are considered noise and are assigned the color black in Fig. 4.26. The center of each subgroup is also marked with an "x". The center is the mean value of the damping estimates in the subgroup and the mean value of the frequency estimates in the subgroup.

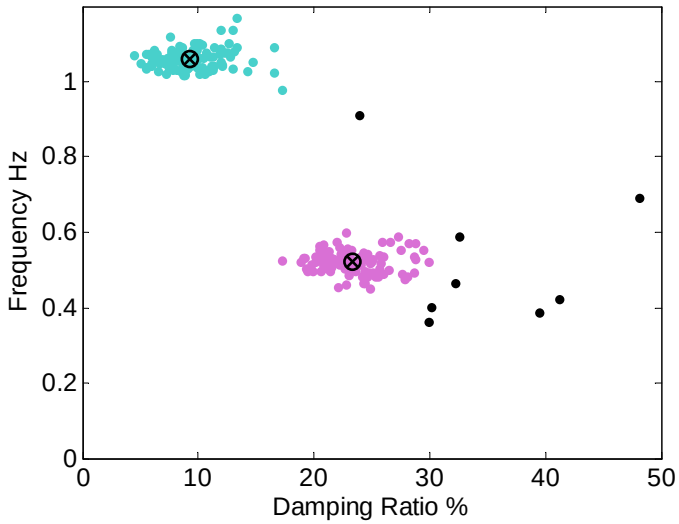

Figure 4.26: Example of how a class identification algorithm detects subgroups of 1.0 Hz and 0.5 Hz modes

The class identification algorithm is used to automate the detection of subgroups of modes. The automated class identification algorithm is applied to an entire 24 hour period of two sets of synchrophasor data to compare the modal content in each set of synchrophasor data. The follwing 5 steps describe how this comparsion is accomplished. The steps are as follows:

- *Step 1:* The Yule-Walker algorithm is used to estimate modal damping and frequency for a 10 minute window of customer-level voltage synchrophasor data.
- *Step 2:* The moving window is applied to 2 hours of data. All modal estimates from each 10 minute window spaning the entire 2 hours is saved.
- *Step 3:* The class identification automatically identifies the center of each detected subgroup created by the saved modal estimates. The center of each detected subgroup for the 2 hour data are saved.
- *Step 4:* Steps 1 to 3 are repeated for the next 2 hours of synchrophasor data and is repeated again until the entire 24 hours of synchrophasor data are examined.
- *Step 5:* Steps 1 to 4 are repeated for the transmission level synchrophasor data.

These steps are applied to synchrophasor data with the results shownin Fig. 4.27. The center of each detected subgroup is shown for an entire day of

customer-level voltage and transmission level synchrophasor data. Fig. 4.27a shows how the 0.5 Hz mode changes throughout the day. The top subplot shows the average frequency of the mode and the bottom subplot shows the average damping of the mode. Each subplot compares the estimates made using the transmission level voltage PMU data taken at Harris Substation (solid line) to the customer-level voltage PMU data taken at UT-Austin (dotted line).

Fig. 4.27b is a plot of the 1.0 Hz mode. The top subplot shows the frequency and the bottom subplot shows the damping comparing the transmission level voltage PMU data taken at Harris Substation (solid line) to the customer-level voltage PMU data taken at UT-Austin (dotted line).

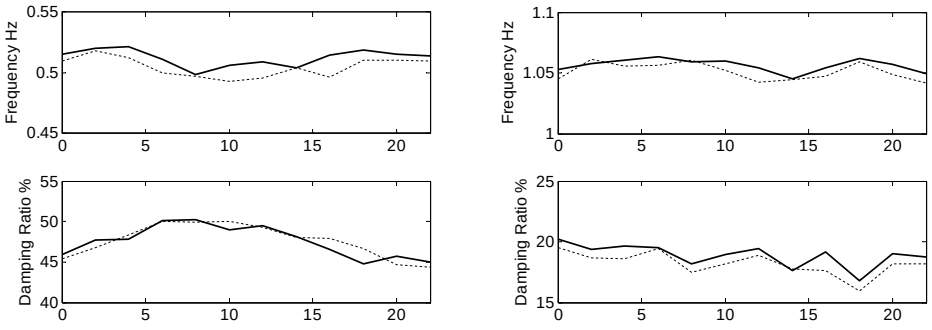

(a) *0.5 Hz mode* Harris Substation (solid line) and UT-Austin (dotted line)

(b) *1.0 Hz mode* Harris Substation (solid line) and UT-Austin (dotted line)

Figure 4.27: Frequency and damping ratio averages for *0.5 Hz and 1.0 Hz modes* at Harris Substation (solid line) and UT-Austin (dotted line) compared for entire day of January 8, 2012

The average modal damping and frequency estimates for the 0.5 Hz and

Table 4.5: Estimated modal damping and frequencies for January 8, 2012 ambient

	Distribution PMU (120 V)		Transmission PMU (69 kV)	
Mode	Frequency	Damping	Frequency	Damping
1	0.50	47.61	0.51	47.53
2	1.05	18.20	1.06	18.89

1.0 Hz mode taken from Fig. 4.27 is summarized in Table 4.5. The estimates based on the customer-level voltage synchrophasor data closely match the estimates based on the transmission synchrophasor data.

The error between the modes estimated from the customer-level voltage PMU data and transmission level voltage PMU data are shown in Fig. 4.28. Fig. 4.28a shows the error for the 0.5 Hz mode and Fig. 4.28b shows the error for the 1.0 Hz mode.

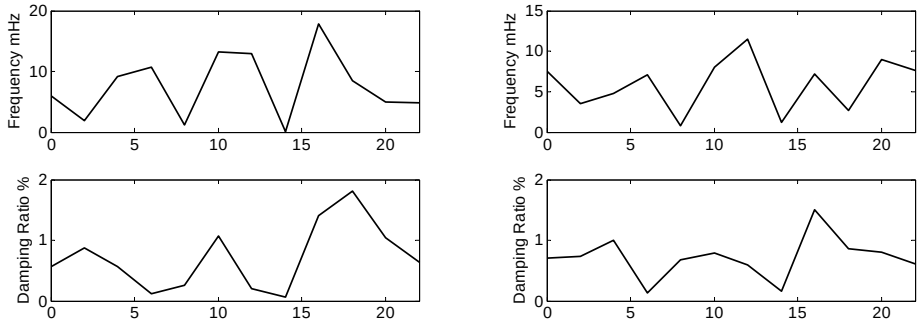

(a) *0.5 Hz mode* (b) *1.0 Hz mode*

Figure 4.28: Error between frequency and damping ratio averages for *0.5 Hz and 1.0 Hz modes* at Harris Substation (solid line) and UT-Austin (dotted line) compared for entire day of January 8, 2012

The error in modal frequency is very small at all times; the units for the y-axis is in mHz. However, for the 0.5 Hz mode, a difference of nearly 2% is seen in the modal damping estimate for the window of data starting at 18:00 UTC. The plot of the modal estimates made for the window of data from 18:00 to 20:00 UTC is shown in Fig. 4.29. The plot shows the range of damping estimates is very high, trailing off especially as the damping estimates increase. Since the error is highest for highly damped modes, this small mismatch is not a problem. Only when damping estimates reach a margin close to 5 to 3% should alarms be raised [24].

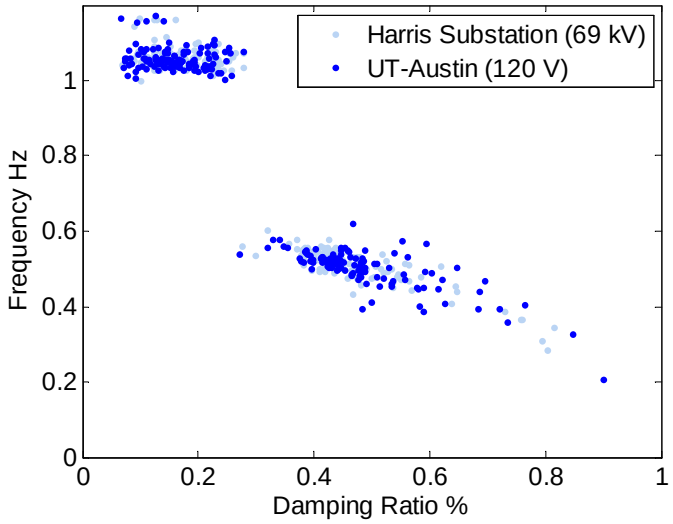

Figure 4.29: Damping error increases only when modes are highly damped for the 0.5 Hz mode

Section 4.5.2 explains the voltage phase angle difference between UT-Austin and Harris Substation by creating a model of the University of Texas

at Austin campus and its connection to the grid. The voltage phase angle difference between these two PMU locations is shown in Figs. 4.23 and 4.24.

4.5.2 Steady State Model of UT Campus

A steady state model is used to analyze the power flow from campus generators to the campus load and determine if the power flow creates the voltage phase angle difference between the UT Austin campus PMU (120-V) and the Harris Substation PMU (69 kV) shown in Fig. 4.24. The University of Texas at Austin campus generates its own power to meet the demands of campus load and creation of chilled water for air conditioning on campus. The campus is connected to the rest of the power grid managed and operated by the Electric Reliability Council of Texas through Harris Substation. This connection to the grid provides frequency and voltage support to the campus power system [74]. The steady state model of this system was created in PSS/E. The data for the PSS/E model was provided in [74, 75].

Figure 4.30 shows the campus power system modeled in PSS/E. The total generating capacity of the system is 140 MW. The main campus load is placed at Bus 2 which is located at the end of the line separating the campus generator bus (Bus 1) from the 12.0 kV Harris substation bus (Bus 2). The PMU located at the 120 V level is located at the campus Engineering Science building (Bus 5) and the 69 kV PMU at Harris Substation 69 kV bus (Bus 3). A small load is located at the 120 V level to represent the load near the customer-level voltage PMU location.

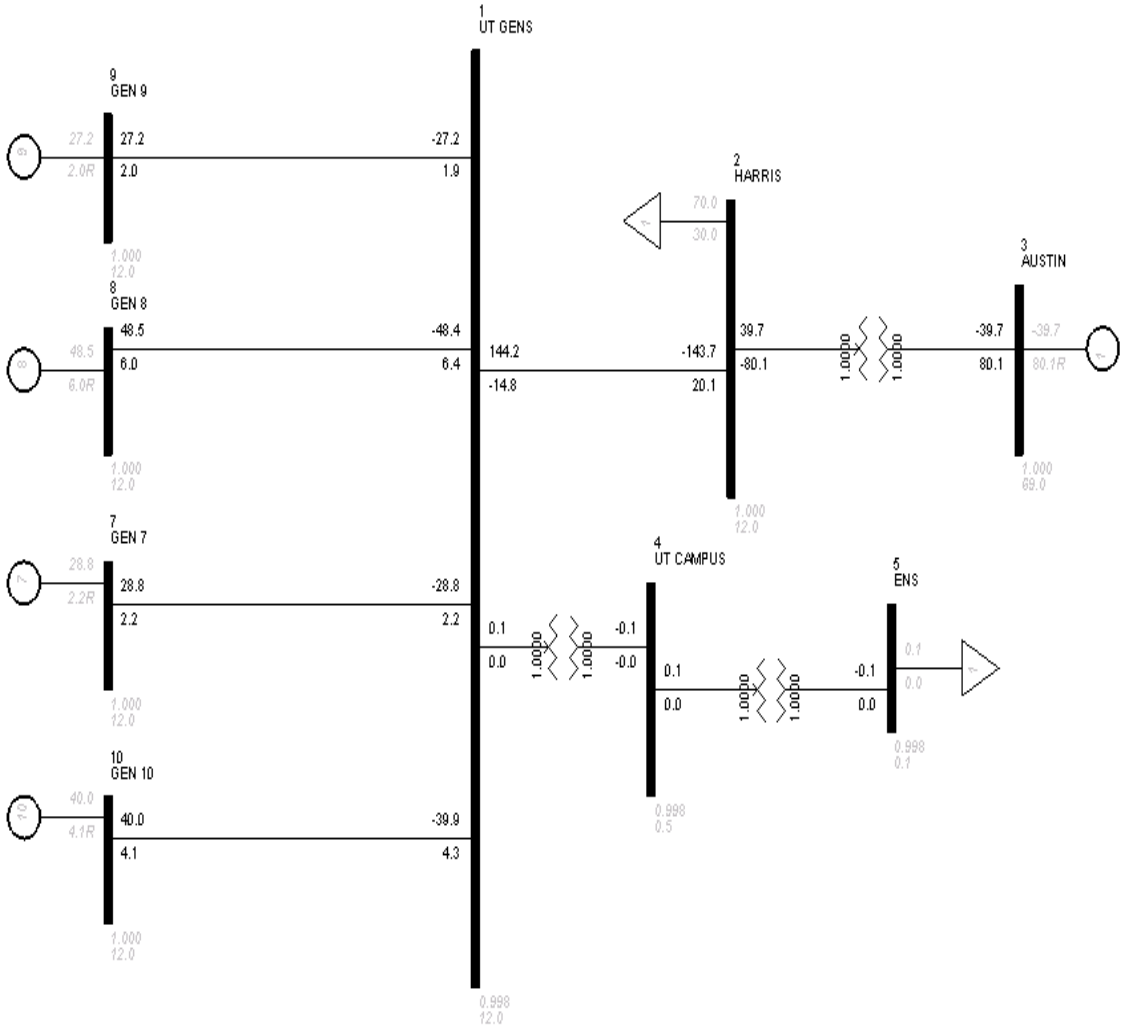

Figure 4.30: PSSE model of UT Austin Campus and Harris Substation

Two different scenarios are used to show how the level of power generated on campus impacts the voltage phase angle between the two PMU locations. For the first scenario, the total campus load and the matching generation is set to 50% capacity. The resulting voltage phase angle difference between Bus 3 and Bus 5 is $\theta = 0.59\,^{\circ}$. This value is similar to what might be expected as shown in the actual PMU measurements plotted in Fig. 4.23. For the second scenario, the generators are run at maximum capacity. The voltage phase angle changes to $\theta = 1.67\,^{\circ}$ indicating that the amount of generation on campus has an impact on voltage phase angle similar to the observation plotted in Figure 4.24. However, the difference in phase angle in the PSS/E simulation does not exactly match the differences seen in the real data. This discrepancy could arise from the approximate values used to model the line impedance in the PSS/E model.

4.6 Summary

The results reported in this chapter make evident that customer-level voltage PMU measurements provide an accurate representation of transient and ambient responses of the transmission power system. The customer-level voltage phase angle measurements were plotted with the state estimated voltage phase angle and shown to be similar. Comparison of transient response effects on frequency and voltage phase angle indicated that the customer-level voltage measurements provided a clear picture of the system transient response. The estimation of modal frequency and damping illustrated the ac-

curacy of distribution measurements as representation of the power system's ambient response. The results from this chapter indicate that use of customer-level voltage PMU measurements are accurate for transmission system analysis and will be used for the remainder of the research presented in this dissertation.

Chapter 5

Algorithm for Screening Synchrophasor Data for Power System Events

Synchrophasor networks generate large volumes of synchrophasor data making it difficult to easily discover meaningful information about power system behavior and events. The purpose of the research presented in this chapter is to take the initial steps necessary to better understand power system behavior by detecting power system events of importance. Events that occur on the grid that are visible in the synchrophasor data include but are not limited to generator unit trips, transmission line trips, and sudden loss of load. To detect power system events, a novel algorithm is created which is applied to automatically detect events in the synchrophasor data. The algorithm detects events based on the abnormal response of the power system to events compared to normal operating conditions. When an event occurs, the normally occurring low-frequency electromechanical oscillations increase in amplitude.

Three different signal processing techniques are utilized to help detect power system events in the synchrophasor data. These techniques are fast Fourier transform method, Matrix-Pencil method, and the Yule-Walker Spectral method and were described in detail in Chapter 3. A fourth method uses

the maximum difference in a window of data to help detect events. All four methods are applied to a moving window of data for an entire hour of synchrophasor data. For the signal processing methods, the peak values for each window are saved. For the maximum difference method, the calculated maximum difference is saved for each window. Statistical methods are applied to the saved peak values to determine if an event occurred for a particular window of data. If two or more methods detect a possible event, the window is marked as containing an event and the data is saved for further analysis. This method is applied to all frequency and relative phase angle difference signals available at the time of the analysis. The number of signals is dependent on the number of network PMUs in operation.

Section 5.1 provides an overview of the synchrophasor data used for event detection and a description of the type of events that are detected. In Section 5.1.2, a description of the screening algorithm development is provided and includes a more detailed description of the signal processing and statistical methods used by the algorithm. In Section 5.3, results from the application of the algorithm to synchrophasor data are described. A chapter summary is provided in Section 5.4.

- **Publication**: Part of the work presented in this chapter has been published in [15–17]
  - Allen, A.J.; Santoso, S.; Muljadi, E.; "Phasor Measurement Unit (PMU) for Wide Area Monitoring, Protection, and Control (WAMPAC)

Applications," NREL Report, December 2012

– Allen, A.J.; Sang-Wook Sohn; Grady, W.M.; Santoso, S.; "Algorithm for Screening PMU Data for Power System Events," IEEE International Smart Grid Technologies, October 2012, Berlin, Germany

– Sang-Wook Sohn; Allen, A.J.; Kulkarni, S.; Grady, W.M.; Santoso, S.; , "Event detection method for the PMUs synchrophasor data," Power Electronics and Machines in Wind Applications (PEMWA), 2012 IEEE , vol., no., pp.1-7, 16-18 July 2012

5.1 Overview

5.1.1 Independent Synchrophasor Network and PMU Data

As described in Chapter 2, large amounts of synchrophasor data are generated by the Texas Independent Synchrophasor Network since the first remote PMU station was added in January 2009. Because so much data has been generated and is still being generated, it is difficult to detect events of interest and analyze them for power system studies. Resources such as ERCOT Daily Grid Operations Reports [12] provide information on sudden loss of power above 450 MW caused by generating unit trips and information on line contingencies (total peak generating capacity in ERCOT is above 65 GW). In addition, it is generally straightforward to visually detect large sudden imbalances in generation and load by monitoring the frequency. However, information related to events like transmission line reclosing and trips and

other equipment trips are not readily available. The research presented herein examines if these system events are visible in the PMU data and if it is possible to automatically detect events of interest.

The term relative phase angle difference (RPAD) was introduced in Chapter 2. The RPAD signal is used by the algorithm to detect power system events as well as the PMU frequency signal. Though the frequency is calculated by the PMU, different categories of events are visible in the frequency data that are not easily detected in the RPAD. Also, the frequency is taken from a single location while the RPAD is actually the angle difference between two separate PMU locations. Some events that occur closer to one PMU location are stronger in the measured signal of that PMU, and therefore may be more easily detected in the frequency signal. The event in the measured RPAD signal may be drowned out by the voltage phase angle from the opposite PMU location. Also, the RPAD may reveal possible event sources that are not as obvious in the frequency signal. One possible drawback is the difficulty to diagnose and to categorize events in the case where are two independent events occurring at the same time at two different locations. However, if this happens, other PMU signals can collectively help decipher the event.

5.1.2 Screening Algorithm

The term *event* in this research is used to describe large disturbances on the power system and sudden changes in power output at wind farms. Large disturbances include but are not limited to short circuits on transmission lines,

protective relay actions required to clear the fault such as transmission line trip and reclosing actions, or a large and sudden loss of generation or load. A sudden change in renewable energy includes but is not limited to large ramping up or down of wind farm power output. Large disturbances excite a single or multiple modes within the power system which can be measured as oscillations in PMU voltage data. These oscillations typically consist of one strong mode with the frequency of the oscillation between 0.1 and 2.0 Hz, the amplitude of the oscillation is typically higher than oscillations induced by random load switching, and the oscillation is quickly damped out if the system is stable. For example, a low-frequency oscillation of 0.3 Hz with a damping constant of 10% has a time constant of 5.3 seconds (the signal would drop to 37% of its original value after 5.3 seconds). This information is used to detect events in the PMU data. However, it is difficult to verify the cause of many of the detected events. The root cause of a few of the detected events can be identified; however, not all causes are known since information on power system disturbances is not always available or shared. Most of the guessed causes of the event are based on clues present in the PMU data. Also, wind power induced events are difficult to detect because detailed measurements of renewable generation power output is necessary for a thorough analysis.

Because the PMU measurements used in this report are taken at customer-level voltage of 120 V, events that occur on the distribution system may be measured as well. However, the voltage magnitude at the customer-voltage level is more heavily impacted by events that occur at the distribution sys-

tem. Large events that occur on the transmission system are also visible at multiple PMU locations rather than at a single PMU location for distribution events. If it is unclear if a detected event occurred on the distribution system or the transmission system, the data from multiple PMUs can be compared during the time of the event and the voltage magnitude can be checked as well. If the event appears at only one PMU location and the voltage magnitude drops significantly (to 95% or less of rated voltage), then the event should not be considered a transmission system event. This type of event should be attributed to the distribution system changes and should not be considered for transmission system analysis. The purpose of the PMU network is to conduct analysis on transmission system behavior but because measurements are taken at customer-level voltage, distribution system events are recorded in addition to transmission system events. Therefore, by using the guidelines above, it is important to distinguish between these two types of events so that distribution system events will not be incorrectly identified and interpreted as transmission system events.

5.2 Screening Algorithm Development

This section describes the algorithm developed to screen PMU data taken from PMUs within the Texas Independent Synchrophasor Network for power system events. The synchrophasor data consist of voltage magnitude, phase angle, and frequency for each PMU station and are saved hourly in comma separated value (CSV) format. All PMU frequencies and all possi-

ble voltage phase angle separations between PMU stations are analyzed. A flowchart describing the algorithm is shown in Fig. 5.1. In the flowchart, the signal to be analyzed for the hourly PMU file uploaded is assigned to the variable y. The algorithm does not analyze the entire hour of data at once, but instead analyzes a window of synchrophasor data, assigned to the variable $yWindow$. The subroutine analysis on the window of data $yWindow$ is applied for each moving window of data until the end of the entire hour of the signal y is reached.

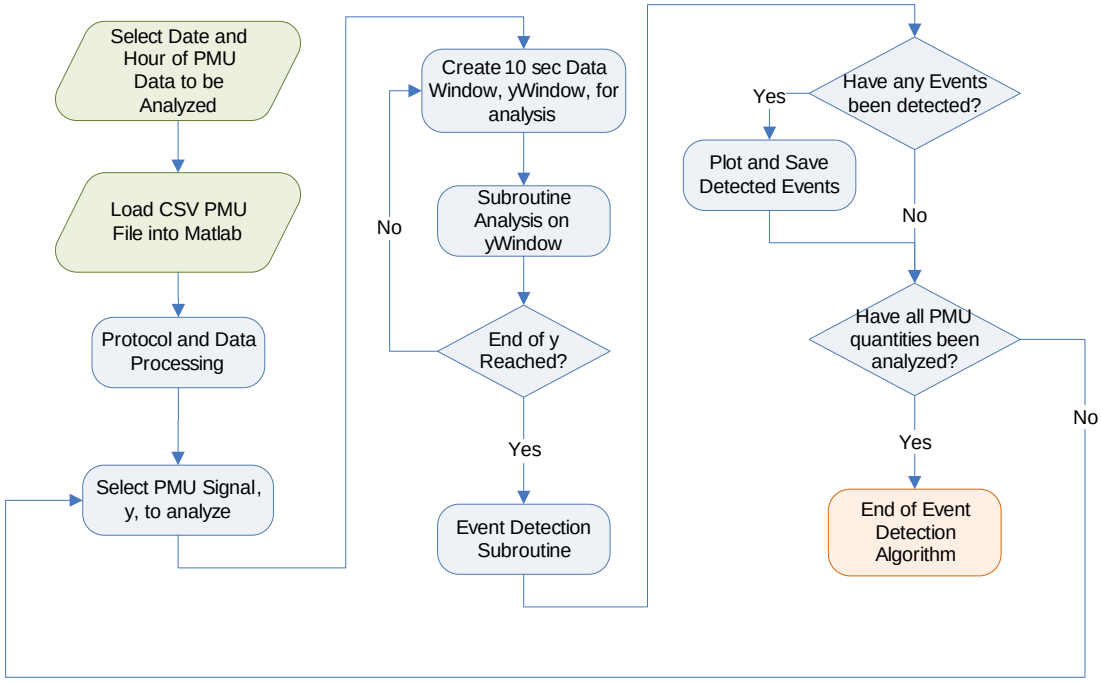

Figure 5.1: Flowchart listing the processes used to screen for events in PMU data

In Section 2.4, the PMU CSV format and the protocol created to orga-

nize and label PMU data for analysis was described. The same methods used to load PMU data for analysis and "unwrap" voltage RPAD data are used in this chapter. To illustrate the amount of information present in PMU data, an entire day of voltage RPAD data between UT-Austin and McDonald is plotted in Fig. 5.2. Each voltage RPAD and PMU frequency data set is screened for possible events.

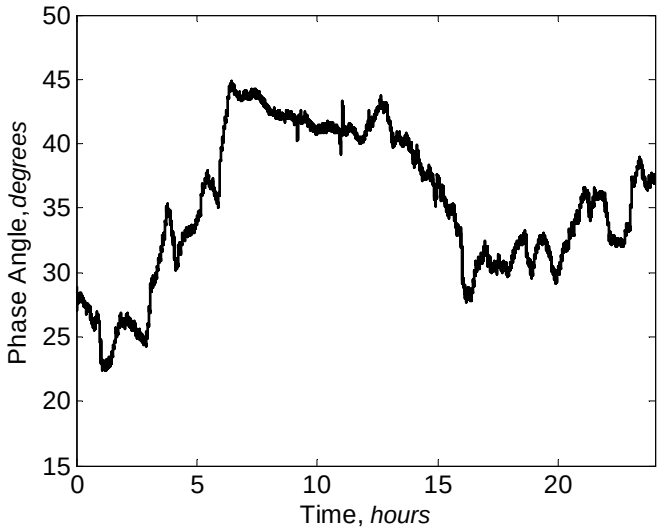

Figure 5.2: Voltage RPAD between UT-Austin and UTPA for 24 hours

Section 5.2.1 describes the methods used to screen for events in the synchrophasor data. Four different methods were used since each method is able to detect different types of events. The methods are Fast-Fourier Transform (FFT), Matrix-Pencil, an analysis based on the difference between the minimum value and maximum value within a window of data (Min-Max method), and Yule-Walker Spectral (YWS) method. The FFT and YWS are spectral

methods while the Matrix-Pencil is parametric. All methods are applied to a window of PMU data where resulting peak values from each method applied to the data window are saved. The peak values from each data window for an entire hour of synchrophasor data are used to detect events. Any peak magnitudes greater than three standard deviations are marked as possible events. Section 5.2.2 describes how the results from each of the methods are used to detect events. If two or more methods detect an event in the same data window that window is marked as containing an event. The event is plotted and data saved for further analysis. The algorithm was developed in Matlab and uses functions from the Signal Processing Toolbox and user-defined functions [59].

5.2.1 Event Screening Methods

In order to screen for events within each hourly PMU file, an overlapping, moving window is applied to the PMU data. The window size is 10 seconds long and overlaps half of the previously windowed data. The moving window method is illustrated in Fig. 5.3.

Each window of data is analyzed for possible events by applying the four different detection methods mentioned. All methods but the Min-Max method are based on the strength of the estimated frequency content. Only frequencies below 2 Hz are examined (the frequency range of inter- and intra-area oscillations [76]). Each method is described in detail below.

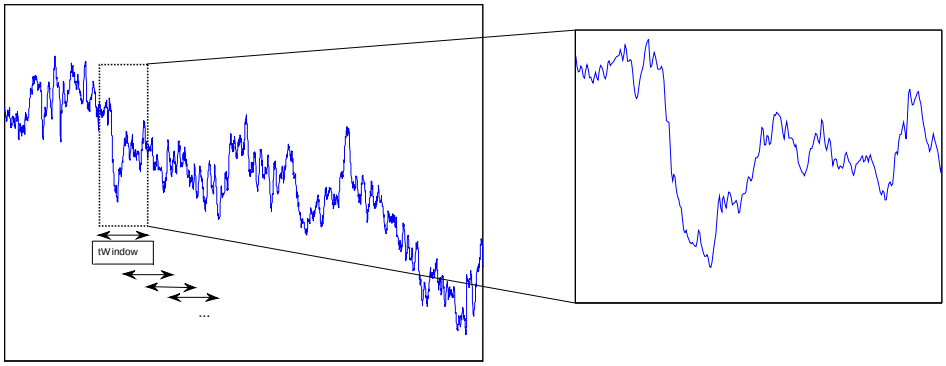

Figure 5.3: Illustration of moving window applied PMU data (right) and 10 second data window for analysis (left)

5.2.1.1 Fast Fourier Transform

Before the method is applied, the data window is differentiated using the Matlab function `diff` to remove dc offset in the data to facilitate detection of events in the low frequency range below 2 Hz. Differentiating the data increases the noise in the data, however, it has been found that the magnitude of frequencies associated with events in the data tend to be very high. Therefore, increased noise is not a concern for this analysis.

The Fast Fourier Transform utilizes the Matlab function `fft` to detect events in the PMU data. This function returns the discrete Fourier transform calculated using the FFT algorithm. The discrete Fourier transform is used to find the strongest frequency component within the data window. The maximum amplitude, $|Y(f)|$, is saved for frequencies in the range of $0 < f \leq 2$ Hz. An example is presented to illustrate how the algorithm uses FFT to detect

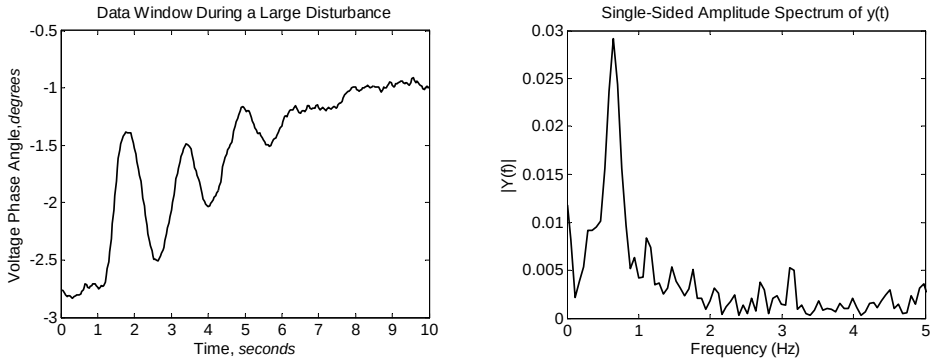

(a) Window of voltage RPAD (b) Spectral Analysis of window

Figure 5.4: Example of RPAD Event and Analysis

events. The method is applied to a data window of the voltage phase angle in Fig. 5.4a containing oscillations induced by a large event. The discrete Fourier transform applied to the data window containing event information is shown in Fig. 5.4b. The Fourier transform in Fig. 5.4b shows a strong 0.64 Hz component. In the algorithm, the peak magnitude, $|Y(f)| = 0.03$, would be saved for this data window.

The FFT method is applied to each 10 second data window for the entire hour of PMU data. The average and standard deviation are calculated for all saved peak magnitudes. Any saved magnitudes above three standard deviations are tagged as possible events. A plot of the peak magnitudes from each 10 second data window is shown for an hour of PMU frequency in Fig. 5.5. The average and standard deviation of the peak magnitudes are indicated. The outliers, or possible events, are also marked in Fig. 5.5.

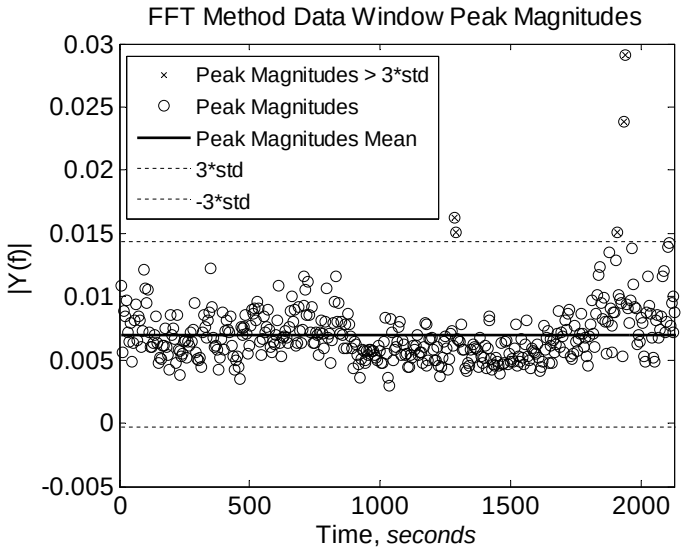

Figure 5.5: For the FFT method, data windows during which the peak magnitude exceeds 3 times the standard deviation of peak magnitudes for the entire hour are marked with an 'x'

5.2.1.2 Matrix Pencil

In this subsection, the Matrix-Pencil method and how it is used in the algorithm to detect events is described. The Matrix Pencil method is applied to a 10 second window of PMU data. Fig. 5.6a shows the reconstructed signal (solid line) using the estimated parameters compared to the original signal (dotted line). Because noise was removed using singular value decomposition (SVD), parameters were not estimated to fit the noise but only the "true" modes present in the data.

The values of the two highest estimated amplitudes are saved for each data window. The method is repeated for the entire hour of data. It is assumed

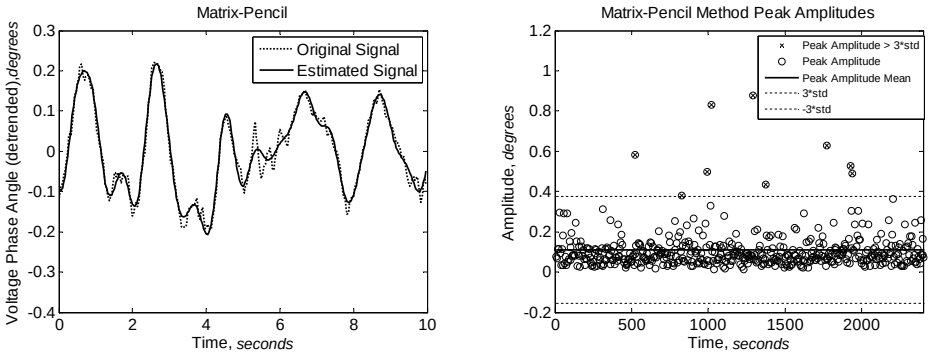

(a) Matrix-Pencil Method used to estimate parameters

(b) Peak magnitudes for an entire hour

Figure 5.6: For the Matrix-Pencil method, data windows during which the peak magnitude exceeds 3 times the standard deviation of peak magnitudes for the entire hour are tagged

that if an event is present in the data, the max amplitude would be significantly larger than the max amplitude from a data window without any events. After the two highest magnitudes are saved for all data windows for the entire hour of synchrophasor data, the averages and standard deviations for the highest and second highest magnitudes are calculated separately. Detection of possible events is similar to the FFT method, any magnitudes above three standard deviations are tagged as possible events as shown in Fig. 5.6b.

5.2.1.3 Yule-Walker Spectral

The Yule-Walker Spectral method is similar to the FFT method but utilizes the `pyulear` function from the Matlab Signal Processing Toolbox [59]. The `pyuler` function calculates the power spectral density (PSD) using the autoregressive (AR) Yule-Walker method. The PSD for a data window con-

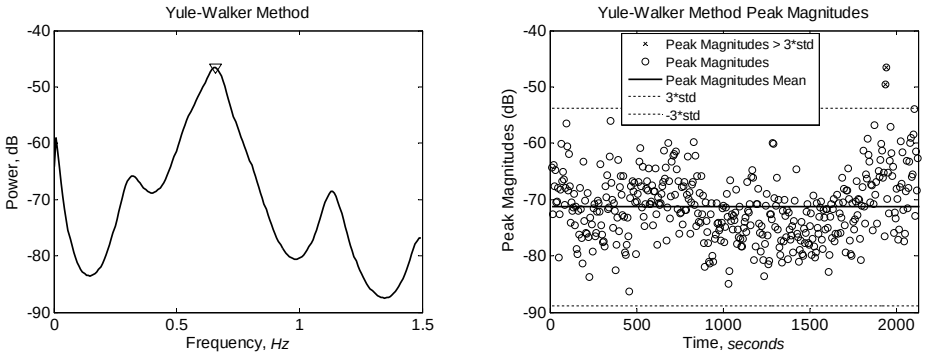

(a) Frequency content in PMU signal during a large disturbance

(b) Peak magnitudes for one hour of PMU data

Figure 5.7: For the Yule-Walker method, data windows during which the peak magnitude exceeds 3 times the standard deviation are tagged

taining an event is given in Fig. 5.7a.

The peak value in the PSD in dB is marked. The peak values for each PSD of the data window are saved. This is repeated for the entire hour. The average and standard deviation of the maximum magnitudes are calculated. Magnitudes above three standard deviations are tagged as possible events as shown in Fig. 5.7b.

5.2.1.4 Min-Max

For this method, the difference between maximum and minimum values within the data window is calculated. The difference for each data window for the entire hour is saved. This method is sensitive because it also detects gradual changes in the signal over the 10 second data window that are not caused by power system events. Possible events are detected by calculating

the average and standard deviation for all the data window differences for the entire hour of PMU data. The differences that exceed three times the standard deviation are marked as possible events as shown in Fig. 5.8.

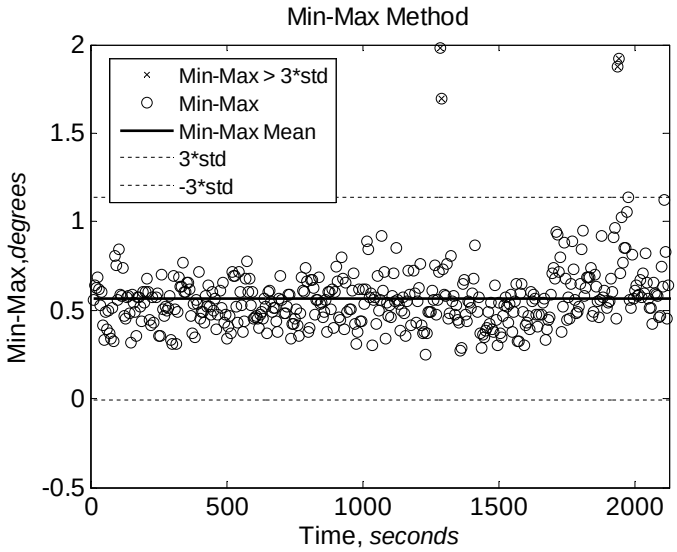

Figure 5.8: For the Min-Max method, data windows during which the difference between minimum and maximum values in a 10 second data window exceeds 3 times the standard deviation are tagged

5.2.2 Method Results for Marking Events

After all methods have been used to screen for possible events in the PMU data, the time stamps of data windows marked as containing possible events are compared for all methods. Fig. 5.9 shows an example of the results for possible events in the RPAD between UT-Austin and McDonald. If two or more methods detect a possible event in the same data window, that data window is marked as containing an event and the synchrophasor PMU data

for that window is saved and plotted. In Fig. 5.9, an event is detected at 1285 seconds by both the Matrix-Pencil and Min-Max methods. Another event is detected at 1935 seconds by all four methods. This event is analyzed further in Section 5.3.1.

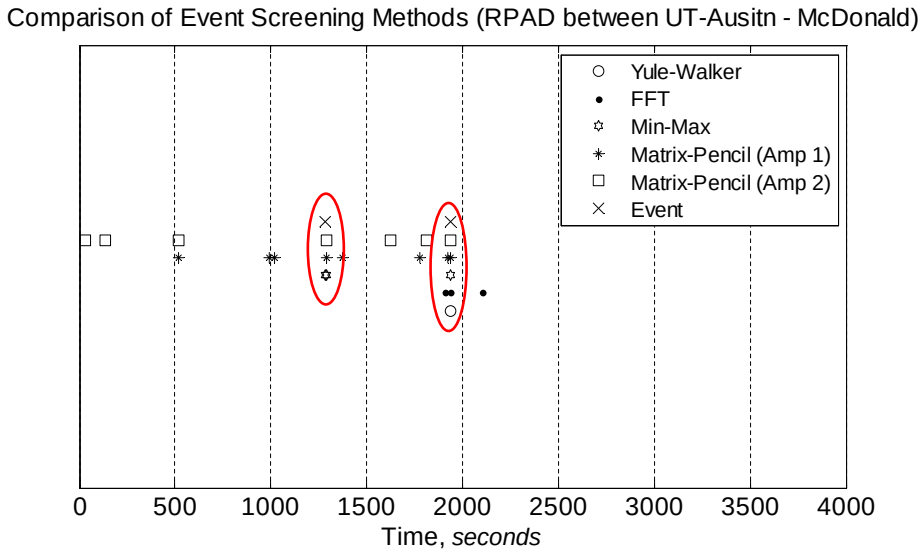

Figure 5.9: Comparison of all the screening algorithms

5.3 Application and Demonstration

The results from the algorithm are examined by screening 24 hours (00:00 to 23:59 UTC) of PMU data for power system events. The UT-Austin PMU and McDonald PMU were operational during this time period. The voltage RPAD between UT-Austin and McDonald and the frequencies at each location are analyzed. An example of 24 hours of UT-Austin PMU frequency is shown in Fig. 5.10 to illustrate the difficulty of visually screening for events in

PMU data. The PMU frequency is a calculated quantity that is based on the measured voltage phase angle [21] and differs slightly across the power system as shown in the PMU frequencies in this section. High precision PMU calculated frequencies provide more information than a single system frequency.

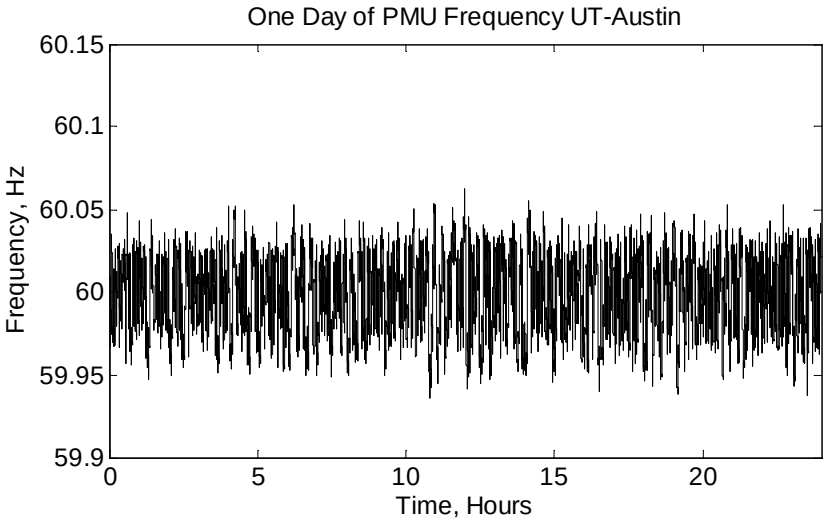

Figure 5.10: One day PMU frequency UT-Austin

Two types of events found in the data are described here to illustrate how the screening algorithm detects events. The first event in Section 5.3.1 was caused by a sudden loss of generation. The event occurred at 23:33 UTC (17:33 CST) and is visible in all three signals. The second event in Section 5.3.2 was probably caused by a recloser operation visible only in the McDonald PMU data. Strong oscillations visible only at the UT-Austin PMU are also examined in Section 5.3.2. The source of the oscillations in the UT-Austin PMU data is unknown.

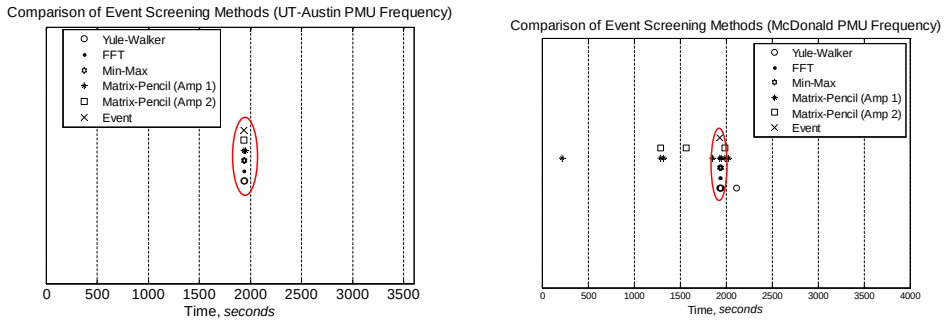

(a) UT-Austin PMU frequency (b) McDonald PMU frequency

Figure 5.11: Comparison of system wide events detected in PMU frequency for hour 23:00 UTC

5.3.1 Screening Results for System Wide Event Caused by Loss of Generation

At 23:33 UTC a generating unit tripped resulted in a loss of 810 MW of generation and a frequency decline to 59.774 Hz. The ERCOT load at the time was 35,000 MW [12]. The frequency at UT-Austin and McDonald are screened for events using the methods described in Section 5.2. The results from the algorithm are shown in Fig. 5.11a and Fig. 5.11b. The generating unit trip was the only event detected in both PMU frequencies and was detected by all four methods in the UT-Austin PMU frequency in Fig. 5.11a. In Fig. 5.11b, the disturbance was detected and tagged in the McDonald PMU frequency but the Matrix-Pencil method detected other possible events as well (represented in Fig. 5.11b as $\square$ and $*$). However, since the Matrix-Pencil method was the only method to detect a possible event, these data windows were not tagged as actual events.

The PMU frequencies data window for the event is plotted in Fig. 5.12.

Both PMU frequencies decline to 59.76 Hz which differs slightly from the ERCOT Grid Report [12] frequency decline possibly because the PMU frequency are taken at specific buses rather than representative of the system frequency. It is possible that the PMU data also has a higher resolution than the ERCOT data.

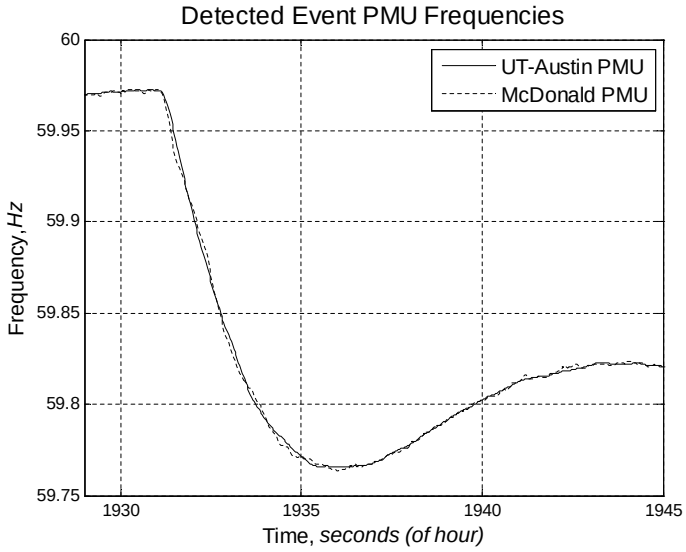

Figure 5.12: Large disturbance caused by a sudden 810 MW loss of generation impact on the UT-Austin PMU and McDonald PMU frequencies

The same generating unit trip was detected in the RPAD between UT-Austin and McDonald as shown in Fig. 5.13. An additional event was detected in the RPAD signal but it is not clear if it is an actual event or if the threshold values in the algorithm are too sensitive. The RPAD during the event is plotted in Fig. 5.14. The voltage phase angle has an approximate initial upswing of 1.5°. The amplitude of the oscillation is not very large and it is possible that

the location of the generating unit that tripped is located far away from the UT-Austin and McDonald PMU stations. The oscillations in the voltage phase angle prior to and after the event are much smaller and have an amplitude between 0.1 to 0.25°.

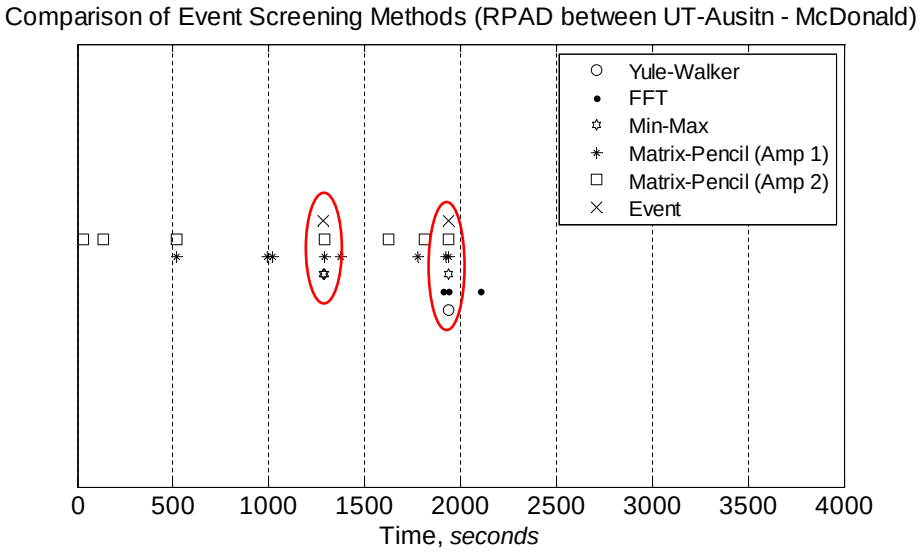

Figure 5.13: Events detected in the voltage RPAD between UT-Austin - McDonald PMU for 23:00 UTC

The examples illustrate that the screening algorithm can very easily detect a large event in all the PMU signals analyzed. Screening for smaller events in the synchrophasor data are examined next.

5.3.2 Screening Results for Local Events with Unknown Causes

The methods are further evaluated by screening PMU frequencies and RPAD data for smaller local events. In this section, an hour of PMU data

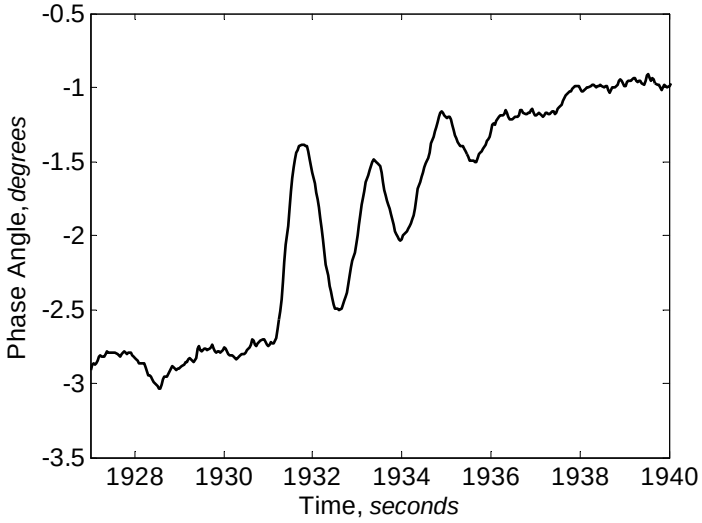

Figure 5.14: Large disturbance caused by a sudden 810 MW loss of generation impact on the voltage RPAD between UT-Austin - McDonald

(17:00 UTC) is screened for possible events. The algorithm is applied to the UT-Austin PMU frequency and the McDonald PMU frequency with results shown in Fig. 5.15a and Fig. 5.15b.

Many of the events detected in the UT-Austin PMU frequency were not detected in the McDonald PMU frequency and vice versa. In the UT-Austin PMU frequency, the events detected starting at approximately 1750 seconds are strong oscillations that are not visible in the McDonald PMU frequency. For comparison, a 20-second window of frequency data is plotted in Fig. 5.16. The UT-Austin frequency (solid line) has stronger, higher magnitude oscillations but it is difficult to identify the strength and frequency of the oscillation based on the plot.

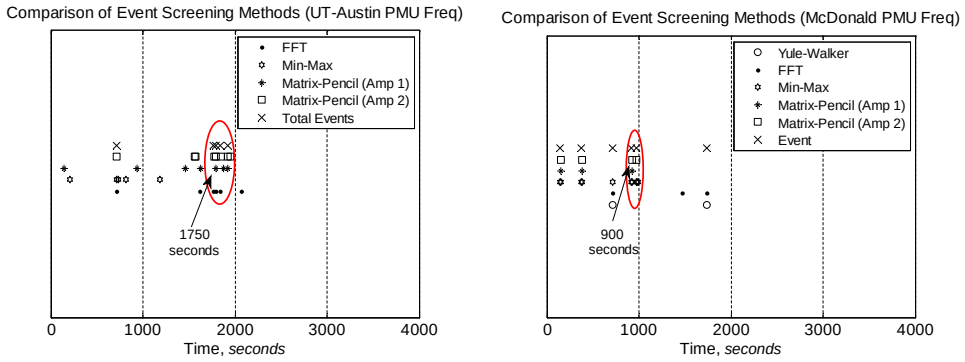

(a) UT-Austin PMU frequency (b) McDonald PMU frequency

Figure 5.15: Comparison of local events detected in PMU frequency for hour 17:00 UTC

The power spectral density (PSD) is calculated to analyze the strength and frequency of the oscillations present in the synchrophasor data. The PSD is stored for each 10 second window and plotted as a contour plot in order to compare the frequency content of the UT-Austin and McDonald PMU signals. The contour plots are shown in Fig. 5.17. From Fig. 5.17 it is easy to see a strong 1 Hz oscillation in the UT-Austin PMU frequency that is not visible in the McDonald PMU frequency for the same time period. The oscillation in the UT-Austin data is strongest from approximately 1600 to 2000 seconds as indicated by the dark red. This is approximately the same time period that the algorithm tagged as a possible event. A 1 Hz oscillation indicates intra-area oscillations [76] (one machine oscillating against a group of machines), but the exact cause of the 1 Hz oscillation is currently unknown. In the contour plot, the frequency on the y-axis is the frequency content of the PMU frequency signal. The PMU frequency is not measured, but calculated from the voltage

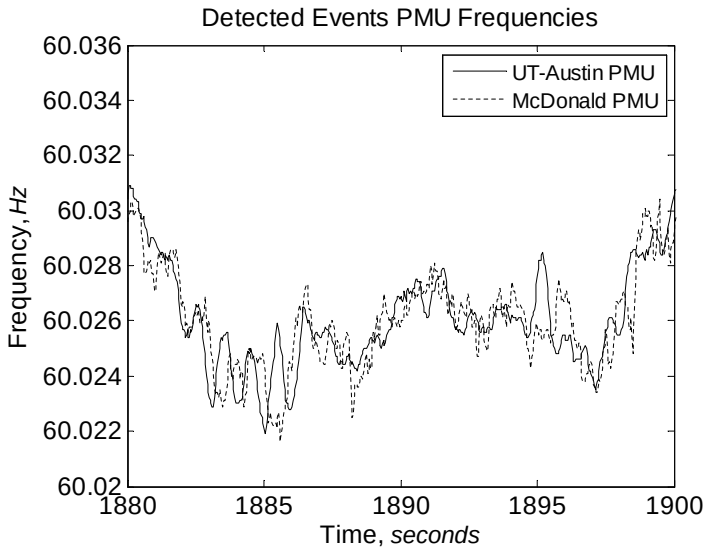

Figure 5.16: Small disturbance event detected in the UT-Austin PMU frequency but not in the McDonald PMU frequency

angle.

In the McDonald PMU frequency, the events detected starting at approximately 900 seconds are damped oscillations that are not visible in the UT-Austin PMU frequency. A 40 second window of frequency data is plotted in Fig. 5.18. The McDonald PMU frequency (dotted line) contains many damped oscillations that are not present in the UT-Austin PMU frequency (solid line). The cause of these oscillations will become apparent when examining the voltage phase angle.

The screening results for PMU RPAD data for one hour (17:00 UTC) is given in Fig. 5.19. The algorithm is able to detect events that were seen in the McDonald PMU frequency at approximately 900 to 1000 seconds shown

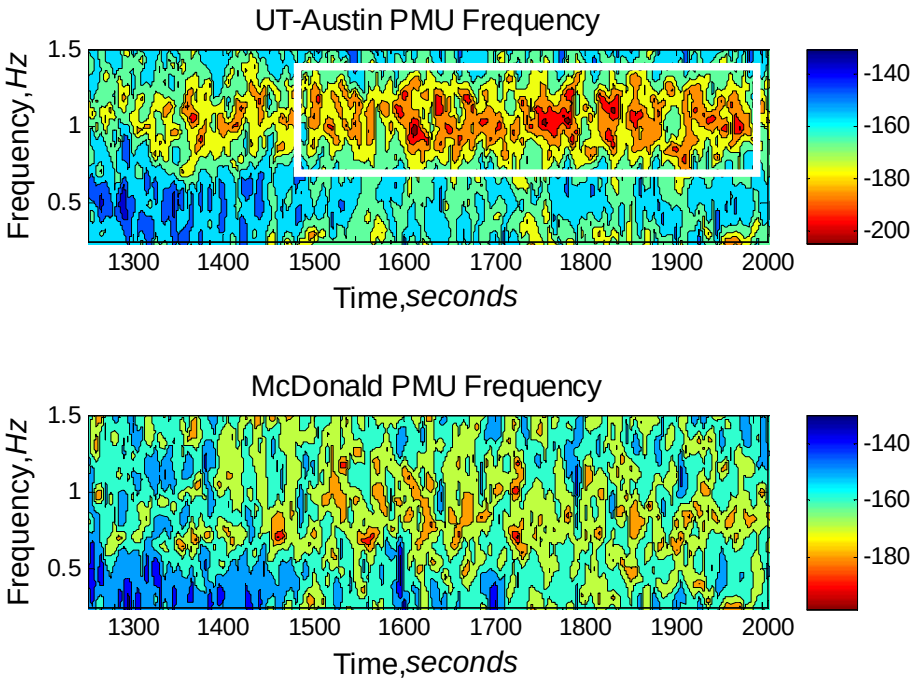

Figure 5.17: Contour plot of the PSD (low-frequency content over time) shows a 1 Hz oscillation present in the UT-Austin PMU frequency signal (top) but the 1 Hz oscillation is absent in the McDonald PMU frequency signal (bottom)

in Fig. 5.15b and Fig. 5.18. However, the events detected in the UT-Austin frequency at approximately 1750 to 2000 seconds (refer to Fig. 5.15a) were not as clearly visible in the voltage phase angle. The FFT and Matrix-Pencil methods were able to detect the oscillation during the 1750 to 2000 second time frame but since these methods did not detect the oscillation simultaneously, they were not tagged as events in the results from the PMU RPAD analysis.

The contour plot for the RPAD signal in Fig. 5.20 indicates that the 1

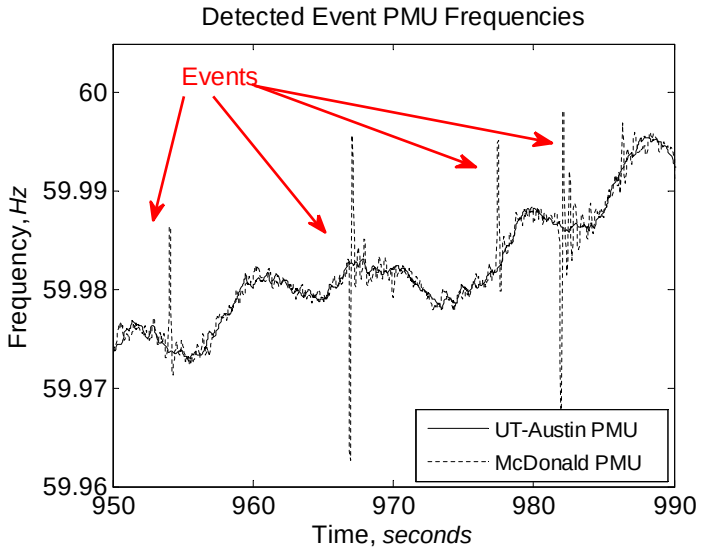

Figure 5.18: Small disturbance event detected in the McDonald PMU frequency (dotted line) but not in the UT-Austin PMU frequency (solid line)

Hz oscillation is strong during the same time period as shown in Fig. 5.17 (top) but contains an approximate 0.6 to 0.7 Hz oscillation as well. The contour plot for the entire hour of data shows that the 1 Hz oscillation is not as strong at other times.

The events detected in the McDonald PMU frequency in Fig. 5.18 were also detected in the PMU voltage phase angle. The RPAD between UT-Austin - McDonald for this series of events is plotted in Fig. 5.21. The sudden change and return of the phase angle indicates multiple reclosing events. Since the oscillations are only visible in the McDonald PMU frequency, it is assumed that the event occurred near McDonald (local event). However, it is difficult to tell at what voltage level the recloser is located (distribution or transmission

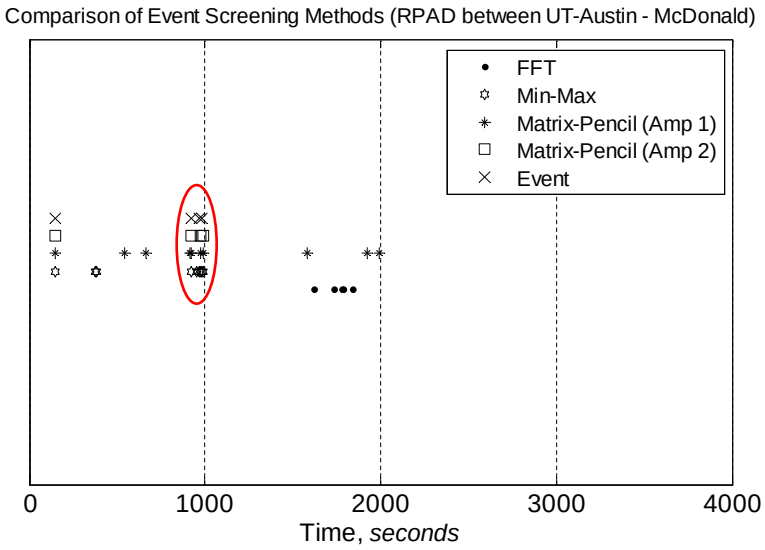

Figure 5.19: Events detected in the voltage RPAD between UT-Austin - McDonald PMU for 17:00 UTC

voltage level). It can be concluded that the recloser is most likely not located at a distribution feeder directly upstream from the PMU station, otherwise a reclosing event could cause the PMU to lose power and the PMU would be unable to measure and transmit voltage phasor data. The measured voltage magnitude at McDonald is too noisy to extract any conclusions.

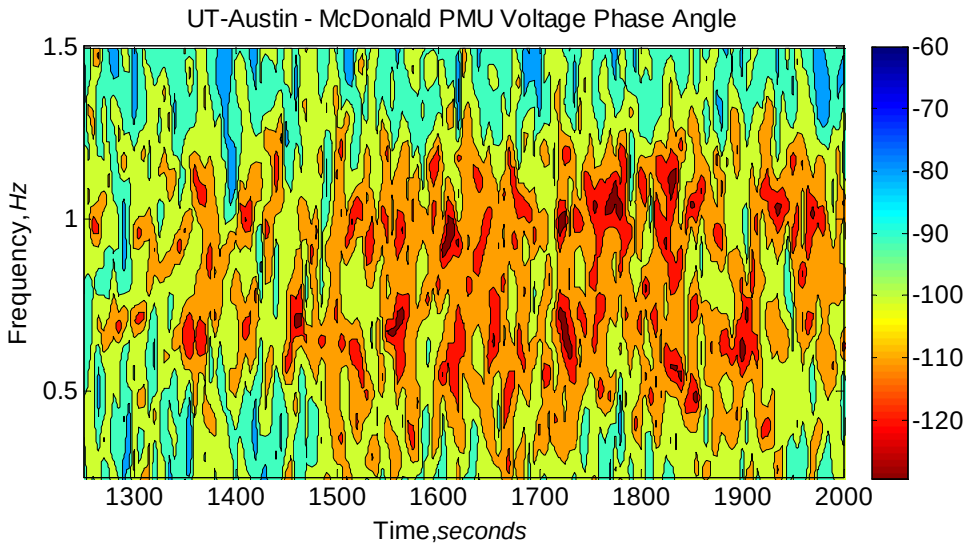

Figure 5.20: Contour plot of the PSD (low-frequency content over time) in the voltage RPAD over time shows a strong 1 Hz oscillation as well as another 0.6 to 0.7 Hz oscillation

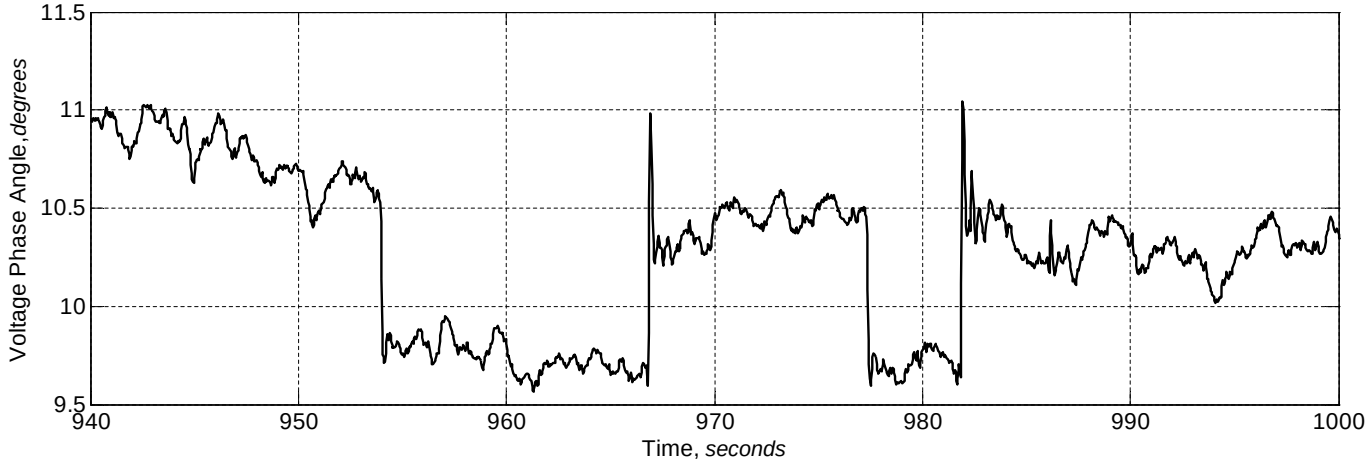

Figure 5.21: Small disturbance event detected in the voltage RPAD between UT-Austin - McDonald PMU

5.4 Summary

In this Chapter, the algorithm used to screen PMU data generated by the University of Texas at Austin synchrophasor network for power system events was described. The algorithm used four different methods to screen for possible events. Each method is applied to a moving window of PMU data. The FFT and Yule-Walker methods are based on using the maximum magnitude of the spectral content of PMU signals to detect possible events. The Matrix-Pencil method is a parametric method that estimates parameters to fit the PMU signal. The two maximum amplitudes are used to screen for possible events. The Min-Max method screens for large fluctuations in the PMU data. Results from the four methods are collected for one hour of PMU data. Any values from each method that exceed three standard deviations away from the mean are marked as possible events. A data window is marked as containing an event if two or more methods detect a possible event in the same data window.

The algorithm was applied to 24 hours of PMU data to analyze how well the algorithm was able to detect large and small events. A large event caused by a sudden loss of generation was easily detected in both the UT-Austin and McDonald PMU frequencies and the voltage phase angle separation between the two PMU stations. Two smaller events were present in the PMU data as well. In the UT-Austin PMU frequency, a strong oscillation at approximately 1 Hz was visible but was not present in the McDonald PMU frequency. A reclosing event was detected in the McDonald PMU frequency and voltage

phase angle. However, it is difficult to determine if the reclosing event was located on the distribution or transmission system. Once an event is detected by the algorithm, the data window containing the event is saved for further analysis. The common quantitative characteristics for each event category and the ranges of characteristics for each event category are described in Chapter 6.

Chapter 6

Creation of Event Categories Based on Detected Events in Synchrophasor Data

In this chapter, power system event categories are created based on the events detected in the synchrophasor RPAD and frequency signals by the screening algorithm presented in Chapter 5. Creation of event categories also includes identifying numerical characteristics for each category and determining the ranges of characteristics for each event category. The characteristics examined include the magnitude, the rate of change, the frequency content of the signal, the duration, and the step change amount. A description of how these categories are created based on common visual characteristics is provided in Section 6.1. Examples of events in the RPAD and frequency signals are provided and described in Subsections 6.1.1.1 and 6.1.1.2, respectively. These event categories were selected after examining many events that occur at different times of the day, seasons, and are measured at different locations within the PMU network. A variety of methods are applied to the data to extract different characteristics from each group. The numerical characteristics from each event category are described in Section 6.2. The ranges for each type of event are described for RPAD and frequency events in Subsections 6.2.1 and 6.2.3, respectively.

- **Publication**: Part of the work presented in this chapter has been published in [15]
  - Allen, A.J.; Santoso, S.; Muljadi, E.; "Phasor Measurement Unit (PMU) for Wide Area Monitoring, Protection, and Control (WAMPAC) Applications," NREL Report, December 2012

6.1 Event Categorization Based on Visual Analysis

This section discusses the categorization of events detected by the screening algorithm, based on common visual characteristics. These different categorizes and examples from each category are described and provided in this section. Subsection 6.1.1 describes the different event categories. In Subsubsections 6.1.1.1 and 6.1.1.2 the events as seen in the RPAD and frequency data are described, respectively. Example events from the synchrophasor data are provided as well.

6.1.1 Event Categories

The categories of detected events for RPAD and frequency signals are proposed in Table 6.1. Events were extracted from nine days' worth of data taken from different seasons of the year and from different years (from 2010 to 2012). Based on the types of events extracted from these days, the categories were selected using common visual characteristics (oscillations, impulses, step change, and rate of change). The RPAD has three categories with a total of 7 subcategories. The frequency also has three categories with a total of 7

subcategories.

Voltage RPAD		Frequency	
Category	Sub Category	Category	Sub Category
Impulse	Single (small)	Impulse	Small
	Single (large)		Large
Transient	Damped	Transient	Damped
	Sustained		Sustained
Step Change	Momentary (small)	Rise or Drop	Rise
	Momentary (large)		Drop
	Sustained		Unit Trip

Table 6.1: Categories presented for PMU RPAD and Frequency events

While the main categories were based on visual inspection, the subcategories were created after the quantitative characteristics from each category were extracted. The subcategories allow for more precise selection of thresholds when determining the category and subcategory of an event in the PMU data. The categories and subcategories are explained in more detail for the RPAD and frequency signals in Subsections 6.1.1.1 and 6.1.1.2, respectively. The typical ranges seen for each category is given in Subsections 6.2.2 and 6.2.3.0.4.

6.1.1.1 Voltage RPAD Event Categories

The event categories seen in the voltage RPAD are presented here with examples shown for each category. The RPAD is approximately proportional to the real power flow between two buses. A sudden change in the RPAD indicates a sudden change in power flow somewhere between the two buses. The events presented here are events in which the RPAD behavior suddenly

changes. When this type of event occurs it is assumed that the power flow somewhere between the two PMU measurements changes as well. In the case of an impulse event, the power flow change typically occurs near only one of the PMU stations as explained in Section 6.1.1.2. This may be interpreted as a sudden surge or drop of power caused by energizing of a motor or transformer or other switching event where the power quickly returns to pre-event conditions seen prior to the event. Step change events may be interpreted as a shift in power caused by events such as a transmission line trip or a generating unit trip. The cause of transient events at this time is unknown, but one possibility is that they may be caused by some switching event, occurring at a distance from the PMU station, causing power flows throughout the system to oscillate with higher magnitude change in the RPAD as compared to normal operating conditions. These oscillations are mostly within the mechanical time constant range of synchronous generator power plants within the area. The categories for the RPAD are examined in further detail below.

6.1.1.1.1 Impulse The first event category is for an impulse event as detected in the RPAD signal. The duration of the impulse is very short and the change in the value of the RPAD varies. The rate of change of the RPAD during the impulse event is typically very high. Two examples of the event are presented below. The first impulse event in Fig. 6.1a falls under the Single (large) subcategory and has duration of 0.33 seconds (20 cycles) and a magnitude of 1.7°. The ramp-up and -down rates are 15.9 deg/sec and 8.5

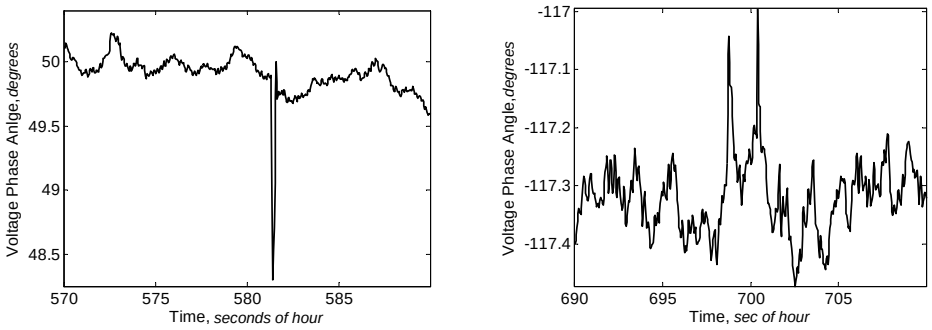

(a) Single (large) Impulse Event (b) Single (small) Impulse Event

Figure 6.1: Examples of RPAD Impulse event in the Voltage RPAD between UT-Austin and UTPA

deg/sec, respectively. The ramp rates are approximations and because the 30 Hz sampling rate of the PMU data, higher frequency oscillations above 15 Hz are not recorded.

This type of event is only seen at the McDonald PMU station but the cause is unknown. After recording the timestamps of the occurrence of seven days' worth of impulse events, it was found that the event is not periodic. Impulse events seem to occur randomly throughout the day. The impulse in the RPAD is thought to arise from a temporary imbalance in load and generation locally or might be caused by self-clearing faults. Analysis of probable causes of impulse events is described in Subsections 6.1.1.2 and 6.1.1.2.1.

The second type of impulse event falls under the Single (small) subcategory and is usually located near a peak of oscillations in the RPAD and sometimes appears as a pair of impulse events. This may also indicate a switching or reclosing event. Referring to Fig. 6.1b, the duration of the impulse event is

0.47 seconds (about 28 cycles) for the first impulse occurring at 698.8 seconds and 0.13 seconds (about 8 cycles) for the second impulse occurring at 700.4 seconds. The change in angle is 0.25 degrees for the first impulse and 0.22 degrees for the second. The ramp-up and -down rates for the first impulse are 1.86 deg/sec and 0.64 deg/sec, respectively. The ramp up and down rates for the second impulse are 3.35 deg/sec and 2.44 deg/sec, respectively.

The impulse events shown in Figs. 6.1a and 6.1b are not caused by dropped data. Dropped data are detected by the screening algorithm but are also easy to identify visually because of the smoothness of the data (the RPAD would remain constant for the duration of the dropped data). The dropped data points are recorded as zeros in the frequency data which can also be used as a way to check if the detected event is actually an error in the data. Successful fault clearing may produce the phenomena indicated in Fig. 6.1b; two sequential events occurring two seconds apart.

6.1.1.1.2 Transient The next event category is damped and sustained transients in voltage RPAD data. The causes of these events are unknown but the common characteristic is higher magnitude oscillations compared to normal operating conditions. This low frequency oscillation may indicate an oscillation between a large generator or group of generators near the PMU station and the rest of system. These types of events differ from typical damped oscillations known as ambient response of the system that is typically seen in synchrophasor data. The amplitude is typically larger and the oscillations

during a transient event are not as noisy as ambient data. The duration, amplitude, and smoothness of the detected damped oscillation events vary as well. Three examples of damped transients are given below. The first damped transient event in Fig. 6.2a lasts 5.07 seconds and the amplitude of the largest swing is 0.41 degrees. The frequency of the oscillation is 1.17 Hz.

In the following damped transient event in Fig. 6.2b, the duration of the event is 4.4 seconds and the largest swing is 0.96 degrees. The frequency of the oscillation is 0.59 Hz.

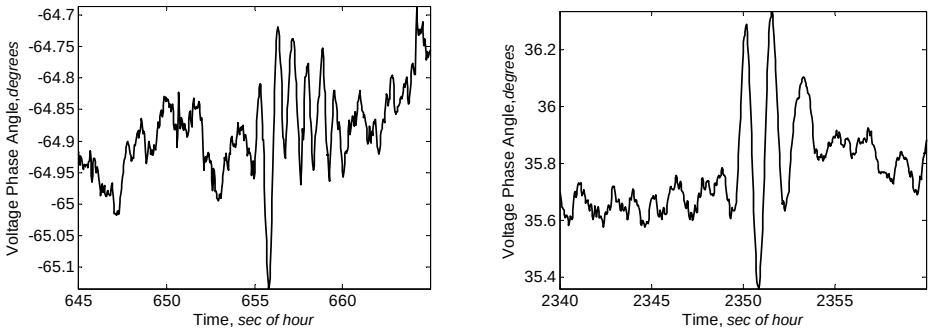

(a) Damped Transient Event (RPAD between UT-Austin and Waco)

(b) Damped Transient Event (RPAD between UTPA and Waco)

Figure 6.2: Examples of RPAD Damped Transient Events

The detected frequencies in the signal that are of interest fall below 2.0 Hz. This range of frequencies is typical to inter- and intra- area oscillations [76]. It is thought that the cause of the oscillation is due to system modes being excited by a switching type event. However, for most cases, the root cause of each switching event is unknown. One example of a sustained transient event is provided in Fig. 6.3a. For a sustained transient event in the RPAD data,

the signal is not as smooth because it contains other frequencies. A zoomed view of the oscillation is provided in Fig. 6.3b where the oscillations in the voltage RPAD are clear.

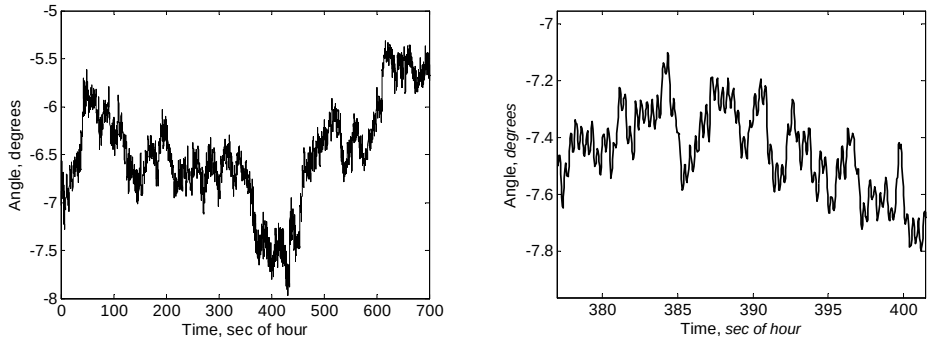

(a) Sustained Transient in RPAD (b) A zoomed view of Transient

Figure 6.3: Example of RPAD Sustained Transient (RPAD between UT-Austin and McDonald)

A sustained transient event is easily identified when examining the PSD contour plot shown in Fig. 6.4 starting at approximately 350 seconds. The frequency of this type of oscillation is approximately 2.8 Hz, higher than the frequencies seen in the damped transients shown in the previous examples.

6.1.1.1.3 Step Change in RPAD The following events are categorized as step changes in the RPAD data. During a step change event, the RPAD suddenly changes from one value to another lower or higher value. The direction of the change depends on the reference point from which phase angle is measured and the effect of the change of power flow caused by the event. The change in the RPAD can vary, from less than 1 degree to up to 10 degrees

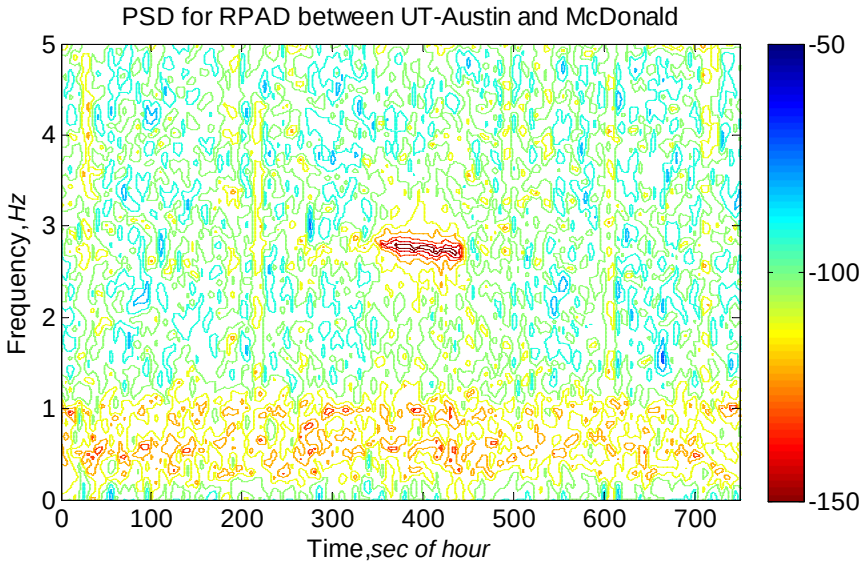

Figure 6.4: Contour plot of the PSD (low-frequency content over time) for a voltage RPAD Sustained Transient Event (RPAD between UT-Austin and McDonald)

or more. Large system changes in power flow such as a generator unit trip can result in larger step changes. Though the exact cause is unknown, it is assumed that smaller RPAD step changes are caused by transmission line trip or reclose events and larger step changes are caused by generator unit trips. The step changes in the RPAD caused by generating unit trips can be confirmed in the ERCOT Daily Grid Reports where sudden loss of generation events above 450 MW are reported [12].

Transmission line trips can occur when a fault is detected on the line. A line trip causes the redirection of power to surrounding transmission lines causing a change in the measured RPAD. In the case where an auto-reclosing

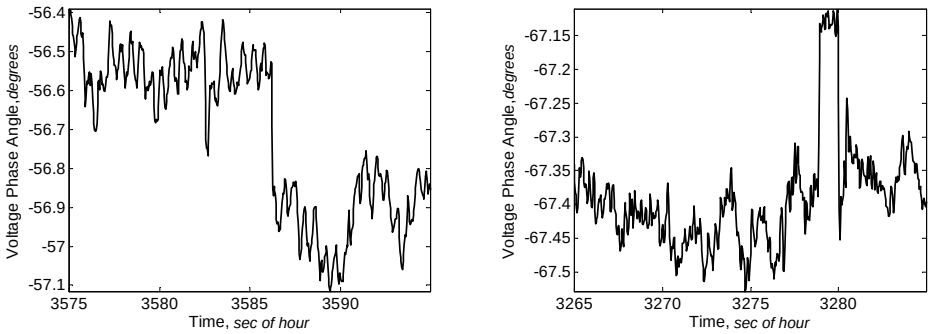

(a) Sustained Step Change Event (McDonald and Waco)

(b) Momentary Step Change Event (UT-Austin and Waco)

Figure 6.5: Example of RPAD Step Change Events

practice is utilized, breakers on both ends of the line will reclose automatically, typically after a period of 2 seconds following the initial line trip. If the fault is temporary, the line reclosing operation will likely be successful and no further protective action is needed. As a result power will return to its original value and the RPAD will return to its pre-fault value as well. If the fault persists, breakers will trip the line again and the reclosing operation is repeated as necessary. However, reclosing events do not normally occur more than three times. For permanent faults, the last trip operation of the sequence will result in the protected line remaining offline. Depending on the utility, voltage level, and type of line, the number of trips and reclosing actions and the wait period between reclose and trip actions will vary [77]. Fig. 6.5a represents a sustained step change event. For this event, the RPAD drops from -56.53 degrees to -56.85 degrees. The ramp rate is 4.86 deg/sec. The event here appears to be caused by a transmission line trip.

In the second event in Fig. 6.5b, a momentary step change occurs. The RPAD starts at -67.39 degrees and rises to −67.13 degrees before back down to −67.45 degrees. The duration of the event is 1.23 seconds (74 cycles) and the ramp up rate is 2.57 deg/sec and the ramp down rate is 2.56 deg/sec. Again, because the RPAD suddenly switches to a new value and then returns to approximately its original value, it is assumed that the cause of the event was a transmission line reclose event.

6.1.1.2 Frequency Event Categories

The event categories seen in the frequency are presented here with examples shown for each category. Though the PMU frequency is calculated using the voltage RPAD data, some events are more easily detected in the frequency signal compared to the RPAD signal. For example, a sudden large imbalance in load and generation caused by a generating unit trip would cause the frequency across the entire system to drop significantly. The drop in frequency and rate of change depend on the amount of power lost and the inertia of the system. The frequency drop during a generating unit trip is of significantly greater magnitude than the frequency during normal operating conditions and can easily be detected.

Smaller system wide imbalances in load and generation also cause sudden frequency rises and drops that are not visible in the RPAD. The frequency also shows events that are local to the PMU station and does not rely on the difference between two PMU stations such as is needed by the RPAD signals.

If an event is detected in the frequency at only one PMU station and is not visible in any of the other PMU frequencies, it is likely that an event occurred near the PMU station where the event was detected. Impulse events are predominantly local events and some transient events are local and are most likely caused by equipment or events located nearby. Local events do not indicate an imbalance in system load and generation.

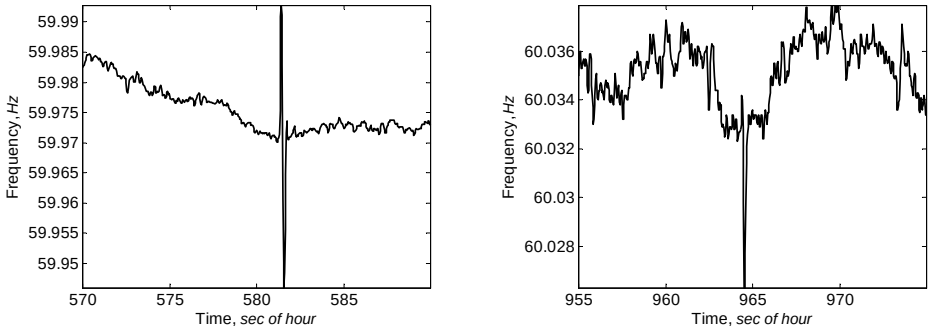

(a) Full-cycle Transient Event (b) Half-cycle Transient Event

Figure 6.6: Examples of Frequency Impulse Events

6.1.1.2.1 Impulse Impulse type events seen in the frequency are presented here. The frequency impulse is similar to a high frequency oscillation with duration of either one cycle or one half of a cycle and fall into subcategories large impulse or small impulse. The events are only seen in the McDonald frequency data, indicating that some sort of switching type event or motor starting occurs near the McDonald PMU station on either the transmission or distribution voltage level. It is possible that these types of events cause a frequency event because of a sudden difference between the local load and

generation. This type of event occurs frequently and may represent a temporary imbalance in load and generation locally. Another event that could cause a local imbalance includes a sudden trip and reclose of a large load (such as a processing plant). Impulse events seen in a PMU frequency are always seen in the corresponding RPADs. The frequency signals are used to determine at which station a local event occurs. The RPAD signal cannot be used to determine where a local event occurs because two PMU measurements are involved. For example, if an impulse event is detected in the frequency at McDonald the same impulse event is seen in the McDonald-UTAustin and McDonald-UTPA RPADs. This always occurs specifically for impulse events but is not always true for other event categories.

The first example in Fig. 6.6a is of an impulse with the "full-cycle" impulse and belongs to the large impulse subcategory. The duration of the event is 0.47 seconds (28 "60 Hz" cycles) and the impulse magnitude is 42.3 mHz. The ramp rate from peak to peak is 253.8 mHz/sec. The second example in Fig. 6.6b is of a "half-cycle" impulse and belongs to the small impulse subcategory. The duration of the event is 0.4 seconds (24 "60 Hz" cycles) and the impulse magnitude is 7.1 mHz. The ramp down and up rates are 26.43 mHz/sec and 58.87 mHz/sec.

6.1.1.2.2 Transient Transient events in the frequency data are not as common as impulse events. An example of a damped oscillation is provided in Fig. 6.7a where the duration of the event is 5 seconds. The largest amplitude

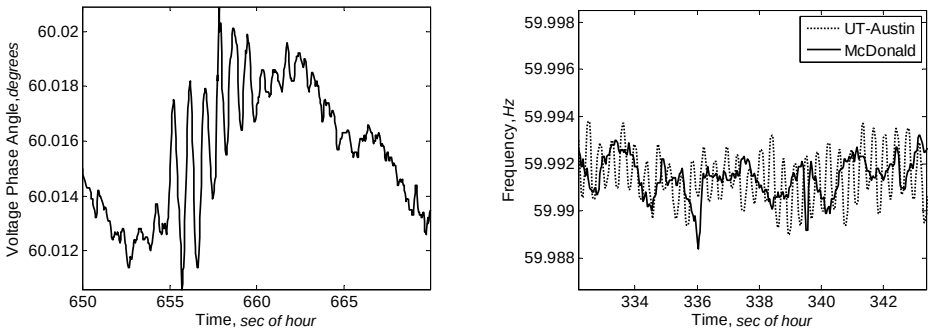

(a) Damped Transient Event (b) Sustained Transient Event

Figure 6.7: Examples of Transient Events in PMU Frequency

peak to peak during the event is 10 mHz. The frequency of the oscillation is 1.23 Hz. The frequency of the oscillation falls within the intra-area oscillation range. Intra-area oscillations are caused by one synchronous machine oscillating against a group of machines in the area.

An example of a sustained transient event is given in Fig. 6.7b. The sustained transient event is detected in the UT-Austin PMU signal but is not present in the McDonald PMU signal. Though it is easy to see in Fig. 6.7b that the event is seen only at UT-Austin, the PSD contour plot provides a simpler way to visually detect sustained transient events including when the transient begins and ends and the approximate frequency of the transient. The PSD contour plot is shown in Fig. 6.8.

6.1.1.2.3 Sudden Drops or Rises in Frequency Small drops or rises caused by sudden imbalances between the load and generation are detected in the PMU frequency data. These types of events are also typically detected

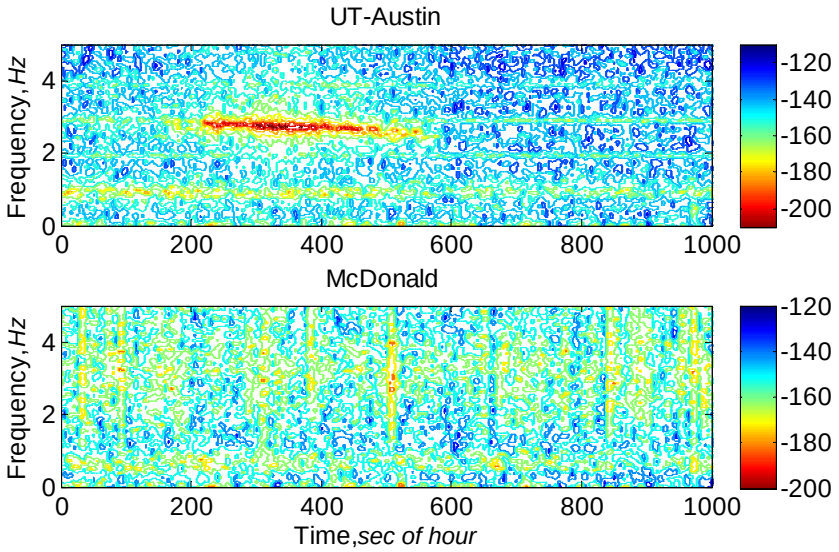

Figure 6.8: Contour plot of the PSD (low-frequency content over time) for a sustained frequency transient event

at all PMU locations at the time of the event. An example of an imbalance caused by higher generation compared to load (the frequency increases above 60 Hz) event is given in Fig. 6.9a. The event does not have a duration but the rate of change of frequency from the bend at the start to the peak before the frequency begins to drop is 5.22 mHz/sec, significantly slower compared to the impulse event in the frequency. This event category differs from the impulse frequency event because these types of events are seen throughout the entire system whereas an impulse event is only seen at a single PMU location. An imbalance caused by higher amount of load compared to generation (the frequency drops below 60 Hz) is seen in Fig. 6.9b.

A zoomed out view of the frequency in Fig. 6.10a provides a clearer

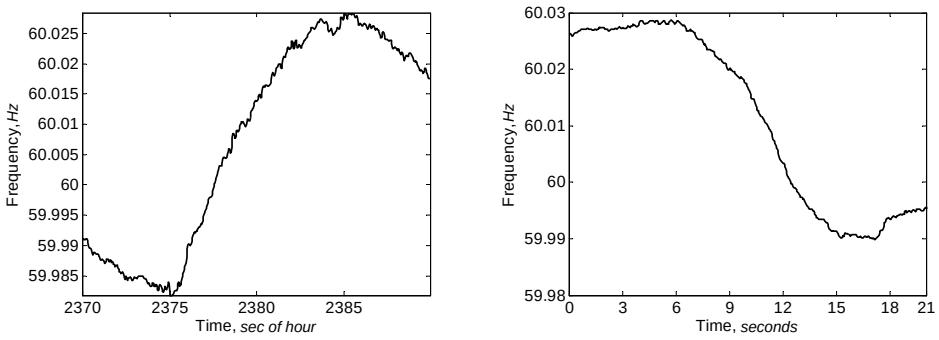

(a) Sudden Rise in Frequency (b) Sudden Drop in Frequency

Figure 6.9: Examples of Frequency Rise and Drop

picture of how a frequency rise or drop event differs from normal operating conditions. During normal operating conditions, variations in the frequency are always occurring, but during a rise in frequency event indicated by the red arrow, the frequency rises at a more rapid rate than is typical. Another system wide frequency event occurs around the 1300 second mark, where the frequency drop is of a lower magnitude (approximately 250 mHz).

Fig. 6.10b presents how an impulse event is a local event and is visible only at a single PMU station. The event was detected in the McDonald PMU frequency but is not present in either the UT-Austin or UTPA PMU frequencies. These examples illustrate that a PMU frequency contains system wide information as well as local information. The variation in PMU frequencies during a large loss of generation in Section 6.2.3 also illustrates how the frequency differs across the power system during a drop in frequency event.

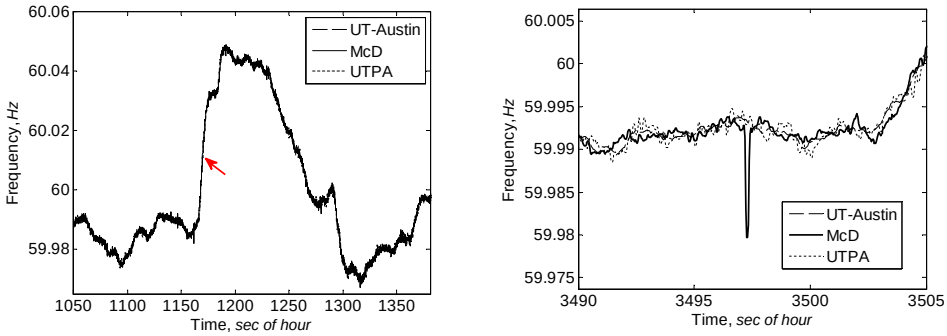

(a) System wide frequency event seen by all PMUs

(b) A local frequency event only seen by McDonald PMU

Figure 6.10: Examples of Frequency Events that are visible system wide and visible only at a single PMU station

6.2 Algorithm Development

Once the events have been placed into the separate categories outlined in Section 6.2.3, the characteristics from each type of event are extracted to determine which numerical characteristics are common to each category. An algorithm is written that utilizes the common characteristics to automatically identify events. For example, if an event has a strong 0.56 Hz frequency, the event will be identified as a transient event. In this section, the RPAD categories are examined first, followed by the frequency categories. For both the RPAD and the frequency, the characteristics that are unique to each category are identified. A flowchart of the algorithm to automatically categorize events and the useful characteristics in each category is given for the RPAD and the frequency.

6.2.1 Extracted Characteristics for RPAD

This section examines the characteristics that are common to categories in the RPAD data described in Section 6.1.1. The categories are impulse, transient, and step change. The methods that are used to extract these characteristics are similar to the methods described in Chapter 5 used to screen the synchrophasor data for events. The methods are FFT, Yule-Walker Spectral, differential of the synchrophasor data, and Matrix-Pencil. The FFT and Yule-Walker Spectral methods are spectral methods used to identify strong oscillations within the PMU data. The differential of the PMU data is used to detect sudden changes in the data. The Matrix-Pencil method can be used to identify damping and strength of oscillations in the PMU data. The following subsections describe the characteristics for each category.

The flowchart for the algorithm for the categorization of events in the RPAD data is given in Fig. 6.11. It is assumed that each identified event falls into at least one of the categories: Sustained Step Change Event, Momentary Step Change Event, Impulse Event, or Transient Event.

Two functions are used to categorize the events based on the extracted characteristics. The first function determines if the event is a transient event by examining the peak power for frequencies below 1.2 Hz. If the detected peaks are above a selected threshold, then the event is identified as a transient event. The power for an inter- or intra-area oscillation during a transient event is typically very high. To illustrate, an example of a transient event and its characteristics is provided. The detected event in the RPAD data is shown

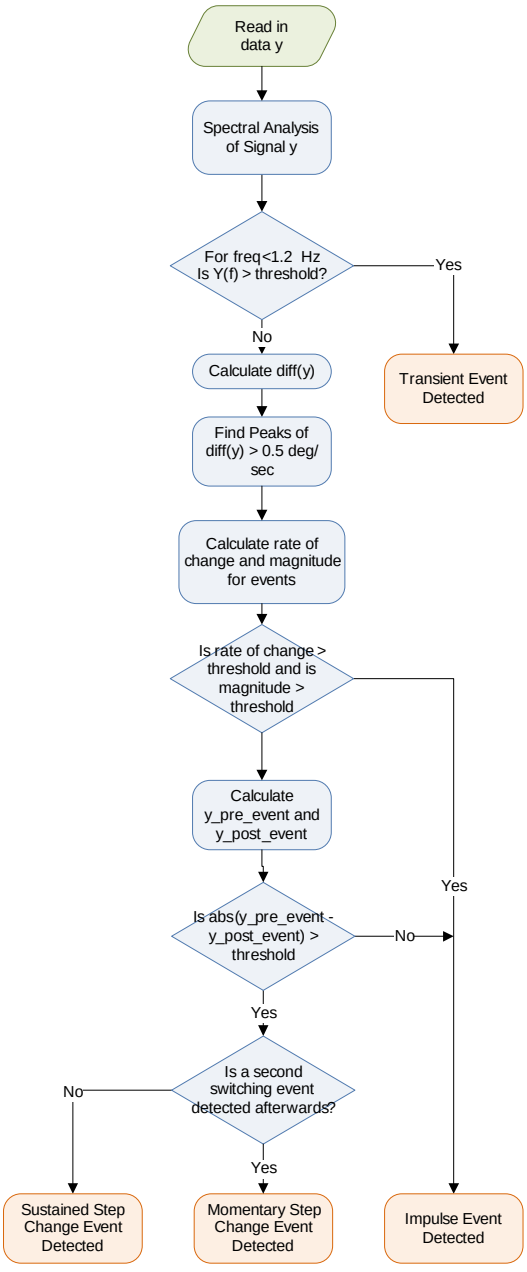

Figure 6.11: Flowchart for Algorithm to Categorize RPAD Events

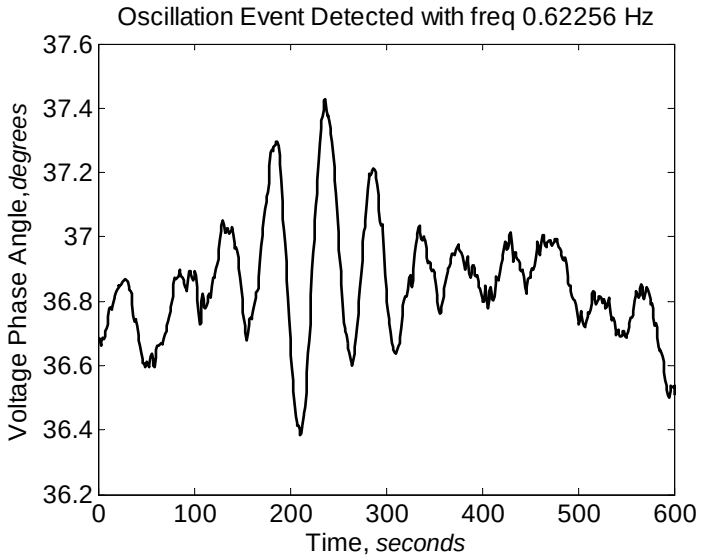

Figure 6.12: Example of PMU RPAD Oscillation Event

in Fig. 6.12. The event was originally detected by the screening algorithm from Chapter 5. Once the event was detected, the algorithm examines the frequency content of the signal. The Yule-Walker Spectral method is used to find the strength of the frequency content in the signal. The frequency content below 2.0 Hz is examined and if the peak power for a frequency below 2.0 Hz is above the selected threshold, the event is identified as an oscillation event.

The Yule-Walker calculated power spectral density for frequencies below 2.0 Hz is shown in Fig. 6.13a. The peak frequency of 0.62 Hz indicated is well above the selected threshold of -80 dB. For the algorithm, the threshold was selected based on examining multiple transient events that have been detected by the screening algorithm. For comparison, the Yule-Walker calculated power spectral density for a non-transient event is shown in Fig. 6.13b.

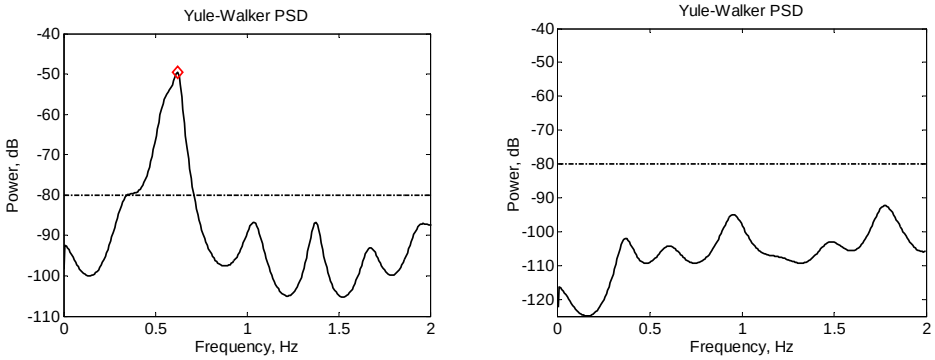

(a) Transient Event PSD (b) Non-Transient Event PSD

Figure 6.13: Yule-Walker PSD comparison between Transient and Non-transient Events

The peak dBs of frequencies of interest fall well below the −80 dB threshold.

The second function identifies the detected event as either an impulse event, a momentary step change event, or a sustained step change event in the RPAD. The function uses the differential of the PMU RPAD signal to determine if the event is a possible step change or impulse event. The peaks in the differential of the signal are detected and if the peaks cross a certain threshold, the event is tagged as a possible step change or impulse event and evaluated further. For the RPAD, the thresholds of the rate of change of RPAD for impulse and step change events are above 0.08 deg/sec or below −0.05 deg/sec. An example of an impulse event in Fig. 6.14 is used to illustrate how the function is able to categorize impulse type events. The differential in Fig. 6.15a has two peaks with only one (indicated by a red diamond) exceeding the defined threshold. This detected peak time is marked as a possible impulse or trip event. The possible event is indicated in the original plot of the data

in Fig. 6.15b. At this step, the function has not yet identified the event as an impulse or step change event but only as a possible impulse or a possible step change event.

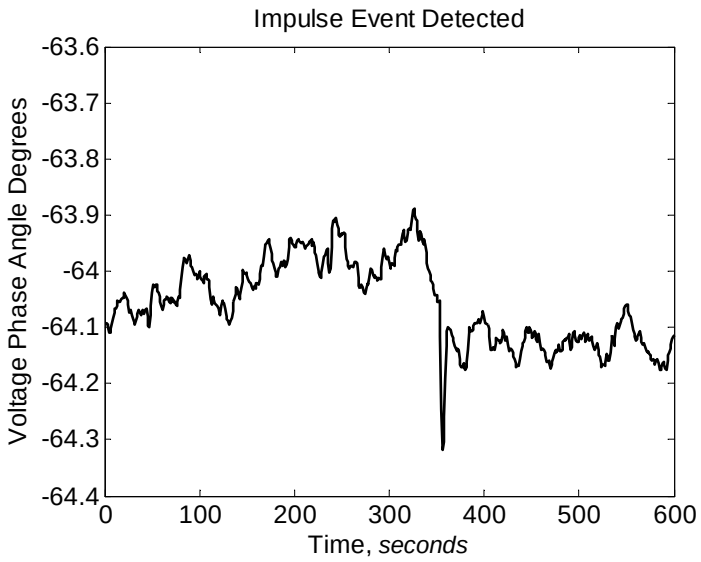

Figure 6.14: An Event is Detected in the RPAD signal

The possible event in the original data is analyzed further to determine if the event is an impulse or a step change. The algorithm identifies the start of the ramping period and the end of the ramping period. With the starting and ending points identified, the ramp rate in degrees per second of the event is calculated. For the example event, the ramp down rate as calculated by the algorithm is 2.66 deg/sec and is highlighted in red in Fig. 6.16a.

Next, to differentiate between step change or impulse events, the average value of 0.33 seconds (20 cycles) of the RPAD before the start point of the detected ramp, $y_{preevent}$, and the average value of 0.33 seconds of RPAD after

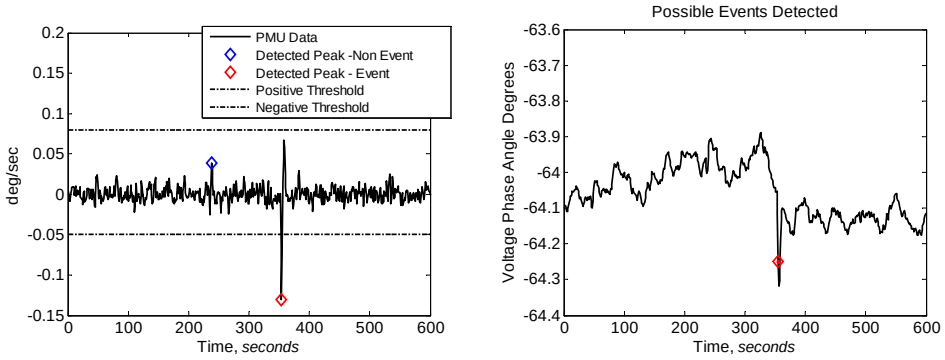

(a) Events detected in differentiated RPAD signal

(b) Event time marked in original RPAD signal

Figure 6.15: Methods Used to Detect an Impulse Event using the differentiated RPAD signal

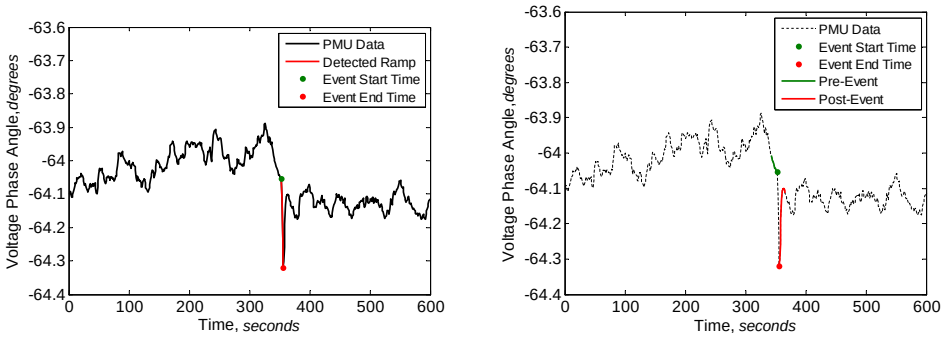

(a) The Start and End times and ramping period of impulse event

(b) The Pre-Event period in green and the Post-Event period in red

Figure 6.16: Methods Used to Determine if Detected Event is an Impulse Event

the end point of the detected ramp, $y_{postevent}$, are compared. This step of the algorithm is illustrated in Fig. 6.16b where $y_{preevent}$ (in green) and $y_{postevent}$ (in red) are highlighted. If the event is a line trip, the RPAD prior to the event suddenly changes and remains at the new value. Therefore, if the differ-

ence between $y_{preevent}$ and $y_{postevent}$ exceeds the selected threshold, the event is tagged as a trip event. Otherwise, the event is considered an impulse event. In the example provided, the jump falls below the selected threshold and the event is correctly identified as an impulse event by the algorithm.

If the jump exceeds the threshold, the event is considered either a sustained or momentary step change event. To differentiate between sustained and momentary step change events, the number and timestamps of each detected ramp up and ramp down events are examined. For example, if a ramp up time is quickly followed by a ramp down time or vice versa the event is tagged as a momentary step change event. If there is a single ramp up or ramp down event that is not an impulse, the event is a sustained step change event. Examples of a line reclose event (step) and line trip event (sustained) are given in Fig. 6.17a and 6.17b.

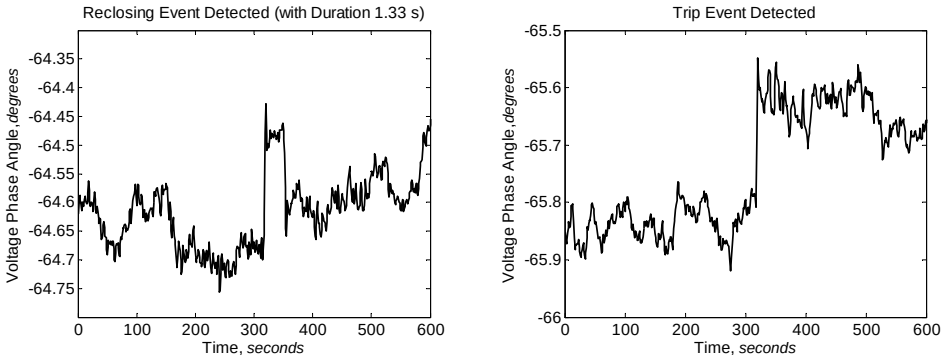

(a) Momentary step change event (b) Sustained step change event

Figure 6.17: Examples of step change event

6.2.2 Summary of RPAD Event Categories

After extracting common characteristics from 62 impulse events, 39 transient events, and 87 step change events, an approximate range of the event characteristics was determined. The magnitude, ramp rate, duration, frequency, and step change content of the events were extracted and saved. Note, that when using the RPAD, which is the voltage phase angle between two buses separated by an unknown network, the RPAD difference indicates the strength of the effective tie line between two buses. It is also shows the measure of stability of power systems. Large value of RPAD indicates a weaker tie between the two areas. Table 6.2 summarizes available characteristics for each category.

Category	Subcategory	Magnitude (deg)	Ramp Rate (deg/sec)	Duration (sec)	Frequency (Hz)	Step Change (deg)
Impulse	Single (small)	0.18-0.4	0.5-5.5	0.167-0.5	-	-
	Single (large)	1.4-1.7	7.0-16.0	0.167-0.5	-	-
Transient	Damped	0.15-1.5	-	<12	0.4-1.25	-
	Sustained	0.1-1.6	-	>12	0.8-3.0	-
Phase Angle Change	Momentary (small)	-	0.75-3.25	0.5-1.5	-	0.2-0.6
	Momentary (large)	-	2-10	0.5-1.5	-	0.95-1.15
	Sustained	-	1-5	-	-	0.15-0.75

Table 6.2: Summary of Characteristics from Events detected in RPAD Data

6.2.3 Extracted Characteristics for PMU Frequency Data

A different algorithm is used for categorizing events in the PMU frequency data. The algorithm is similar to the algorithm used to categorize events in the RPAD data with changes made to include events only present in the frequency signal and to create new threshold values since fluctuations in frequency are smaller than fluctuations in RPAD. The category for events present only in the frequency is the sudden rise or drop in frequency. Step change events are not included because these types of events are present in the RPAD only.

A flowchart for the frequency categorizing method is given in Fig. 6.18. The signal is examined by all functions because it is possible for an event to belong to multiple categories. The flowchart below shows how each of the tags for the three categories is decided. After the tags have been assigned, they are examined to determine which category or categories the event belongs to.

In this section, examples of the events and the analysis used to identify the events are given. The first category that is examined is for impulse events which can fall into two different subcategories. The next event category is for transient events. The third event category is a rise or drop in frequency. For the first category, where possible impulse events are identified, the differential of the PMU frequency signal is used. Peaks in the differential are identified at three different levels. The first level is for impulses with the highest magnitude. An example of the impulse in the frequency data is given below in Fig. 6.19a. This type of event is only found at the McDonald PMU station and could be

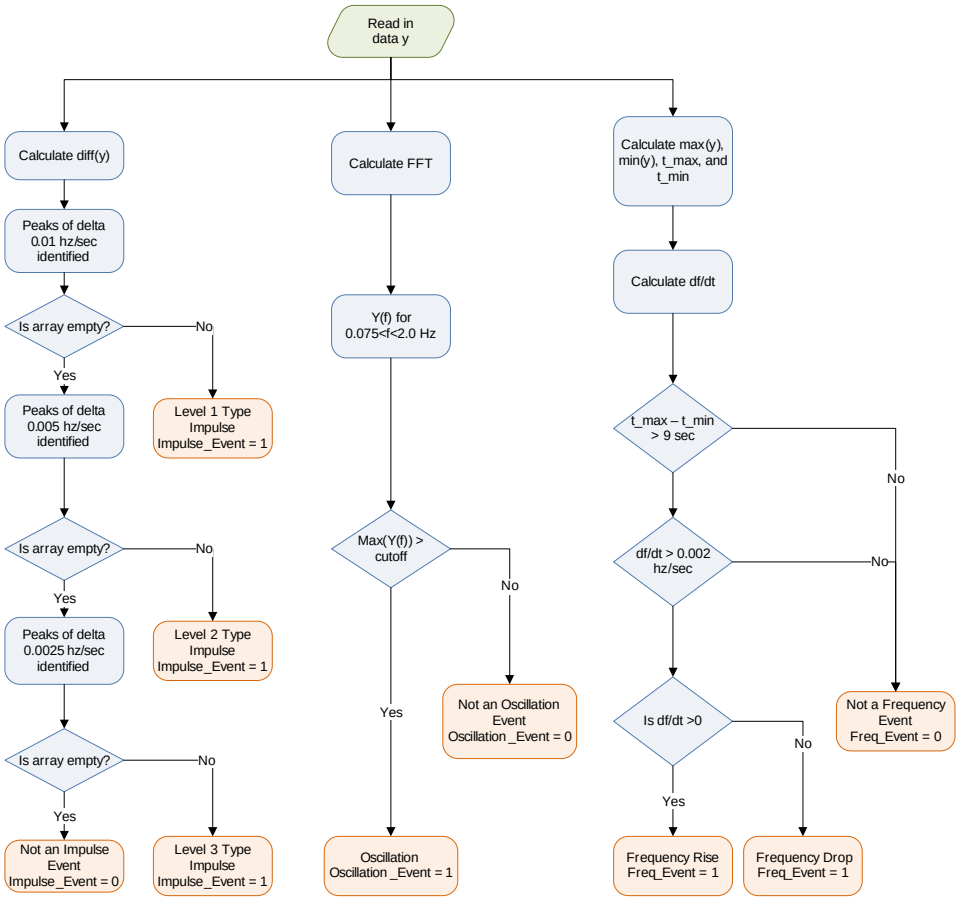

Figure 6.18: Flowchart for the algorithm to categorize frequency events

caused by equipment on the distribution side located near the station. For the first level, the peaks in the differential of the signal are identified when previous values exceed 0.01 Hz/sec. An example of the peaks identified for the impulse event given in Fig. 6.19b is shown.

The next step is to determine if the detected peaks exceed the selected threshold values. In the case below, all the detected peaks exceed the thresh-

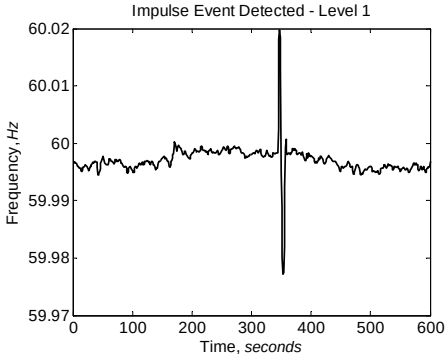

(a) Level 1 Impulse Event

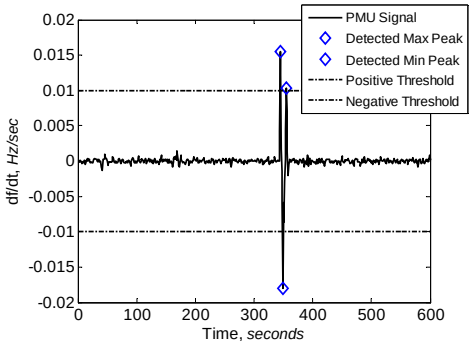

(b) Peaks of the differential

Figure 6.19: Example of Level 1 Impulse Event and how it is detected in the differential of the PMU frequency signal through comparison of a selected threshold value

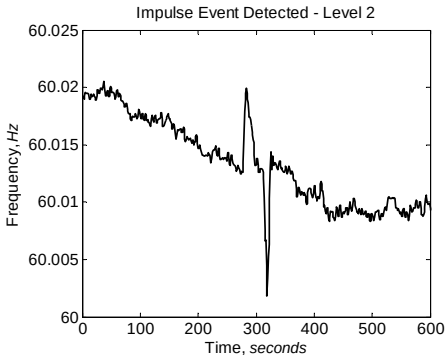

(a) Level 2 Impulse Event

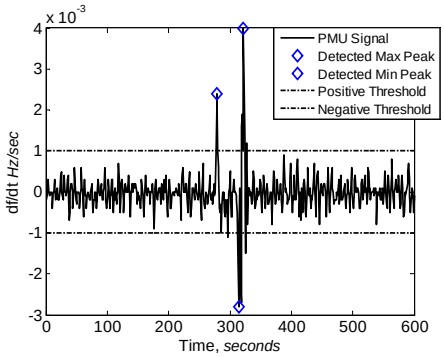

(b) Peaks of the differential

Figure 6.20: Example of Level 2 Impulse Event and how it is detected in the differential of the PMU frequency signal through comparison of a selected threshold value

old. Examples of level 2 and level 3 impulse events are provided in Figs. 6.20a to 6.21b. The peak detection and threshold values are different for all impulse event levels. The first event level is an example of the large impulse event subcategory. The second and third levels are examples of the small impulse

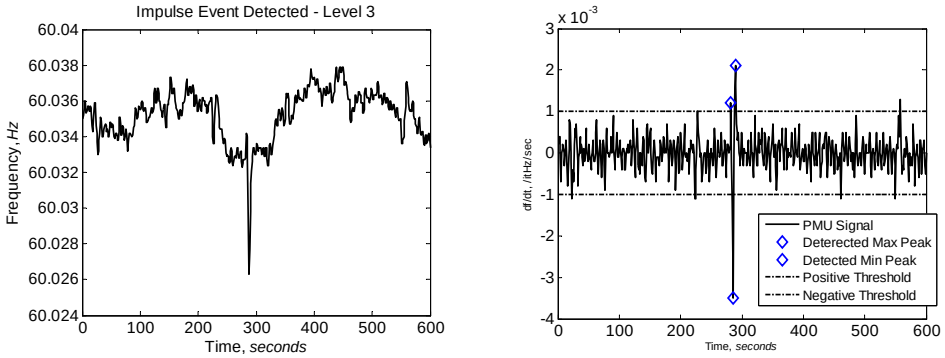

(a) Level 3 Impulse Event (b) Peaks of the differential

Figure 6.21: Example of Level 3 Impulse Event and how it is detected in the differential of the PMU frequency signal through comparison of a selected threshold value

event subcategory.

The next event category that is analyzed is a transient. The FFT of the PMU frequency signal is used to detect transient events. Transient events are typically excited by switching of either equipment in the power system or of load or generation. Because of the structure of the power system network, the damped transient events of interest that are excited fall into the range of frequencies that are below 2.0 Hz. From examining the PMU data, frequencies above 2.0 Hz are present but the cause and origin of these oscillations are not well understood at this time. These frequencies may be examined in future work and help categorize power system events further. An example of a transient event is given in Figs. 6.22a and 6.22b. The FFT as applied to the differential of the frequency (to remove DC offset) is given as well. The peaks are detected in the 0.05 to 2.0 Hz frequency range and if the

peaks fall above the selected threshold the algorithm assigns a transient event tag.

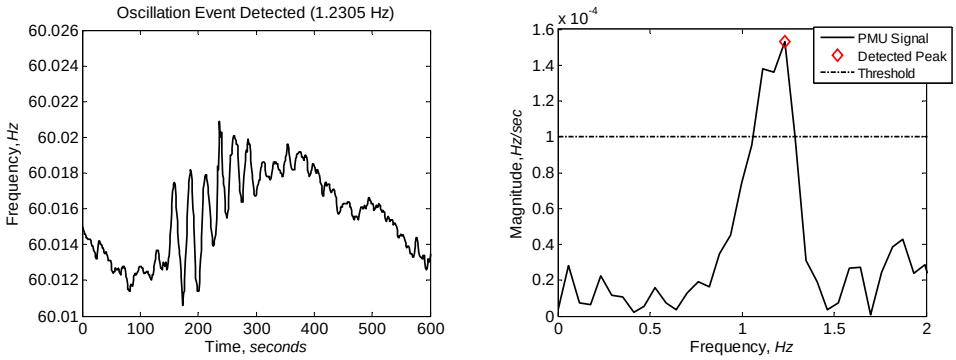

(a) An transient event (b) The spectral analysis of event

Figure 6.22: Example of a transient event and the spectral analysis of the event which contains frequencies that exceeds the threshold used to indicate a detected event

To illustrate the difficulty of visually screening PMU data for oscillation type events, a zoomed out plot of the frequency containing the event over a period of 400 seconds is given in Fig. 6.23. The event starts at 255 seconds.

Next, to determine if the event is a rise or drop in frequency event, the maximum and minimum values and the times at which these occur within a 20 second window are extracted. The time between the maximum and minimum values is calculated as well as the slope between the maximum and minimum. The first step examines if the time difference is greater than 9 seconds. This step eliminates events where there are sudden large changes in the signal such as seen during impulse events. Next if the slope is greater than 2 mHz/sec, the event is placed in the rise or drop in frequency category. If the slope is too

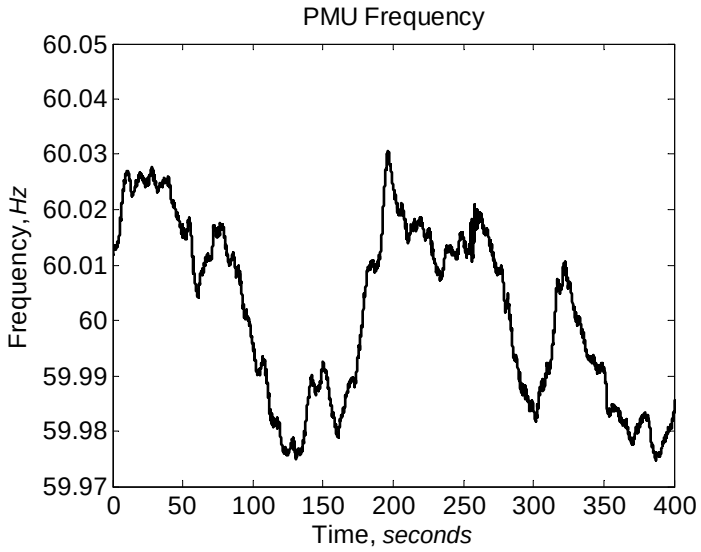

Figure 6.23: From a 400 second window of frequency data, it is difficult to visually detect events

gradual, the event is most likely not a rise or drop in frequency event. The sign of the slope is used to determine if the event belongs to a rise in frequency or a drop in frequency subcategory. If the event is a rise in frequency event, the frequency increases and the slope is positive. If the event is a drop in frequency event, the frequency decreases and the slope is negative. Examples of both types of events are provided in Figs. 6.24a and 6.24b. The rises and drops presented in this section are from small sudden imbalances between load and generation.

An example of a drop in frequency event is provided in Fig. 6.25 when a sudden loss of large generation of 478 MW on January 25, 2012 at 7:13 UTC occurred.

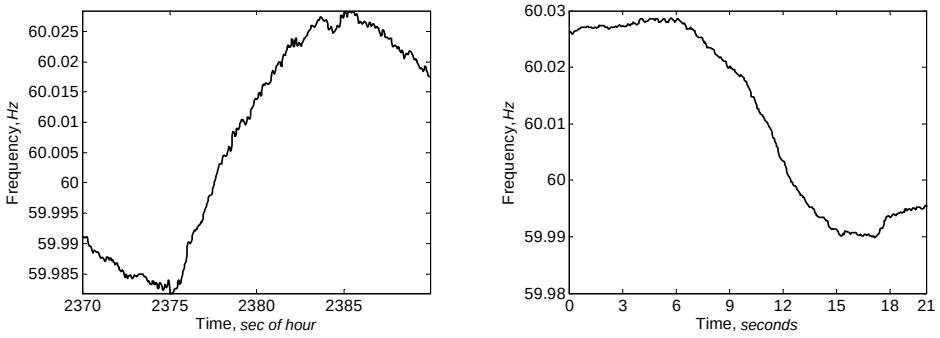

(a) Sudden rise (b) Sudden drop

Figure 6.24: Example of sudden rise and sudden drop in the PMU frequency signal

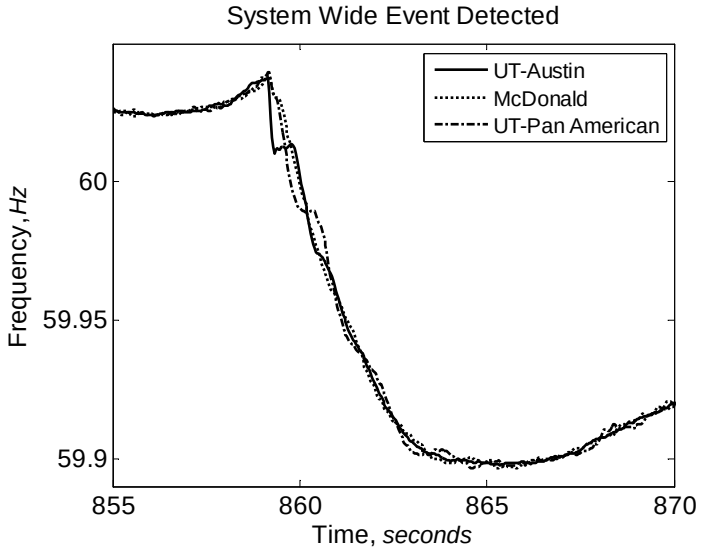

Figure 6.25: Another example of a frequency drop event on January 25, 2012 7:13 UTC

The event was detected at all PMUs in operation at the time of the event. The frequency at the time of the event is given in Fig. 6.25. A more detailed view in Fig. 6.26a shows the initial rate of change of frequency is

much higher at UT-Austin and the frequency begins to oscillate against the frequency at UT-Pan American. The initial rate of change of frequency is approximate 300 mHz/sec and eventually the rate of change of frequency changes to approximately 22.4 mHz/sec (from the start of the event to the nadir). A zoomed in view of the beginning of the event is also given in Fig. 6.26b. The frequency at UT-Austin begins to drop before the other frequencies at the other PMU locations. The rate of change of frequency characteristic taken for unit trip events is measured taking the frequency and time at the start of the event and the frequency and time at the minimum nadir of the event.

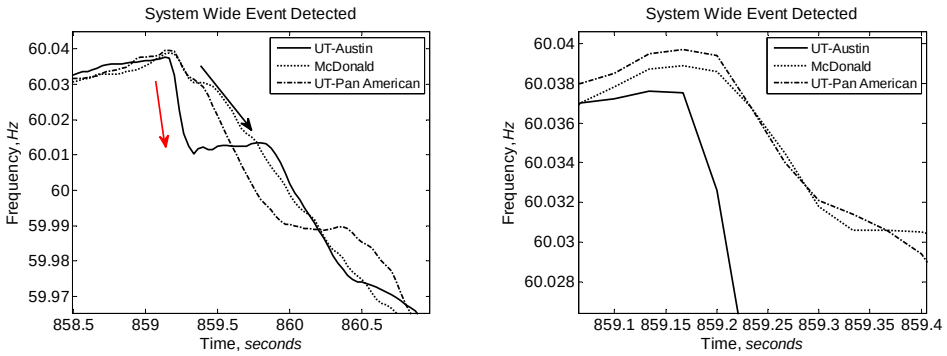

(a) Zoomed view shows oscillations in the frequency

(b) Zoomed view shows drop at UT-Austin

Figure 6.26: Zoomed in view of event shows that the frequencies at each location begin to drop at different times with UT-Austin dropping sooner and more rapidly

The event is also tagged as an oscillation event in the UT-Austin (1.17 Hz) and UT-Pan American (0.70 Hz) frequency data. The events are also categorized as impulse events because of sudden changes in the frequency.

6.2.3.0.4 Summary of Frequency Event Categories After extracting common characteristics from 82 impulse events, 35 transient events, and 93 rise or drop events, an approximate range for characteristics of these event categories was determined. The magnitude, ramp rates, duration, frequency content, and change in frequency of the events were extracted and saved. Table 6.3 summarizes available characteristics for each category.

Category	Subcategory	Magnitude (mHz)	Magnitude Peak to Peak (mHz)	Ramp Rate (mHz/sec)	Ramp Rate Peak to Peak (mHz/sec)	Duration (sec)	Freq (Hz)	Delta Freq (Hz)
Impulse	Single	3-9	-	10-900	-	0.267-0.5	-	-
	Multiple	20-25, 3-10	40-50	25-250	250-500	0.3-0.6333	-	-
Transient	Damped	5-325	-	-	-	0.4-7	0.3-5.0	-
	Sustained	0.1-1.6	-	-	-	>12	0.8-3.0	-
Rise or Drop in Frequency	Rise	-	-	0.8-3	-	-	-	0.015-0.04
	Drop	-	-	2-8	-	-	-	0.02-0.1
	Unit Trip	-	-	15-30	-	-	-	0.1-0.21

Table 6.3: Summary of Characteristics from Events detected in Frequency Data

6.3 Summary

In this chapter, the events detected from the screening algorithm are placed into categories based on common characteristics. First, the events are placed into categories based on visual inspection. These categories are impulse, transient, and step change for RPAD events and impulse, transient, and sudden rise or drop in frequency for frequency events. The common quantitative characteristics for each event category and the ranges of characteristics for each event category are identified.

Chapter 7

Influence of Wind Power on Synchrophasor Data

In this chapter, synchrophasor and wind power data are used to study the relationship between wind power and the relative phase angle difference. The observations made from synchrophasor and wind power output data show that wind power has a strong influence on RPAD as seen in the linear relationship between RPAD and wind power and in the influence on modal content of electromechanical oscillations in the RPAD. The linear relationship between the voltage RPAD and wind power penetration is explored first in Section 7.1. Even though the weak relationship between power transfer and the voltage RPAD across large distances was discussed previously in Section 2.4.1, the power transfer from wind power plants in West Texas to major load centers in Central Texas has a strong linear relationship to the measured voltage RPAD between McDonald (West Texas) and UT-Austin (Central Texas).

Next, the relationship between synchrophasor modal content and levels of wind power are studied. Initial observations indicate correlation between wind power penetration levels and the appearance of an approximately 2 Hz mode (strongest at McDonald, but visible throughout the system) [9, 18]. The

impact of wind power on modal frequency estimates extracted from the synchrophasor data are examined in Section 7.2. A chapter summary is presented in Section 7.3.

- **Publication**: Part of the work presented in this chapter has been published in [15, 18]
  - Allen, A.J.; Santoso, S.; Grady, W.M.; , "Voltage phase angle variation in relation to wind power," Power and Energy Society General Meeting, 2010 IEEE , vol., no., pp.1-7, 25-29 July 2010
  - Allen, A.J.; Santoso, S.; Muljadi, E.; "Phasor Measurement Unit (PMU) for Wide Area Monitoring, Protection, and Control (WAMPAC) Applications," NREL Report, December 2012

7.1 ERCOT Wind Power Data and Relationship to Voltage RAPD

Total wind power and total generation data required for this research was captured from the ERCOT web site (no longer available) starting January 27, 2009 to November 6, 2010. The data on the website included the aggregate wind power, aggregate generation, aggregate load, system frequency, and zonal pricing (before ERCOT switched to nodal pricing) and was updated at one-minute intervals. The time stamp for this data employs Central Time zone and is not synchronized with the GPS time stamp used to time stamp the synchrophasor data. The collected data also has many missing data points.

Gaps range from a few hours in a day to months' worth of missing data. Aggregate wind power and generation are now available online as hourly averages in portable document format (PDF). The resolution of this data is too low for thorough analysis.

An example of one day of wind power and wind power penetration is provided in Fig. 7.1. The left y-axis corresponds to the wind power (MW) and the right y-axis corresponds to the wind power penetration (%). The wind power penetration within ERCOT is calculated using the aggregate wind power and total generation data. The time stamp is converted to UTC to match the synchrophasor data time stamp for easy comparison to PMU data. During the date of the examples provided, the Central Time conversion is UTC - 05:00 during Central Daylight Time and UTC - 06:00 during Central Standard Time. For example, in Fig. 7.1, the peak wind power of 4330 MW occurs at 05:00 UTC or at 00:00 CST.

Initial observations also show that during higher levels of wind power penetration, the voltage RPAD between UT-Austin and McDonald is closely correlated to the wind power penetration as shown in Fig. 7.2. This information reveals that the voltage synchrophasor data can be used to study power flows over a large system.

The highlighted areas in Fig. 7.2 show the periods of data to be evaluated for dynamic modal behavior in Subsection 7.2. The time stamp converted to equivalent Central Time are provided for convenience as well. The blue highlighted area is the wind power penetration and voltage RPAD during a

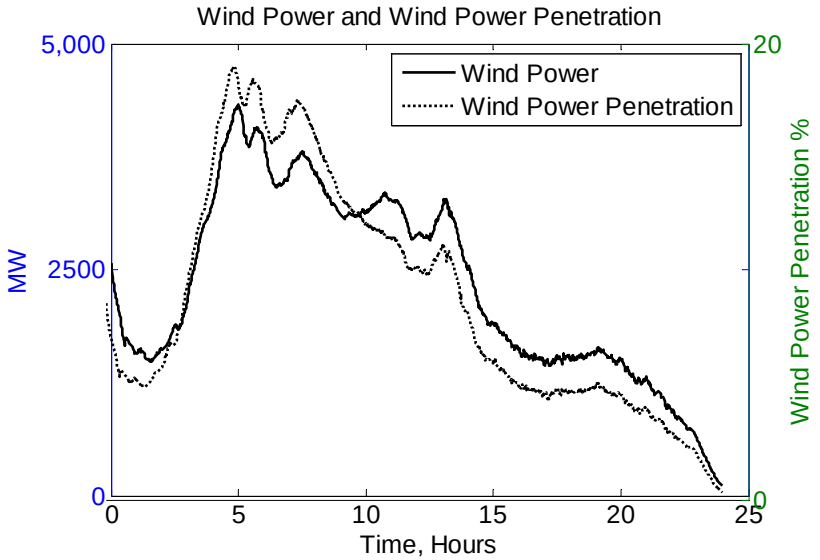

Figure 7.1: Aggregate wind power and wind power penetration within ERCOT for April 13, 2009 (UTC)

period of "high wind" and occurs at 1:00 to 3:00 Central Time (1:00 to 3:00 AM). The time at which high wind penetration typically occurs during Texas' spring season ranges from late at night to the early hours of the morning. This is when power output of wind power plants is highest and total generation in the system is lowest. The red highlighted area is the wind power penetration and voltage RPAD during a period of "low wind" and occurs at 11:00 to 13:00 Central Time (11:00 AM to 1:00 PM).

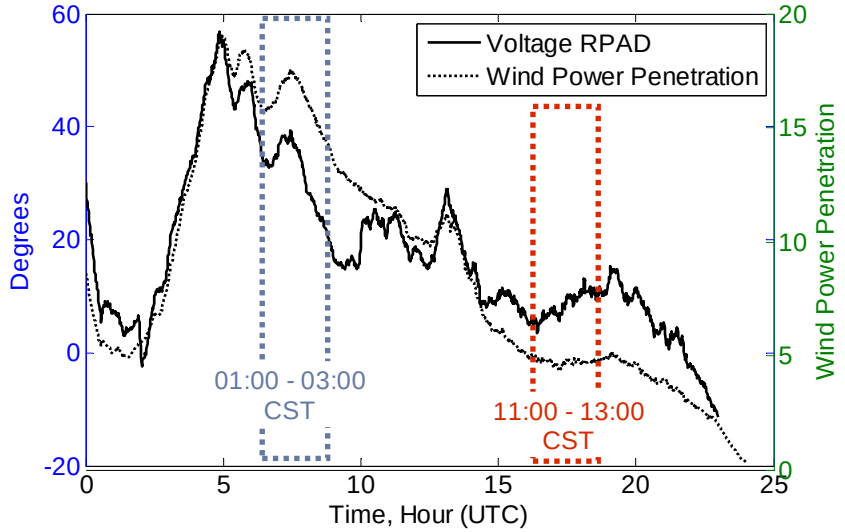

Figure 7.2: Voltage RPAD and Wind Power Penetration for April 13, 2009

7.2 ERCOT Wind Power Data and Relationship to Modes in Synchrophasor Data

The modal frequency and damping of low-frequency oscillations in the PMU data are made using the auto-regressive parameter estimation is available in the Matlab Signal Processing Toolbox [59]. The number of modes estimated is set to 32 but only modes with frequency under 3 Hz are examined in this section. Estimates are made for a moving window of 5 minutes of synchrophasor data. The estimates from each window are saved and plotted over a period of 2 hours. The frequency estimates, plotted on the y-axis, and the damping ratio estimates, plotted on the x-axis, made during a period of "low wind" power penetration is provided in Fig. 7.3. The data used for the analysis is the data highlighted in red in Fig. 7.2. The estimates are made

using data from 16:00 to 18:00 UTC (11:00 to 13:00 Central Time) when the wind power penetration is between 4.6% and 5%. The wind power during this time period is between 1500 and 1620 MW. There are clusters around the 1 Hz and 0.5 Hz modes which are always present within ERCOT. Other modes are present from 1.5 Hz to 3 Hz but are not as tightly clustered. This type of pattern is seen in time periods when the wind power penetration levels are low during the early months of 2009.

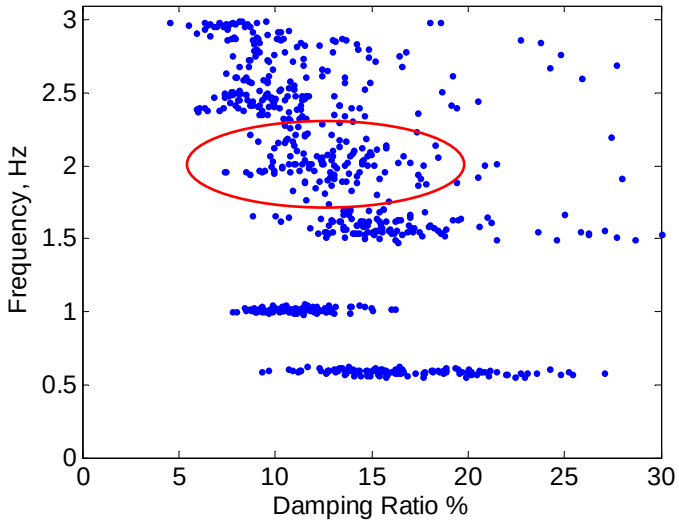

Figure 7.3: Modal Frequency and Damping Estimates for "low wind" conditions in April 13, 2009

A time period of "high wind" power penetration is examined. The data used for the analysis is the data highlighted in blue in Fig. 7.2. The data time period is from 6:00 to 8:00 UTC (1:00 to 3:00 Central Time) when the wind power penetration is between 15 and 18%. The wind power during this time

period is between 3425 and 3940 MW. The same clusters around 1 Hz and 0.5 Hz are seen, however, the modes around 2 Hz and 1.5 Hz are more tightly clustered. This pattern is seen during periods of "high wind" in early 2009.

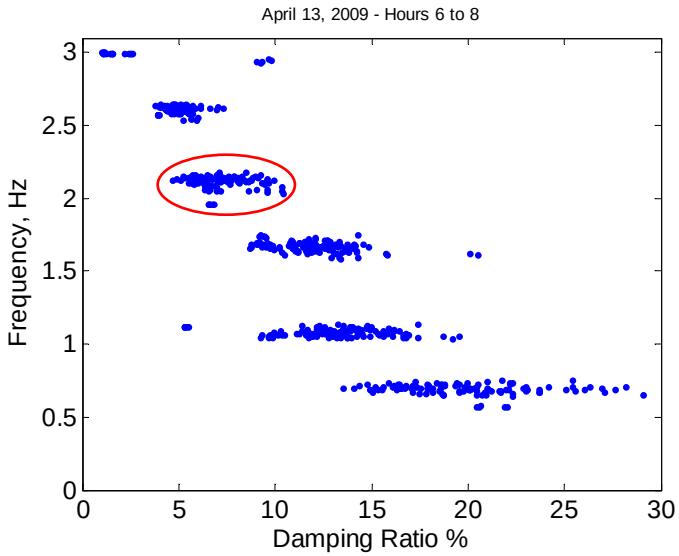

Figure 7.4: Modal Frequency and Damping Estimates for "high wind" conditions in April 13, 2009

It was observed that this pattern of tightly clustered modes of 2 Hz during "high wind" scenarios began to change in late 2009 and early 2010. To illustrate this, a day with a similar wind profile was found in early 2010. The wind penetration and voltage RPAD between UT-Austin and McDonald are shown in Fig. 7.5. The wind power penetration and the voltage RPAD follow each other closely, especially during sudden ramping periods in wind power.

The highlighted areas in Fig. 7.5 show the periods of data to be evaluated for dynamic modal behavior. The time stamp converted to equivalent

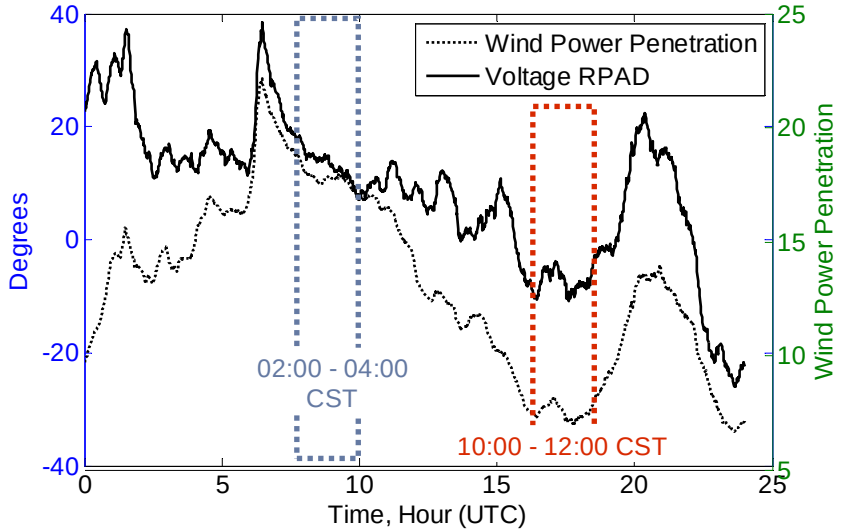

Figure 7.5: Voltage RPAD and Wind Power Penetration for January 18, 2010

Central Time are provided for convenience as well. The blue highlighted area is the wind power penetration and voltage RPAD during a period of "high wind" and occurs at 2:00 to 4:00 Central Time (2:00 to 4:00 AM). The red highlighted area is the wind power penetration and voltage RPAD during a period of "low wind" and occurs at 10:00 to 12:00 Central Time (10:00 AM to 12:00 PM).

The frequency and damping estimates in the voltage RPAD are saved for a period of 2 hours during "high wind" power penetration. The data is taken from 8:00 to 10:00 UTC and the wind power penetration during this period is between 16.8 and 18%. The wind power during this time period is between 4575 and 4830 MW. However, in this case the frequency estimates are not as tightly clustered around 2 Hz as during the April 2009 case. Multiple

days of data are examined to show that the relationship between the wind power and the clustering of the approximate 2 Hz mode is not as strong as would be expected from analysis of early 2009 data.

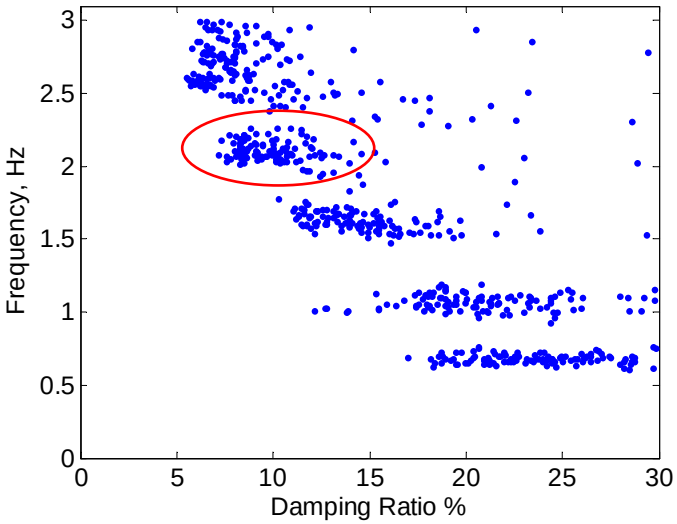

Figure 7.6: Modal Frequency and Damping Estimates for "high wind" conditions in January 18, 2010

Modal frequency and damping estimates are also made for a period of the same day when the wind power output is low as shown in Fig. 7.7. The data is taken from 16:00 to 18:00 UTC and the wind power penetration during this period is between 7 and 7.8%. The wind power during this time period is between 2275 and 2625 MW. However, the approximate 2 Hz data is tightly clustered which is the opposite of what occurred in the April 2009 case.

The two cases provided above show that the relationship between frequencies present in the PMU data and wind power penetration has changed

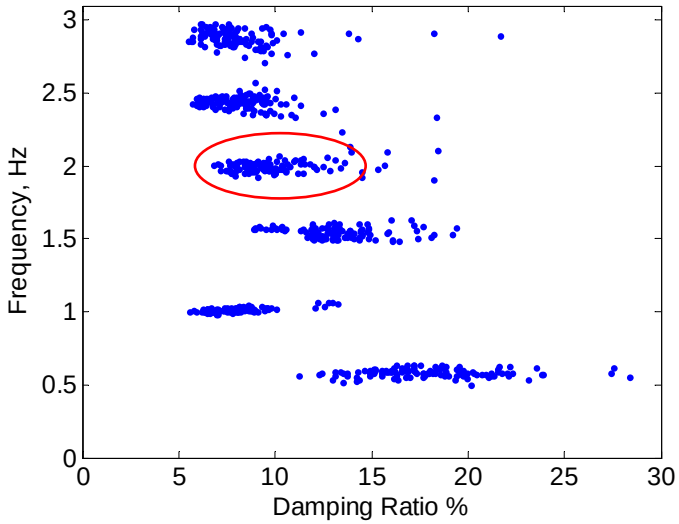

Figure 7.7: Modal Frequency and Damping Estimates for "low wind" conditions in January 18, 2010 -the 2 Hz oscillation are still present even though the wind penetration levels are low

over time. Possible reasons for these changes may include new transmission in wind-rich resource areas, new wind plants or conventional generators coming online, retirement of old generators or other significant system changes. An annual report on the Electric Systems Constraints and Needs released at the end of December in 2010 includes a summary of major completed transmission improvements [78]. In the summary is a list of improvements made in 2009 and 2010 including two transmission line rebuilds and a new autotransformer all located in West Texas. The same report for the following year also shows upgrades to transmission lines in the northwest region of ERCOT that could also have an impact on the dynamic modal behavior of the system [79]. A few

more examples of estimated modes during high wind power penetration are provided in Figs. 7.9 to 7.10 in order to illustrate that the cluster of modal estimates around 2 Hz is not always present.

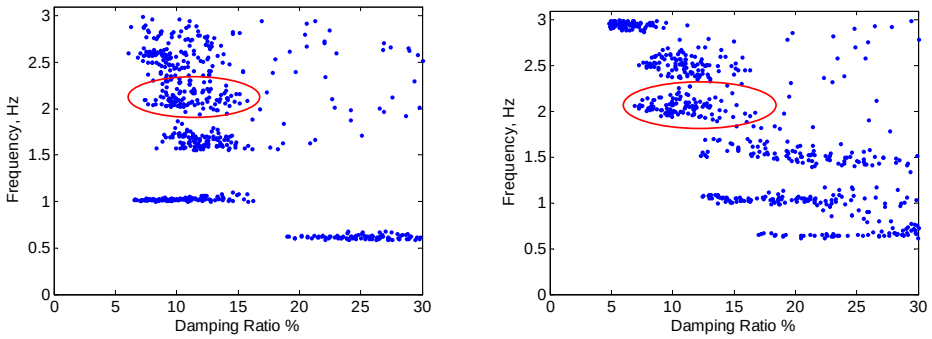

(a) January 27, 2012 9:00 to 11:00 UTC

(b) November 8, 2010 (UTC) 4:00 to 6:00 UTC

Figure 7.8: Modal Frequency and Damping Estimates for "high wind" conditions

In Fig. 7.8a, the wind power output during the duration of the analysis on January 27, 2012 was 6000 to 6500 MW and the wind power penetration was above 20% during this period. The wind data taken starting in August of 2010 to the present can be found in ERCOT Wind Integration Reports [80]. The data was taken from 3:00 to 5:00 Central Time or 9:00 to 11:00 UTC. The approximate 2 Hz mode at this time is spread out along both the y-axis and the x-axis, consistent with observations made that during high wind conditions, the modal estimates do not cluster tightly around 2 Hz.

In Fig. 7.8b, the wind power output during the duration of the analysis on November 8, 2010 was approximately 6000 MW and the wind power

penetration was approximately 20%. The data was taken from 22:00 to 00:00 November 7, 2010 Central Time or 4:00 to 6:00 November 8, 2010 UTC. The modal estimates are also not tightly clustered around 2 Hz even though the wind penetration is high.

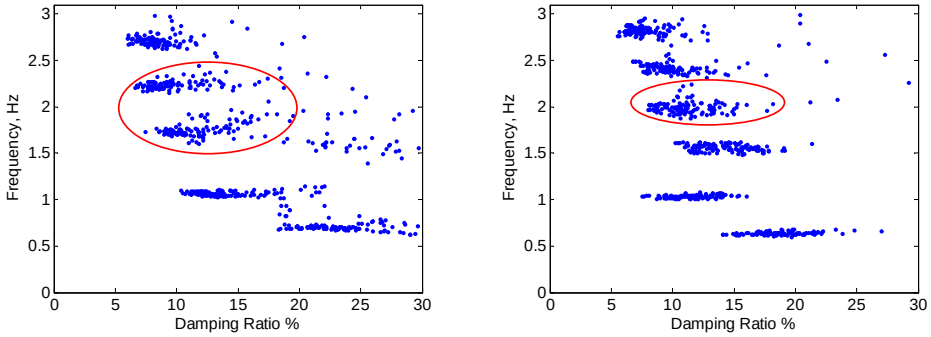

(a) October 7, 2011 at 8:00 to 10:00 UTC

(b) October 7, 2011 at 19:00 to 21:00 UTC

Figure 7.9: Modal Frequency and Damping Estimates for "high wind" conditions

In Fig. 7.9a, the wind power penetration was above 20% and the wind power is approximately 7000 MW at 9:00 UTC. The figure shows that the frequency estimates (the spread across the y-axis) are more tightly clustered but the damping estimates change throughout the 2 hour window of data. Another change is that the modal frequency has shifted so that there is no longer a 2 Hz mode but instead two neighboring modes located at 2.26 Hz and 1.74 Hz. Another example taken from the same day in Fig. 7.9b shows modal estimates made during a new record for wind power when the wind power output reached 7,400 MW at 20:06 UTC. The modal frequencies during this time of the day have changed so that now there is a modal frequency at 2 Hz.

The mode is not as tightly clustered as was seen in the examples from early 2009. The change in modal frequency and the spread of the damping as well as the tightness of the clustering of the modal estimates indicates that a lot of different variables besides wind power and wind penetration could have an effect on the modes present in the power system.

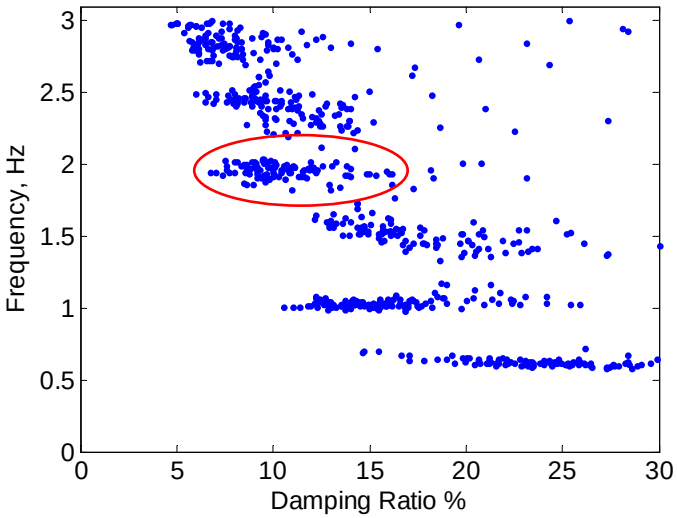

Figure 7.10: Modal Frequency and Damping Estimates for "high wind" conditions in November 1, 2011 at 00:00 to 02:00 UTC

A final example in Fig.7.10 is taken during a time when the wind power output of 3000 MW; which is approximately the same as the wind power output during the April 13, 2009 case. However, here the wind power penetration is lower at about 7 to 9%. Fig. 7.10 shows the modal estimates from 00:00 to 02:00 UTC.

A comparison of all the modes during high penetration levels is given in

Figs. 7.11 to 7.13. Each comparison is of a typical high wind modal behavior in April 2009 to high wind modal behavior examples from January 2010 to January 2012. When comparing the modal behavior, it is easier to see how the modes have changed over time. In all cases the spread along the x-axis is greater and shifted toward the right, meaning the modes are better damped. When the oscillations are better damped, damping estimates are more difficult to make since the oscillation in the signal has a shorter duration compared to a lightly damped oscillation. The frequency estimates also change, but these changes are not consistent and even change throughout the day. For example, the modes for Figs. 7.12a and 7.12b are both taken from the same day but the frequencies are different. Later in the day in Fig. **??** there is a frequency at almost exactly 2 Hz but early in the day in Figs. 7.12b there is a frequency below 2 Hz.

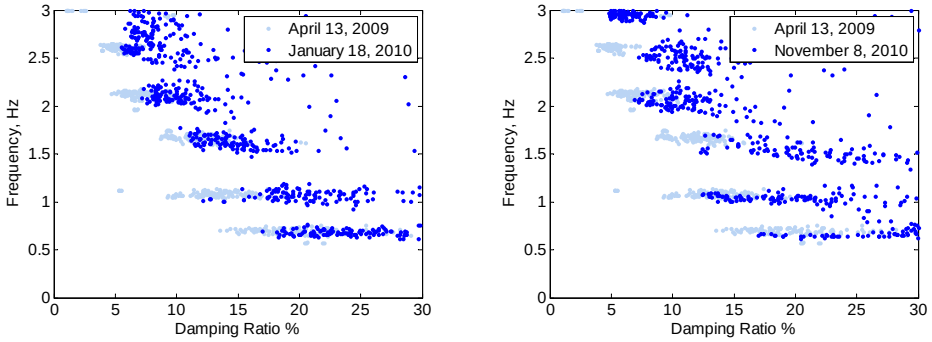

(a) Comparison to January 2010 modes

(b) Comparison to November 2010 modes

Figure 7.11: Comparison of modes during "high wind" conditions to modes during similar conditions in April 2009

These examples illustrate the power of PMUs to document changes

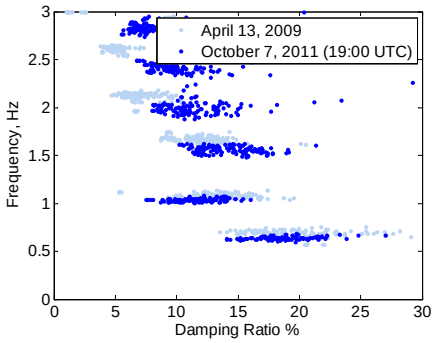

(a) Comparison to October 2011 (19:00 UTC) modes

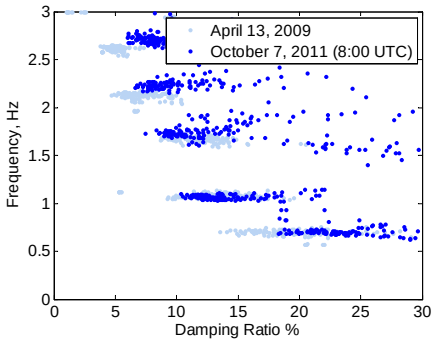

(b) Comparison to October 2011 (8:00 UTC) modes

Figure 7.12: Comparison of modes during "high wind" conditions to modes during similar conditions in April 2009

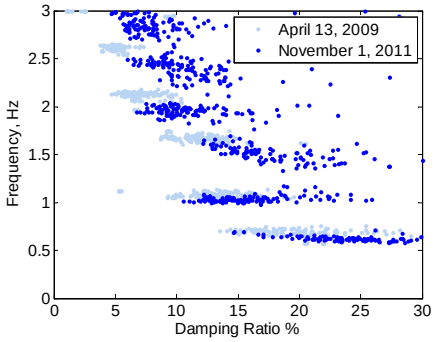

(a) Comparison to November 2011 modes

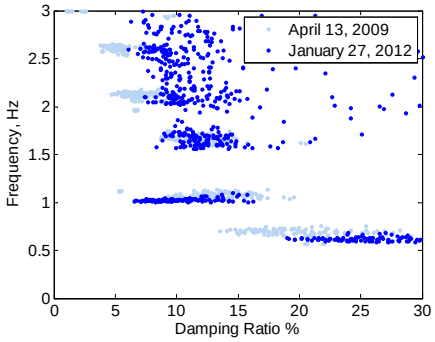

(b) Comparison to January 2012 modes

Figure 7.13: Comparison of modes during "high wind" conditions to modes during similar conditions in April 2009

in power system behavior over time. However, the data used to find the relationship between trends measured by PMUs and the wind power output for ERCOT is limited. At this time, it is not possible to make a conclusive statement about the effect wind power has on the power system as measured

by PMUs. The ERCOT wind data is not always available, and is limited to less than 2 years of data taken at a rate of one sample per minute. ERCOT wind data is now only available in PDF format as hourly averages. The wind data used is aggregated wind power for all of ERCOT and does not take into account variation in output between wind resource regions. As more wind power plants are installed over a larger geographical area, it will become difficult to use the limited number of PMUs currently in the system to make accurate analysis on the effects of wind power on synchrophasor data. As more PMUs are installed and more wind data becomes available, a more accurate analysis can be conducted, and PMUs will become a more valuable tool for tracking long term bulk power system behavior changes, particularly changes resulting from adoption of wind and other variable generation.

7.3 Summary

In this chapter, the relationship between wind power and voltage RPAD behavior was examined. The linear relationship between synchrophasor voltage RPAD (between UT-Austin and McDonald PMU stations) and the wind power output was shown to exist during periods of "high wind" scenarios. This was typically when the wind power penetration levels were above 12%. The linear relationship disappeared when the wind power penetration levels dropped. The modal content of the synchrophasor data taken during different periods of wind power penetration was examined as well. Initial observations indicate correlation between wind power penetration levels and the appearance

of an approximately 2 Hz mode (strongest at McDonald, but visible throughout the system). These observations were first made near the beginning of the synchrophasor network's initiation (in early 2009). After examining many days of synchrophasor and wind data, it was observed that a pattern of tightly clustered modes around 2 Hz appears during "high wind" scenarios prior to approximately mid-2009. However, the pattern of tightly clustered modes around 2 Hz began to change in late 2009 and early 2010. The typical behavior from early 2009 is compared to typical behavior seen in early 2010 to the present.

Chapter 8

Conclusion

The research presented in this dissertation is based on synchronized phasor measurement data, or synchrophasor data, taken at customer-level voltage as measured by the Texas Independent Synchrophasor Network. The customer-level synchrophasor data are first validated before being used for transmission level power system analysis. The methods and results of the validation processes are summarized in Section 8.1 of this chapter. After validation of the customer-level synchrophasor data, information from the data is extracted using statistical and signal processing techniques. First, an algorithm was created to automatically find power system events in the synchrophasor data. Next, categories for the events found in the synchrophasor data were created. Section 8.2 summarizes the research and results for the algorithm and creation of the event categories. Finally, Section 8.3 summarizes the work done using the synchrophasor data to discover trends in power system data due to changing levels of wind power penetration within ERCOT.

8.1 Validation of customer-level voltage synchrophasor data for analysis of transmission system behavior

The results from the research reported in Chapter 4 make evident that customer-level voltage synchrophasor data provide an accurate representation of transmission level power system behavior. Both power system behavior during normal operating conditions and during a large disturbance are examined. In Chapter 4, the customer-level voltage synchrophasor data is shown to accurately capture the transmission system response to multiple generating unit trip events. The drop in frequency as captured by the customer-level voltage synchrophasor data is compared to the frequency drops recorded and published by ERCOT in Daily Grid Operations Reports. The voltage phase angles and magnitudes during the same generating unit trip events are also examined. It is shown that the voltage magnitude is too noisy to be used for analysis of power system events. Next, the customer-level voltage phase angle measurements were compared to the state estimated 69 kV voltage phase angle and shown to be similar. The state estimated phase angles were examined for buses located near PMU stations within the synchrophasor network. Next, customer-level synchrophasor data is compared to synchrophasor data taken from a PMU installed at 69 kV. The transmission level PMU is located near the UT-Austin campus which is the location of a customer-level voltage PMU station. The comparison of transient response effects on frequency and voltage phase angle indicates that the customer-level synchrophasor data provide a clear picture of the system transient response. The estimation of modal fre-

quency and damping illustrated the accuracy of customer-level synchrophasor data as representation of the power system's ambient response. However, the relative phase angle difference between the UT-Austin customer level location and the 69 kV PMU location shows sudden "jumps" or changes in value. A simulation of the campus shows that these phase angle jumps are influenced by changes in load current. These results reported in Chapter 4 indicate that use of customer-level voltage PMU measurements are accurate for transmission system analysis and the synchrophasor data is used for the remainder of the research presented in this dissertation.

In addition, background information on the Texas Independent Synchrophasor Network is provided in Chapter 2 and includes a brief introduction to synchrophasors and their applications, PMU placement within ERCOT for power system event monitoring purposes, hardware used in the network, and the synchrophasor data format and pre-processing methods. The methods used to analyze the synchrophasor data throughout the dissertation is described in Chapter 3.

8.2 Automatic detection and categorization of power system events as captured by synchrophasor data

A novel algorithm to help extract useful information for power system analysis out of the large volume of synchrophasor data was created. A description of the algorithm and results from application of the algorithm to synchrophasor data is given in Chapter 5. The algorithm used four different

methods to screen for possible events and each method is applied to a moving window of PMU data. These methods were described in Chapters 3 and 5. Statistical techniques are applied to the results of these four methods to determine if an event occurred. The algorithm was applied to 24 hours of PMU data to analyze how well the algorithm was able to detect large and small events. A variety of events were detected, including a sudden loss of generation that was visible system wide as well as smaller local events that were visible at only a single PMU station. Once an event is detected by the algorithm, the data window containing the event is saved for further analysis.

The common quantitative characteristics for each event category and the ranges of characteristics for each event category are described in Chapter 6. First the events are placed into categories based on visual inspection. These categories are impulse, transient, and step change for RPAD events and impulse, transient, and change in frequency for frequency events. The common quantitative characteristics for each event category and the ranges of characteristics for each event category are also provided.

MATLAB software was used to analyze synchrophasor data and create the algorithm to detect events.

8.3 Identify trends in power system behavior related to wind power

The impact of increasing penetration of wind power on power system behavior is not completely known. The grid operated by ERCOT provides

a unique opportunity to study the impact of high levels of wind penetration. With the installation of PMUs across ERCOT, the impact of wind power on power system behavior can now be analyzed in new ways. Wind power and total generation data was captured from ERCOT's website. This information was collected over a period of 2 years and is compared to the synchrophasor data collected by the Texas Independent Synchrophasor Network over the same period of time. The relationship between the relative phase angle difference (between West Texas where many wind farms are located and Central Texas) and the wind power penetration levels are highly linearly correlated during periods of high levels of wind power penetration above 15% in the examples shown. Once the wind power penetration reduces to below 10%, the wind power penetration levels and relative phase angle difference are uncorrelated. The low frequency electromechanical oscillations present in the synchrophasor data are analyzed and the damping and frequency content are compared to different wind power penetration levels. Initially, the relationship between high levels of wind power penetration and a 2 Hz mode present in the synchrophasor data was strong. However, it is possible that changes to grid topology impacted this relationship and the 2 Hz mode is not as strong during periods of high wind power penetration.

All synchrophasor data are taken from the Texas Independent Synchrophasor Network and are used in all the listed research objectives. Additional data is provided by ERCOT as used in the approach. Analysis of all data was done in MATLAB.

Appendices

Appendix A

Power System Stability Monitoring Methods List

The expanded acronyms of the methods used for power system stability monitoring as summarized in Fig. 3.4 are provided here. References for most methods are also cited. The overview of the methods listed here is taken from [6] and [4].

Ambient Response

- Without Probing → Parametric → Recursive
  - Least-Squares
    - Least-Mean Squares (LMS) [81]
    - Robust Regularized Recursive Least-Squares (R3LS) [82]
- Without Probing → Parametric → Non-Recursive → Time-Domain
  - Yule-Walker
    - Autoregressive (AR) [52]
    - Autoregressive + Kalman Filter (AR+KF) [83]
    - Interleaved Prony (IP) [84]

        * Autoregressive Moving Average (ARMA) [72]
    - Subspace
        * Canonical Variate Algorithm (CVA) [85]
        * Numerical Algorithm for Subspace State-Space System Identification (N4SID) [86], [4]
        * Multivariate Output Error State-Space Algorithm (MOESP) [87], [88]
- Without Probing → Parametric → Non-Recursive → Frequency-Domain
    - Second-Order Frequency Regression (SOFR) [89]
    - Yule-Walker with Spectral Analysis (YWS) [61], [4]
    - Frequency-Domain Decomposition (FDD) [90], [24]
- Without Probing → Non-Parametric
    - Spectral Methods
        * Fast-Fourier Transform (FFT)
        * Welch Periodogram [91]
    - High Order Spectral (HOS)
        * Bispectrum & Bicoherence [92]
        * Trispectrum [47]
    - Basic Function Decomposition
        * Principal Component Analysis (PCA) [93]

- With Probing
  - System Identification with Known Input

  Transient Response

- Linear → Time-Domain
  - Prony [50], [51], [53]
  - Matrix-Pencil (MP) [58], [24]
  - Eigensystem Realization Algorithm (ERA) [94], [95]
  - Hankel Total Least-Squares (HTLS) [96], [24]
- Linear → Frequency-Domain
  - z-Transform Identification (z-ID)
  - Frequency-Domain Identification (f-ID) [4, 97]
- Non-Linear → Parametric
  - Wavelets [98], [99]
  - HilbertHuang Transform (HHT) [47], [4]
- Non-Linear → Non-Parametric
  - Frequency-Domain Pattern Recognition (FDPR) [100]
  - Short-Time Forier Transform (STFT)

Appendix B

Unwrapping Function for Synchrophasor Phase Angles

The code for the function written in Matlab to unwrap the voltage phase angle as measured at each PMU station is given here. A description of the funciton is also provided.

The differential of the voltage angle is used to detect jumps which appear as -360 degree or 360 degree spikes in the differentiated signal. The place in the signal where these spikes apear are used to move the signal up 180 or down 180 degrees depending on the direction of the spike. The signal is adjusted by finding first spike that is -360 degrees. The rest of the signal following the detected spike is adjusted by adding 360 degrees. The next -360 spike is found and the signal following that spike is adjusted by adding 360 degrees. This continues untill all -360 spikes have been adjusted for. Next, the 360 degree spikes are found and adjusted for. The location in the signal where the first 360 degree spike occurs is detected and -360 degrees is added to the rest of the signal following the detected spike. This is repeated until all 360 degree spikes are adjusted for.

```
% Input is the PMU angle, output is the unwrapped angle
function [ang_unwrap] = fAngleUnwrap(V1ang)

% differential of the PMU angle
angdiff = V1ang(2:end) - V1ang(1:end-1);

posjmp = find(angdiff<-300); % detect jumps
negjmp = find(angdiff>300); % detect jumps

if ~isempty(posjmp) % correct jumps
    for qt = 1:length(posjmp)
        x = [V1ang(1:posjmp(qt));
                V1ang(posjmp(qt)+1:end)+360];
        V1ang = x;
    end
end

if ~isempty(negjmp) % correct jumps
    for qt = 1:length(negjmp)
        x = [V1ang(1:negjmp(qt));
                V1ang(negjmp(qt)+1:end)-360];
        V1ang = x;
    end
end

% final unwrapped voltage angle
ang_unwrap = V1ang;
```

Bibliography

[1] K. Martin and J. Carroll. Phasing in the technology. *Power and Energy Magazine, IEEE*, 6(5):24 –33, september-october 2008.

[2] Office of the Govenor Economic Development & Tourism. Wind energy potential and wind farm locations in texas. Online, March 2012.

[3] P. Kundur, N.J. Balu, and M.G. Lauby. *Power system stability and control*. The EPRI power system engineering series. McGraw-Hill, 1994.

[4] A.R. Messina. *Inter-area Oscillations in Power Systems: A Nonlinear and Nonstationary Perspective*. Power Electronics and Power Systems. Springer, 2009.

[5] J.F. Hauer and J.G. DeSteese. *A tutorial on detection and characterization of special behavior in large electric power systems*. Pacific Northwest National Laboratory, 2004.

[6] J. Thambirajah, E. Barocio, and N.F. Thornhill. Comparative review of methods for stability monitoring in electrical power systems and vibrating structures. *Generation, Transmission Distribution, IET*, 4(10):1086 –1103, october 2010.

[7] S. Sharma, Shun-Hsien Huang, and N.D.R. Sarma. System inertial frequency response estimation and impact of renewable resources in ercot interconnection. In *Power and Energy Society General Meeting, 2011 IEEE*, pages 1 –6, july 2011.

[8] NASPI. North american synchrophasor initiative mission statement, December 2012.

[9] W.M. Grady and D. Costello. Implementation and application of an independent texas synchrophasor network. In *Protective Relay Engineers, 2010 63rd Annual Conference for*, pages 1 –12, 29 2010-april 1 2010.

[10] W. Mac Grady. The texas synchrophasor network, December 2012.

[11] III E.O. Schweitzer and D. Hou. Filtering for protective relays. In *WESCANEX 93. 'Communications, Computers and Power in the Modern Environment.' Conference Proceedings., IEEE*, pages 15 –23, 1993.

[12] ERCOT. Ercot daily grid operations reports. Now defunct.

[13] ERCOT. Ercot operations messages.

[14] A.J. Allen, Sang-Wook Sohn, W.M. Grady, and S. Santoso. Validation of distribution level measurements for power system monitoring and low frequency oscillation analysis. In *Power Electronics and Machines in Wind Applications (PEMWA), 2012 IEEE*, pages 1 –5, july 2012.

[15] S.; Muljadi E.; Allen, A.J.; Santoso. Phasor measurement unit (pmu) for wide area monitoring, protection, and control (wampac) applications. Technical report, National Renewable Energy Laboratory (NREL), 2012.

[16] W.M.; Santoso S. Allen, A.J.; Sang-Wook Sohn; Grady. Algorithm for screening pmu data for power system events. In *IEEE International Smart Grid Technologies, 2012 IEEE*, 2012.

[17] S.W. Sohn, A.J. Allen, S. Kulkarni, W.M. Grady, and S. Santoso. Event detection method for the pmus synchrophasor data. In *Power Electronics and Machines in Wind Applications (PEMWA), 2012 IEEE*, pages 1–7. IEEE, 2012.

[18] A.J. Allen, S. Santoso, and W.M. Grady. Voltage phase angle variation in relation to wind power. In *Power and Energy Society General Meeting, 2010 IEEE*, pages 1 –7, july 2010.

[19] M.; Muljadi E.; Santoso S.; Allen, A.J.; Singh. Measurement-based investigation of inter- and intra-area effects of wind power plant integration. Power Systems, IEEE Transactions on.

[20] S. Kulkarni, A. Allen, S. Santoso, and WM Grady. Phasor measurement unit placement algorithm. In *Power & Energy Society General Meeting, 2009. PES'09. IEEE*, pages 1–6. IEEE, 2009.

[21] A.G. Phadke and J.S. Thorp. *Synchronized phasor measurements and their applications*. Power electronics and power systems. Springer, 2008.

[22] Ieee standard for synchrophasor measurements for power systems. *IEEE Std C37.118.1-2011 (Revision of IEEE Std C37.118-2005)*, pages 1 –61, 28 2011.

[23] A.G. Phadke and J.S. Thorp. History and applications of phasor measurements. In *Power Systems Conference and Exposition, 2006. PSCE '06. 2006 IEEE PES*, pages 331 –335, 29 2006-nov. 1 2006.

[24] Guoping Liu, J. Quintero, and V. Venkatasubramanian. Oscillation monitoring system based on wide area synchrophasors in power systems. In *Bulk Power System Dynamics and Control - VII. Revitalizing Operational Reliability, 2007 iREP Symposium*, pages 1 –13, aug. 2007.

[25] Zhian Zhong, Chunchun Xu, B.J. Billian, Li Zhang, S.-J.S. Tsai, R.W. Conners, V.A. Centeno, A.G. Phadke, and Yilu Liu. Power system frequency monitoring network (fnet) implementation. *Power Systems, IEEE Transactions on*, 20(4):1914 – 1921, nov. 2005.

[26] M. Parashar and Jianzhong Mo. Real time dynamics monitoring system (rtdms): Phasor applications for the control room. In *System Sciences, 2009. HICSS '09. 42nd Hawaii International Conference on*, pages 1 –11, jan. 2009.

[27] E. O. Schweitzer, A. Guzman, H. J. Altuve, D. A. Tziouvaras, and J. Needs. Real-time synchrophasor applications in power system control and protection. In *Developments in Power System Protection (DPSP*

2010). Managing the Change, 10th IET International Conference on, pages 1 –5, 29 2010-april 1 2010.

[28] E. Martínez, N. Juárez, A. Guzmán, G. Zweigle, and J. León. Using synchronized phasor angle difference for wide-area protection and control. In *proceedings of the 33rd Annual Western Protective Relay Conference, Spokane, WA*, 2006.

[29] E. Price. Practical considerations for implementing wide area monitoring, protection and control. In *Protective Relay Engineers, 2006. 59th Annual Conference for*, page 12 pp., april 2006.

[30] G. Benmouyal, E.O. Schweitzer, and A. Guzman. Synchronized phasor measurement in protective relays for protection, control, and analysis of electric power systems. In *Protective Relay Engineers, 2004 57th Annual Conference for*, pages 419 – 450, mar-1 apr 2004.

[31] Power System Relaying Committee Report of Working Group C-14 Of the System Protection Subcommittee. Use of synchrophasor measurements in protective relaying applications. Technical report, 2012.

[32] A.G. Phadke, J.S. Thorp, R.F. Nuqui, and M. Zhou. Recent developments in state estimation with phasor measurements. In *Power Systems Conference and Exposition, 2009. PSCE '09. IEEE/PES*, pages 1 –7, march 2009.

[33] T.L. Baldwin, L. Mili, Jr. Boisen, M.B., and R. Adapa. Power system observability with minimal phasor measurement placement. *Power Systems, IEEE Transactions on*, 8(2):707 –715, may 1993.

[34] B. Milosevic and M. Begovic. Nondominated sorting genetic algorithm for optimal phasor measurement placement. *Power Systems, IEEE Transactions on*, 18(1):69 – 75, feb 2003.

[35] R.F. Nuqui and A.G. Phadke. Phasor measurement unit placement techniques for complete and incomplete observability. *Power Delivery, IEEE Transactions on*, 20(4):2381 – 2388, oct. 2005.

[36] I.W. Slutsker, S. Mokhtari, L.A. Jaques, J.M.G. Provost, M.B. Perez, J.B. Sierra, F.G. Gonzalez, and J.M.M. Figueroa. Implementation of phasor measurements in state estimator at sevillana de electricidad. In *Power Industry Computer Application Conference, 1995. Conference Proceedings., 1995 IEEE*, pages 392 –398, may 1995.

[37] A.G. Phadke. Synchronized phasor measurements in power systems. *Computer Applications in Power, IEEE*, 6(2):10 –15, april 1993.

[38] F. Hashiesh, H.E. Mostafa, A.-R. Khatib, I. Helal, and M.M. Mansour. An intelligent wide area synchrophasor based system for predicting and mitigating transient instabilities. *Smart Grid, IEEE Transactions on*, 3(2):645 –652, june 2012.

[39] C. Wang, C.X. Dou, X.B. Li, and Q.Q. Jia. A wams/pmu-based fault location technique. *Electric Power Systems Research*, 77(8):936–945, 2007.

[40] Electric reliability council of texas (ercot), October 2012.

[41] Schweitzer engineering laboratories, inc., October 2012.

[42] Schweitzer Engineering Laboratories, Inc. *Instruction Manual for SEL-2401 Satellite-Synchronized Clock*.

[43] Schweitzer Engineering Laboratories, Inc. *Instruction Manual for SEL-421 Relay - Protection and Automation System*, 2011.

[44] Schweitzer Engineering Laboratories, Inc. *Instruction Manual for SEL-3378 Synchrophasor Vector Processor*, 2008.

[45] Schweitzer Engineering Laboratories, Inc. *Instruction Manual for SEL-5078 SYNCHROWave Central Software*, 2012.

[46] D.N. Kosterev, C.W. Taylor, and W.A. Mittelstadt. Model validation for the august 10, 1996 wscc system outage. *Power Systems, IEEE Transactions on*, 14(3):967 –979, aug 1999.

[47] A.R. Messina and V. Vittal. Nonlinear, non-stationary analysis of interarea oscillations via hilbert spectral analysis. *Power Systems, IEEE Transactions on*, 21(3):1234–1241, 2006.

[48] J.W. Pierre, Ning Zhou, F.K. Tuffner, J.F. Hauer, D.J. Trudnowski, and W.A. Mittelstadt. Probing signal design for power system identification. *Power Systems, IEEE Transactions on*, 25(2):835 –843, may 2010.

[49] J.F. Hauer, W.A. Mittelstadt, K.E. Martin, J.W. Burns, H. Lee, J.W. Pierre, and D.J. Trudnowski. Use of the wecc wams in wide-area probing tests for validation of system performance and modeling. *Power Systems, IEEE Transactions on*, 24(1):250 –257, feb. 2009.

[50] J.F. Hauer, C.J. Demeure, and L.L. Scharf. Initial results in prony analysis of power system response signals. *Power Systems, IEEE Transactions on*, 5(1):80 –89, feb 1990.

[51] J.F. Hauer. Application of prony analysis to the determination of modal content and equivalent models for measured power system response. *Power Systems, IEEE Transactions on*, 6(3):1062 –1068, aug 1991.

[52] J.W. Pierre, D.J. Trudnowski, and M.K. Donnelly. Initial results in electromechanical mode identification from ambient data. *Power Systems, IEEE Transactions on*, 12(3):1245 –1251, aug 1997.

[53] D.J. Trudnowski, J.M. Johnson, and J.F. Hauer. Making prony analysis more accurate using multiple signals. *Power Systems, IEEE Transactions on*, 14(1):226 –231, feb 1999.

[54] T.J. Browne, V. Vittal, G.T. Heydt, and A.R. Messina. A comparative assessment of two techniques for modal identification from power system measurements. *Power Systems, IEEE Transactions on*, 23(3):1408 – 1415, aug. 2008.

[55] Surya Santoso Jamie Ramos Aparajita Sant, W.M. Grady. A screening procedure for synchrophasor data using the prony method to detect power systems events. In *Power and Energy Society General Meeting, 2012 IEEE*, 2012.

[56] G. Yanfeng and A. Guzmn. Synchrophasor-based online modal analysis to mitigate power system interarea oscillation.

[57] Ning Zhou, J.W. Pierre, and D. Trudnowski. A stepwise regression method for estimating dominant electromechanical modes. *Power Systems, IEEE Transactions on*, 27(2):1051 –1059, may 2012.

[58] T.K. Sarkar and O. Pereira. Using the matrix pencil method to estimate the parameters of a sum of complex exponentials. *Antennas and Propagation Magazine, IEEE*, 37(1):48 –55, feb 1995.

[59] MATLAB. *MATLAB version 7.12.0.635 (R2011a).* The MathWorks Inc., Natick, Massachusetts, 2012.

[60] M.H. Hayes. *Statistical digital signal processing and modeling.* John Wiley & Sons, 1996.

[61] D.J. Trudnowski, J.W. Pierre, Ning Zhou, J.F. Hauer, and M. Parashar. Performance of three mode-meter block-processing algorithms for automated dynamic stability assessment. *Power Systems, IEEE Transactions on*, 23(2):680 –690, may 2008.

[62] P. Stoica and R.L. Moses. *Introduction to spectral analysis*. Prentice Hall, 1997.

[63] L. Vanfretti, R. Garcia-Valle, K. Uhlen, E. Johansson, D. Trudnowski, J.W. Pierre, J.H. Chow, O. Samuelsson, J. andstergaard, and K.E. Martin. Estimation of eastern denmark's electromechanical modes from ambient phasor measurement data. In *Power and Energy Society General Meeting, 2010 IEEE*, pages 1 –8, july 2010.

[64] R.C. Dugan, S. Santoso, M.F. McGranaghan, and H.W. Beaty. *Electrical power systems quality*. McGraw-Hill professional engineering. McGraw-Hill, 2002.

[65] Jody Verboomen, Dirk Van Hertem, Pieter H Schavemaker, Wil L Kling, and Ronnie Belmans. Phase shifting transformers: principles and applications. In *Future Power Systems, 2005 International Conference on*, pages 6–pp. IEEE, 2005.

[66] Vance Beauregard. Small signal stability analysis study: study prepared by powertech labs inc. for ercot. Power Point Presentation, April 2002.

[67] R. W. Cummings. Overview of frequency response initiative. Power Point Presentation, March 2010.

[68] Jingyuan Dong, Tao Xia, Yingchen Zhang, Yilu Liu, L. Beard, and T. Bilke. Monitoring the north american interconnections at distribution level. In *Power Energy Society General Meeting, 2009. PES '09. IEEE*, pages 1 –8, july 2009.

[69] V. M. Venkatasubramanian and Yuan Li. Analysis of 1996 western aermican electric blackouts. In *Bulk Power System Dynamics and Control*, August 2004.

[70] A. Monticelli. *State estimation in electric power systems: a generalized approach*. Kluwer international series in engineering and computer science. Kluwer Academic Publishers, 1999.

[71] M. Crow. *Computational methods for electric power systems*. Electric power engineering series. CRC Press, 2003.

[72] R.W. Wies, J.W. Pierre, and D.J. Trudnowski. Use of arma block processing for estimating stationary low-frequency electromechanical modes of power systems. In *Power Engineering Society General Meeting, 2003, IEEE*, volume 4, page 4 vol. 2666, july 2003.

[73] M. Ester, H.P. Kriegel, J. Sander, and X. Xu. A density-based algorithm for discovering clusters in large spatial databases with noise. In *Proceed-*

ings of the 2nd International Conference on Knowledge Discovery and Data mining, volume 1996, pages 226–231. AAAI Press, 1996.

[74] University of Texas Austin Utilities & Energy Management. University of texas austin power plant and chilling stations, October 2011.

[75] M. R. Rylander. *Nonlinear Power Electronic Loads: Modeling and Impact on Power System Transient Response and Stability*. PhD thesis, Dept. Elect. and Comp. Eng., Univ. of Texas, Austin, 2008.

[76] G. Rogers. *Power System Oscillations*. Kluwer international series in engineering and computer science: Power electronics & power systems. Kluwer Academic, 2000.

[77] Midwest Reliability Organization Protective Relay Subcommittee. Considerations for transmission reclosing practices in the mro area. Technical report, Midwest Reliability Organization, 2009.

[78] ERCOT. Report on existing and potential electric system constraints and needs. Technical report, Electric Reliability Council of Texas, 2010.

[79] ERCOT. Report on existing and potential electric system constraints and needs. Technical report, Electric Reliability Council of Texas, 2011.

[80] ERCOT. Ercot wind integration reports, October 2012.

[81] R.W. Wies and J.W. Pierre. Use of least-mean squares (lms) adaptive filtering technique for estimating low-frequency electromechanical modes

in power systems. In *American Control Conference, 2002. Proceedings of the 2002*, volume 6, pages 4867 – 4873 vol.6, 2002.

[82] Ning Zhou, D.J. Trudnowski, J.W. Pierre, and W.A. Mittelstadt. Electromechanical mode online estimation using regularized robust rls methods. *Power Systems, IEEE Transactions on*, 23(4):1670 –1680, nov. 2008.

[83] P. Korba, M. Larsson, and C. Rehtanz. Detection of oscillations in power systems using kalman filtering techniques. In *Control Applications, 2003. CCA 2003. Proceedings of 2003 IEEE Conference on*, volume 1, pages 183 – 188 vol.1, june 2003.

[84] G. Ledwich and E. Palmer. Modal estimates from normal operation of power systems. In *Power Engineering Society Winter Meeting, 2000. IEEE*, volume 2, pages 1527 –1531 vol.2, 2000.

[85] N. Zhou, JW Pierre, and RW Wies. Estimation of low-frequency electromechanical modes of power systems from ambient measurements using a subspace method. In *Proceedings of the North American Power Symposium*, 2003.

[86] N. Zhou, J.W. Pierre, and J.F. Hauer. Initial results in power system identification from injected probing signals using a subspace method. *Power Systems, IEEE Transactions on*, 21(3):1296–1302, 2006.

[87] M. Larsson and D.S. Laila. Monitoring of inter-area oscillations under ambient conditions using subspace identification. In *Power & Energy Society General Meeting, 2009. PES'09. IEEE*, pages 1–6. IEEE, 2009.

[88] P.V. Overschee, BLD Moor, D.A. Hensher, J.M. Rose, W.H. Greene, K. Train, W. Greene, E. Krause, J. Gere, and R. Hibbeler. *Subspace Identification for the Linear Systems: Theory–Implementation*. Boston: Kluwer AcademicPublishers, 1996.

[89] N. Kakimoto, M. Sugumi, T. Makino, and K. Tomiyama. Monitoring of interarea oscillation mode by synchronized phasor measurement. *Power Systems, IEEE Transactions on*, 21(1):260–268, 2006.

[90] R. Brincker, L. Zhang, and P. Andersen. Modal identification of output-only systems using frequency domain decomposition. *Smart materials and structures*, 10(3):441, 2001.

[91] D.J. Trudnowski. Estimating electromechanical mode shape from synchrophasor measurements. *Power Systems, IEEE Transactions on*, 23(3):1188–1195, 2008.

[92] A.R. Messina and V. Vittal. Assessment of nonlinear interaction between nonlinearly coupled modes using higher order spectra. *Power Systems, IEEE Transactions on*, 20(1):375 – 383, feb. 2005.

[93] K.K. Anaparthi, B. Chaudhuri, N.F. Thornhill, and B.C. Pal. Coherency identification in power systems through principal component

analysis. *Power Systems, IEEE Transactions on*, 20(3):1658–1660, 2005.

[94] I. Kamwa, R. Grondin, EJ Dickinson, and S. Fortin. A minimal realization approach to reduced-order modelling and modal analysis for power system response signals. *Power Systems, IEEE Transactions on*, 8(3):1020–1029, 1993.

[95] J.N. Juang and R.S. Pappa. An eigensystem realization algorithm for modal parameter identification and model reduction. *Journal of guidance, control, and dynamics*, 8(5), 2012.

[96] JJ Sanchez-Gasca and JH Chow. Computation of power system low-order models from time domain simulations using a hankel matrix. *Power Systems, IEEE Transactions on*, 12(4):1461–1467, 1997.

[97] D.J. Trudnowski and J.W. Pierre. Overview of algorithms for estimating swing modes from measured responses. In *Power Energy Society General Meeting, 2009. PES '09. IEEE*, pages 1 –8, july 2009.

[98] P. Kang and G. Ledwich. Estimating power system modal parameters using wavelets. In *Signal Processing and Its Applications, 1999. ISSPA'99. Proceedings of the Fifth International Symposium on*, volume 2, pages 563–566. IEEE, 1999.

[99] J. Turunen et al. A wavelet-based method for estimating damping in power systems. 2011.

[100] DR Ostojic and GT Heydt. Transient stability assessment by pattern recognition in the frequency domain. *Power Systems, IEEE Transactions on*, 6(1):231–237, 1991.

[101] M. J. Bertin et al. *Pisot and Salem Numbers*. user Verlag, Berlin, 1992.

[102] S. Braun and Y. M. Ram. Determination of structural modes via the prony model: System order and noise induced poles. *The Journal of the Acoustical Society of America*, 81(5):1447–1459, 1987.

[103] J. Eto. Phasor technology research and implementation roadmap. presented to Center for Commercialization of Electric Technologies Phasor Roadmapping Kick-off Meeting, October 2008.

[104] Joonhyun Kim and W.M. Grady. Synchrophasor analysis of 221 generating unit trips in ercot. In *Power and Energy Society General Meeting, 2011 IEEE*, pages 1 –4, july 2011.

[105] Donald K. Knuth. *The TEXbook*. Addison-Wesley, 1984.

[106] R. Kumaresan and D. Tufts. Estimating the parameters of exponentially damped sinusoids and pole-zero modeling in noise. *Acoustics, Speech and Signal Processing, IEEE Transactions on*, 30(6):833 – 840, dec 1982.

[107] Leslie Lamport. *LATEX: A document preparation system*. Addison-Wesley, 2nd edition, 1994.

[108] T. Lobos, Z. Leonowicz, J. Rezmer, and P. Schegner. High-resolution spectrum-estimation methods for signal analysis in power systems. *Instrumentation and Measurement, IEEE Transactions on*, 55(1):219–225, 2006.

[109] F Mittelbach M Goosens and A Samarin. *The LaTeXCompanion*. Addison-Wesley, 1994.

[110] K.E. Martin, G. Benmouyal, M.G. Adamiak, M. Begovic, Jr. Burnett, R.O., K.R. Carr, A. Cobb, J.A. Kusters, S.H. Horowitz, G.R. Jensen, G.L. Michel, R.J. Murphy, A.G. Phadke, M.S. Sachdev, and J.S. Thorp. Ieee standard for synchrophasors for power systems. *Power Delivery, IEEE Transactions on*, 13(1):73 –77, jan 1998.

[111] R.F. Nuqui and A.G. Phadke. Phasor measurement unit placement based on incomplete observability. In *Power Engineering Society Summer Meeting, 2002 IEEE*, volume 2, pages 888 –893 vol.2, july 2002.

[112] D. A. Pierre, D. J. Trudnowski, and J. F. Hauer. Identifying reduced-order models for large nonlinear systems with arbitrary initial conditions and multiple outputs using prony signal analysis. In *American Control Conference, 1990*, pages 149 –154, may 1990.

[113] Alf J. van der Poorten. Some problems of recurrent interest. Technical Report 81-0037, School of Mathematics and Physics, Macquarie University, North Ryde, Australia 2113, August 1981.

[114] P.F. Ribeiro. *Time-Varying Waveform Distortions in Power Systems*. Wiley - IEE. Wiley, 2009.

[115] O. Samuelsson, M. Hemmingsson, A.H. Nielsen, K.O.H. Pedersen, and J. Rasmussen. Monitoring of power system events at transmission and distribution level. *Power Systems, IEEE Transactions on*, 21(2):1007 – 1008, may 2006.

[116] J.J. Sanchez-Gasca and J.H. Chow. Performance comparison of three identification methods for the analysis of electromechanical oscillations. *Power Systems, IEEE Transactions on*, 14(3):995 –1002, August 1999.

[117] Michael Spivak. *The joy of TEX*. American Mathematical Society, Providence, R.I., 2nd edition, 1990.

[118] Zhiyong Yuan, Tao Xia, Yingchen Zhang, Lang Chen, P.N. Markham, R.M. Gardner, and Yilu Liu. Inter-area oscillation analysis using wide area voltage angle measurements from fnet. In *Power and Energy Society General Meeting, 2010 IEEE*, pages 1 –7, july 2010.

[119] R. Zivanovic and C. Cairns. Implementation of pmu technology in state estimation: an overview. In *AFRICON, 1996., IEEE AFRICON 4th*, volume 2, pages 1006 –1011 vol.2, sep 1996.

Vita

Alicia Jen Allen was born in Tulsa, Oklahoma on January 11, 1982, the daughter of Loy Ray Allen and Don-May Allen. She received her M.S. degree in electrical engineering from the University of Texas at Austin in 2007 and her B.S. in electrical engineering from the University of Texas at Austin in 2004. She is currently enrolled in the Ph.D. program in electrical engineering at the University of Texas at Austin. Her research interests include wide area monitoring, protection, and control systems, power system stability, and renewables. She will be joining the National Renewable Energy Laboratory in Golden, CO as a postdoctoral researcher in April 2013.

Permanent address: 1507 Houston St 231
Austin, Texas 78756

This dissertation was typeset with LaTeX[†] by the author.

[†]LaTeX is a document preparation system developed by Leslie Lamport as a special version of Donald Knuth's TeX Program.